Combustion of Gas in Closed, Interconnected Vessels: Pressure Piling

Lars Rogstadkjernet

A thesis submitted in partial fulfilment of the
requirements for the degree of Candidatus Scientiarum

Department of Physics and Technology
University of Bergen
Bergen Norway
November 2004

Preface

This work has been performed as part of the degree Candidatus Scientiarum at the University of Bergen, 2004. Experiments and simulations have been performed in GexCons facilities at Fantoft, Bergen. Without the support from GexCon, this work could not have been possible.

I would especially like to thank my supervisors:

Bjørn Arntzen at UIB
Geir Pedersen at GexCon A/S

Special thanks are also due to the people at GexCon for valuable discussions and help. I would also like to thank Professor Rolf Eckhoff who introduced me to the field of gas explosions and Kåre Slettebakken at the mechanical workshop at the University of Bergen.

Finally I which to thank Sigrunn, Magnus, Iver and Hans who have been waiting patiently at home.

Lars Rogstadkjernet

Abstract

This thesis is the documentation of a study of gas explosions in closed, interconnected vessels. Explosions within such vessels is strongly affected by the characteristics of the geometry, and can, under given conditions, result in very high local peak pressure and rates of pressure rise. In these situations peak pressure and rate of pressure rise can be several factors higher than in comparable single vessel explosions. The term *pressure piling* or *pre-compression* is used to describes explosions that show such characteristics pressure development

The focus for the present work has been to investigate the effect of fuel properties on pressure piling situations. Altogether more than 500 tests have been conducted with variation in some of the key parameters such as volume ratio between chambers, size and shape of transfer connection, location of ignition point and fuel mixtures. In each test, pressure has been measured and pressure time history recorded.

For range of geometries used in this study, the level of pressure piling is consistently lower for hydrogen than for methane. The higher burning velocity of hydrogen is the main cause for this effect. Fast combustion in primary chamber means that the flame uses little time to propagate into the secondary chamber. Consequently only a small portion of gas is able to flow into the secondary chamber and the level of pre-compression is moderate. Subsequent combustion does not result in very high pressure. For this reason lean and rich mixture, which have lower burning velocities, are slightly more prone to pressure piling.

The range of burnable concentrations of hydrogen is very wide (5-75%) and the characteristics of these mixtures change significantly with fuel content. Lean mixtures have a low ratio of laminar to turbulent burning velocity whereas rich mixtures typically will flow more easily. Both these factors have been shown to affect hydrogen's tendency for pressure piling. However, these effects are very geometry dependent and have moderate impact on the general pressure level.

Tests of methane air mixtures with various equivalence ratios show that peak pressure is moderately affected by this parameter. In pressure piling situations, peak pressure will typically be just as high for rich and lean mixture as for stoichiometric equivalent mixtures. For slow-burning mixtures (rich and lean) more gas will have time to flow into the secondary chamber and thereby compensate for the lower energy content in the gas.

In the last phase of this work, the CFD-code FLACS has been used to simulate the experiments and the general trends seen in experiments are also seen in simulations. However FLACS tend to under predict peak pressure due to over prediction of laminar burning velocity in primary chamber. This effect is expected to be less important in larger-scale situations.

Table of Content

CHAPTER 6

Introduction

1.1. Background

Explosions of gaseous flammable mixtures in linked vessels, is recognized as a major source of risk. Vessels connected with tubing are common in process industry, but the concept of connected vessels is also applicable in many other situations. A particular version of such a vessel configuration, or geometry, can be represented as two or several interconnected boxes much like the rooms in a building. A comparable but more complex situation may occur inside electrical casings where numerous wires, circuits and other components efficiently restrict the flow of gas. Explosions within such vessels is strongly affected by the characteristics of the geometry and can, under given conditions, result in very high local peak pressure and rates of pressure rise. In these situations peak pressure and rate of pressure rise can be several factors higher than in comparable explosions in single vessels. For this to occur a number of requirements must be fulfilled, - which of one is that the geometry is able, at least partially, to withstand the initial rise in pressure. The term *pressure piling* or *pre-compression* is used to describes explosions that show such characteristic pressure development and high peak pressure. According to Gleim and Marcy (1952), the term pressure piling was first introduced by Beyling (1906) and referred to situations in which one chamber had "*increased pressure ... prior to its ignition"*. This definition is very wide and will in fact apply for most confined explosions. A narrower and perhaps more applicable definition reserves the term for explosions in which "*the peak pressure exceeds that of a closed spherical vessel under otherwise identical conditions"*. The latter definition facilitates the use of a quantitative measure for pressure piling and will be used throughout this text.

1.2. Motivation

Estimating pressure loads from explosions is central in risk assessments. Even in simple situations prediction of an explosion can be a complex task, and a number of models for estimating pressure loads exist. The developed models varies greatly from the very simple ones that only apply to a limited range of situations, to state of the art CFD-codes (Computational Fluid Dynamic) which solves conservation equations of mass, energy and momentum and account for physical and chemical processes. One of these codes is FLACS (FLame ACceleration Simulator), which has been developed, by CMR and GexCon AS with support from the petroleum industry. In the development of FLACS a vast number of experiments has been carried out in order to provide empirical input data as well as for verification purposes. Much of this work has been oriented toward prediction of large-scale explosion in petroleum industry and the more commercial important hydrocarbon gases have received most attention. Consequently there is both less experience with other gases and less confidence on how well FLACS work with other gases.

Besides the prospects of hydrogen becoming an important energy carrier in the future, the interest in hydrogen is also based on its distinct characteristics that set it apart from the common hydrocarbon gases. The mass of the small H_2 molecule is about 1/8 of the lightest natural gas component, methane. The laminar burning velocity for hydrogen is about six times greater than natural petroleum components (Alkenes and alkynes is not natural constituents in petroleum). Hydrogen's small size, low mass and reactivity affect properties such as diffusivity, viscosity and it's ability to detonate etc. Table 1.1 list some characteristics for several common gases.

Tests conducted in the laboratories at GexCon have revealed situations where extraordinary high pressures occur. These situations have been related to specific mixtures of more reactive gases such as hydrogen and acetylene, and have introduced some uncertainty on how these gases behave with regard to pressure piling. In general these incidents have been related explosion proof casings for electronic components, and is characterized as a single closed vessels with a highly congested interior.

The main objective of this thesis was to investigate pressure piling with hydrogen as fuel gas and to see whether this diverges from that of natural gases, here represented by methane. Experiments were conducted in interconnected closed vessels and vessel-volume, size of connection (orifice) and gas mixture was expected to be important variables. The aim for these

experiments was to provide a basis for comparing the behavior of the different gasses. Experiments were subsequently simulated with FLACS and special focus was given to situations where differences between experiments and simulations were expected to occur.

	H_2	CH_4	C_3H_8	C_2H_4	C_2H_2
Molecular mass	2.02	16.04	44.10	28.05	26.04
Stoichiometric concentration [%fuel]	29.6	9.5	4.0	6.5	7.7
Flammability range[1] [% fuel]	4.0-75	5.0-15.0	2.1-9.5	2.7-36	2.5-100
Maximum explosion pressure [bar]	8.01	8.75	9.28	9.33	9.71
Adiabatic flame temperature constant V [°C]	2755	2591	2633	2735	2918
Laminar burning velocity [2] [m/s]	3,25	0,45	0,43	0,75	1,55
CJ-detonation velocity [3] [m/s]	1968	1802	1804	1822	
Detonation cell size[4] [mm]	10,5	300	50	12	4

Table 1.1 *Some selected characteristics for hydrogen, methane, propane, ethylene and acetylene. Values was found by using the combustion calculator GasEq* or from following sources: [1] (Kutcha 1985), [2](Baker, Cox et al. 1983), [3](Sheperd, Melhem et al. 1991)*

1.3. Basic introduction: pressure piling

To gain insight to the process of pressure piling in a closed vessel one should begin with taking a look at the combustion process in a single chamber vessel. When combustion is initiated inside a closed vessel, a finite amount of energy is released and the system will at any time be defined by the equation of state.

$$pV = nRT \tag{1.1}$$

Assuming adiabatic conditions, a theoretical absolute max value can be calculated and explosion pressures for different chemical substances can be given specific values as shown in Table 1.1 . The values given can be regarded as a maximum attainable pressure for stoichiometric mixture and is close to what could be achieved with a centric ignition in a spherical bomb. Slightly rich mixtures will often produce higher pressure than stoichiometric mixtures, as the as a small excess of fuel will push the equilibrium towards higher yield of products.

**GasEq is a combustion calculator in which calculation are made on the basis of thermal equilibrium and minimization of free energy. For more information se web page listed in the reference list.*

In closed vessel combustion wave propagation is attended by a rise in pressure and mass flow which is first directed away from and later toward the point of ignition. This effect complicates the process of flame propagation and a thorough analysis has been made by Lewis and von Elbe (1987). As the flame travels outward from the ignition point, the temperature and pressure rises in the unburned gas in accordance with the law of adiabatic compression. The increased kinetic energy reduces the energy needed to initiate reaction in the unburnt gas and thereby enhances burning velocity.

As the flame travels outward from the point of ignition, the rate of combustion increases rapidly because of the increased flame area, the increased burning velocity and a relatively higher energy content in the unburnt gas caused by compression. Experiments have shown that in an oblong cylinder (length / radius ≈ 2,5) pressure rise was about 1% when the flame was halfway to the cylinder wall (Beyer 1997). In other words; the major part of pressure rise takes place in the latter part of the combustion process.

As noted earlier, the temperature and pressure of the unburned gas will rise in accordance with the law of adiabatic compression. This will cause a temperature gradient to be set up between the gas burned first and the gas burned last. In the initial phase the gas burns and expand at practically constant pressure and is subsequently compressed almost to its original volume as the last part of gas is consumed. The latter work of compression exceeds that of the former work of expansion since the compression of the gas at the point of ignition takes place at a steadily increasing pressure whereas the expansion took place at the lowest pressure. An analogue argument will also apply for gas burning last which is compressed at steadily increasing pressure up till approximately final pressure and then subsequently expand at high pressure. Consequently the gas burning last lose some of its energy while the gas burning first gains energy in excess of the chemical energy bound within it. This results in a radial temperature gradient in the burned gas, which can amount to as much as 900 K (Jost 1946). Figure 1.1 show how pressure, burning velocity and temperatures vary with chamber radius on an ozone explosion.

Toward the last stage of the combustion process there will be significant gas movement. As the flame propagates trough the last centimeter of compressed gas (from 9b to 10b), the gas will expand to a layer of 3.3-centimeter in thickness at a very short time. An element of gas located at 9b may in this process reach a speed of 14m/s due to the very rapid gas expansion, and elements closer to the wall may achieve even higher velocity (Lewis and von Elbe 1987). However heat loss will become significant in this latter phase when the flame meets the wall and may reduce these effects.

Figure 1.1 also shows how pressure relates to flame position: When the pressure has reached half of its maximum value, the flame front has covered a distance of about 93% (14/15) of the vessel radius.

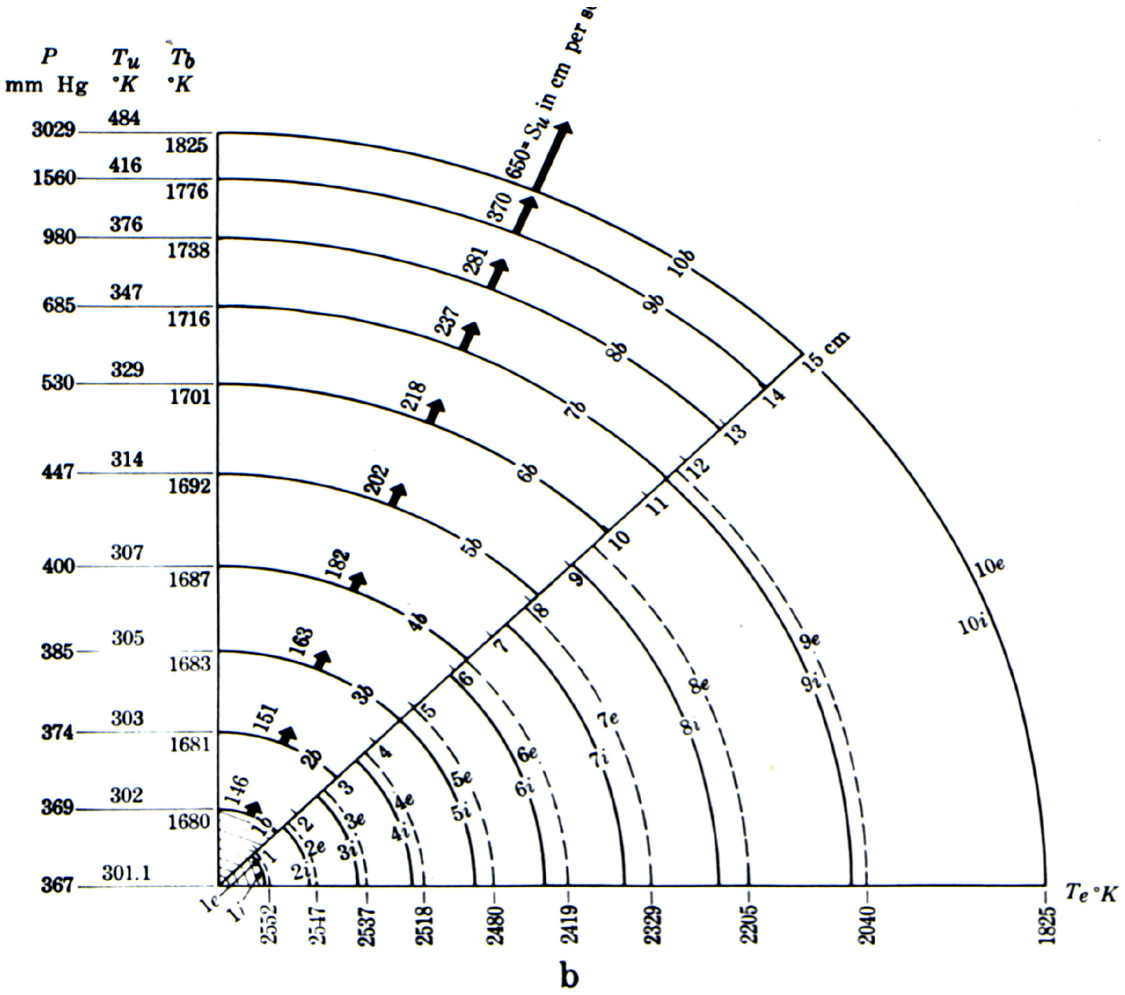

Figure 1.1 *Pressure, Temperature and burning velocity as function of vessel radius for an ozone explosion in a spherical vessel. Subscripts: unburnt (u), burnt (b), initial (i), end (e)(Lewis and von Elbe, 1987).*

The general process described above will be comparable to what will happen in the primary chamber in a double compartment vessel. However, depending on orifice size gas will flow into the secondary chamber and the values given in Figure 1.1 will be reduced. The flame front will no longer be a circular sphere but deform toward the orifice.

In a cylindrical or cubical vessel the flame movement will no longer be strictly radial as gas is pushed toward the corners and resulting in a tangential movement of gas particles. Depending on geometric characteristics, the gas mixture might be agitated and give increased combustion

rate. In the vicinity of the orifice the gas movement is obviously much higher, and as the flame front approaches the orifice it will accelerate and at a certain distance tend to make a sudden transfer into the secondary chamber.

Singh (1984, 1993) has proposed a simple empirical relation for this "*effective entrance", Z,* as a function of orifice diameter, d_c.

$$Z = d_c^{1.8} \tag{1.2}$$

Although this must be assumed to be a very geometry dependent parameter and a poor representation of the actual flow characteristics, it shows that time of flame transfer into the second chamber is dependent on orifice diameter.

When the flame eventually reaches the secondary chamber it will encounter a compressed turbulent mixture. Time between ignition and flame arrival in the secondary chamber, flow through the orifice and volume of the two chambers will decide what pre-ignition pressure will be at this time. As the jet shoot into the secondary chamber, a simultaneous ignition of a large area occurs. The high turbulence level will efficiently distribute radical spices and heat, resulting in a very fast combustion process. Depending on combustion rate and the orifices ability to vent this secondary explosion, very high pressures can occur. Figure 1.2 show a typical pressure curves for a pressure-piling situation.

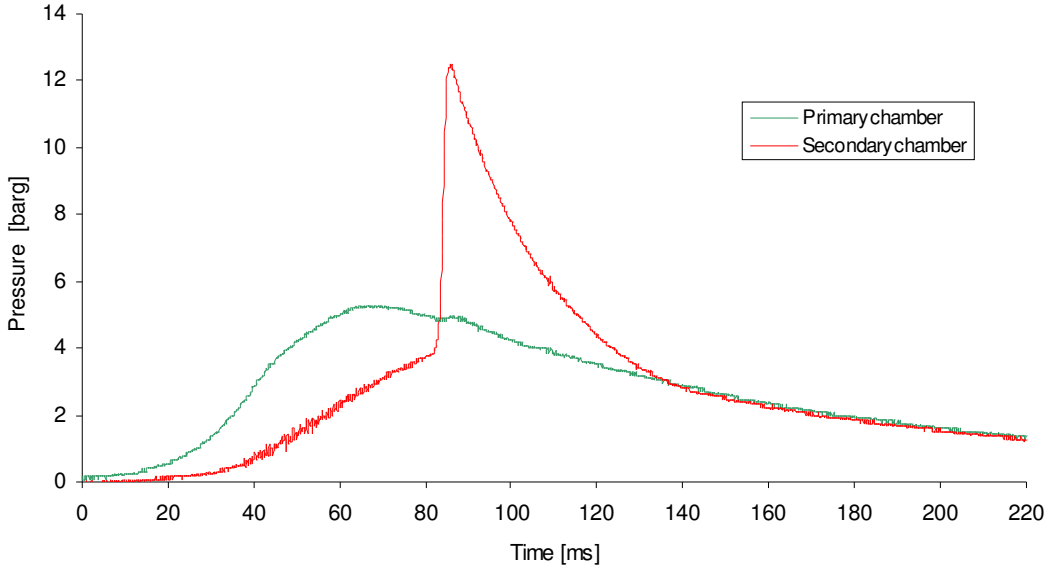

Figure 1.2 *Typical pressure curves from a pressure piling situation. Pressure in the secondary chamber (red) raises steadily until the flame arrives and a very fast combustion occur. At the point where the curves intersect flow direction trough the opening is reversed.*

The process outlined above is very complex an depend on a number of factors:

- Chemical substance
- Laminar and turbulent burning velocity
- Temperature
- Gas composition
- Geometry

In pressure piling situations the geometry is of paramount importance and minor details may be of great significance. The underlying reason for this is that the geometrical shape has a decisive role in restricting flow and generating turbulence which greatly affects the combustion process. Some important geometrical factors are:

- Volume ratio between vessels
- Cross-sectional area of connection
- Scale
- Shape of vessel
- Point of ignition

CHAPTER 2

Previous work

Pressure piling in compartmented vessels was first recognized as a special explosion hazard by Beyling (Grice and Wheeler 1929; Gleim and Marcy 1952). The effect was solely attributed to the pre-compression of the secondary chamber and consequently labeled "*pressure pili*ng".

The work of Beyling was followed up by Grice and Wheeler (1929) who gave the subject a thorough treatment and concluded that the effect was caused by three separate factors:
"Compression of the mixture before ignition"
"Turbulence of the mixture, owing to the rapid inrush of gases..."
"Ignition by a large flame projected through the communicating passage"

A more comprehensive study was made by Gleim and Marcy (1952) who investigated the role of various volume ratios and ignition locations. Their experiments showed higher peak pressures as volume ratio increased ($V_{primary}/V_{secondary}$) and that ignition point was a very important factor in pressure piling. As distance between ignition and the secondary chamber grew larger the more pronounced was the effect of pressure piling.

A significant contribution was also given by Brown (1959) who based on his experiments, concluded that "*the extent of pressure piling…. is independent of the length of the connecting tube*". This can easily be understood since the pressure in the primary chamber is the "driving force" of flame transfer into the second chamber: At the time of flame arrival in the second chamber the pressure will be about the same as when the flame entered the tube. Brown also realized that the cross sectional size was a very important factor and as tube diameter declined, peak pressures got much higher.

In his book on explosions Bartknecht (1981) reports of experiments conducted in double-compartmented vessels. For the ignition compartment, he noted that even the rate of pressure rise in the primary vessel was greatly enchanted when it was connected to a second chamber. Rate of pressure rise was in fact 4 times as high as those found in a single vessel, but without any elevation of max pressure. For the secondary chamber, rate of pressure rise was up to 10 times higher than in single vessel explosions, and max pressure was increased by 10%. The volume ratio in these experiments was only 1:1, and the elevated rate of pressure rise was attributed to jet ignition and turbulence. Bartknecht also reported of large-scale ($6m^3$) experiments with volume ratios of 5:1, in which max pressures increased with a factor of two. In these experiments it was noted that the gas concentration giving the most pronounced effect varied with transfer opening and ignition location. On the basis of experimental tests, Bartknecht concluded that excessive pressure increase would only occur if the ratio between cross-sectional area of transfer opening and vessel volume was less than 0.4 and more than 0.002.

A simple model for pressure piling situations has been presented by Abdullin et al. (1988). In their approach, Abdullin et al.focused on the interaction of two basic factors: combustion rate and the outflow chemically bound energy.

$$B = \frac{Energy\ liberated\ \ in\ combustion}{Energy\ transfered\ \ through\ outflow} \tag{2.1}$$

Based on their simulations the ratio of these two factors (B) was used to define three different regimes.

- For fast combustion ($B>>1$) the general pressure piling process is limited by outflow from the primary chamber. In this situation combustion proceeds as in a single vessels, but with successive transfer of the chemical reaction at the open boundary of the system.
- In the intermediate regime ($B=1$), the “release” of thermal energy by outflow is comparable to the release of thermal energy as heat (combustion) and the interaction effects are strongest: accumulation of gas in secondary vessel, maximum velocity of turbulent combustion, anomalously high pressures etc.
- In the regime of slow combustion ($B<< 1$) all characteristics are determined by the combustion process itself, proceeding as in isolated vessel.

Although the presented model gives some insight in the pressure piling process, it only handles central ignition and have a highly questionable model for turbulent combustion. Hence, its practical relevance is very limited. Abdullin et al. also argued that the pressure piling effect would be more pronounced as vessel sizes got smaller. This was attributed to the relatively higher turbulence intensity expected in the smaller vessels.

Phylaktou and Andrews (1993) used a double compartment vessel and made a thorough investigation of burning velocities and flame movement in different stages of the process. Explosion violence or the rate of pressure rise is strongly related to burning velocity, which in turn is linked to the degree of turbulence. The measurements of burning velocities showed a dramatic increase as the flame propagated into the tube connecting the two vessels. Maximum burning velocity in the tube and the secondary vessel was found to be 370m/s and maximum rate of pressure rise was 2068 bar/s. The fuel used was methane. As the rapid combustion took place in the secondary chamber, pressure surpassed that of the premier chamber and hence flow was reversed. This induced turbulence and combustion rate was then greatly enhanced in the premier chamber as well. This induced yet another change in direction of flow, and a strong, low frequency oscillation was set up in the system. In fact, both compartments showed similar explosion violence. The experimental setup used by Phylaktou and Andrews had a fixed volume ratio of 1:1 and in the strict sense no actual pressure piling occurred. However their work is definitely relevant to pressure piling situations and gives insight to the role of turbulence and flame propagation.

Pressure piling has been thoroughly studied by (Singh 1984; Singh 1993) who investigated several parameters important to pressure piling on the same system in order to assess their relative importance and interrelatedness. Singh studied the role of ignition location, volume ratio and size of transfer opening. Experiments where conducted with a pair of cylindrical chambers connected by small tube in which the diameter could be altered. Experiments were done with volume ratio ranging from 2 till 32, and connecting tube diameter ranging from 12-51mm.

Generally, Singh confirmed much of the earlier findings but was also able to give more precise description of the general trends (effect of ignition point, volume ratio, orifice size)
From experiments of similar setups but different scale, he concluded that max pressure and rate of pressure rise was more pronounced in larger scale setups. Although the conclusion may be

right, the basis for it seems somewhat questionable since Singh did not change the size of the transfer opening. In the smallest setup the hole would therefore be relatively larger and hence result in a more efficient back venting of the secondary explosion.

In his work, Singh presented an approximate model for predicting the peak pressure in the secondary chamber. The model uses empirical parameters to predict pre-ignition pressure in the secondary chamber. It is rather dependent on idealized assumptions to predict flame arrival in second chamber and must be expected to be quite geometry sensitive.

In 1996 Lunn, Holbrow et al. published a report on dust explosions with coal in enclosed interconnected vessels. The experimental setup consisted of several vessels with sizes ranging between $2m^2$ and 20 m^2 connected with 5m tubes of various diameters (15, 25, 50cm). The investigation was mainly focused on volume ratios and diameter of transfer opening. The authors confirmed much of earlier findings and noted that no pressure piling occurred for volume ratios less than ¼. The authors also presented a simple calculation giving a theoretical limit of the maximum attainable peak pressures based on volume ratios (Figure 2.1). Experiments conducted in smaller-scale setup showed higher peak pressures and higher rate of pressure rise, than a similar setup ten times the size. Lunn et al. (1996) stated that for a given tube diameter, pressure piling effects are less pronounced in large-scale situations. Although Singh made the opposite conclusion in his experiments, both conclusions may hold true as there was a considerable difference in scale between the two setups. This would, however, imply that there is something like an optimal size for generating high peak pressures.

Possible combustion of lean hydrogen –air mixtures is a major concern in nuclear reactor industry especially because of the compartmented structures involved. In general these investigations are concerned with mixtures of low hydrogen content (8-14%). Kanzleiter and Ficher (1994) conducted a series of test on lean hydrogen deflagration in large-scale multi-compartmented geometries. Their setup consisted of several interconnected volumes ranging from 41 to $480m^3$. After ignition in the primary chamber, the flame propagated trough a narrow connection to the secondary chamber where very high rates of pressure rise were registered.

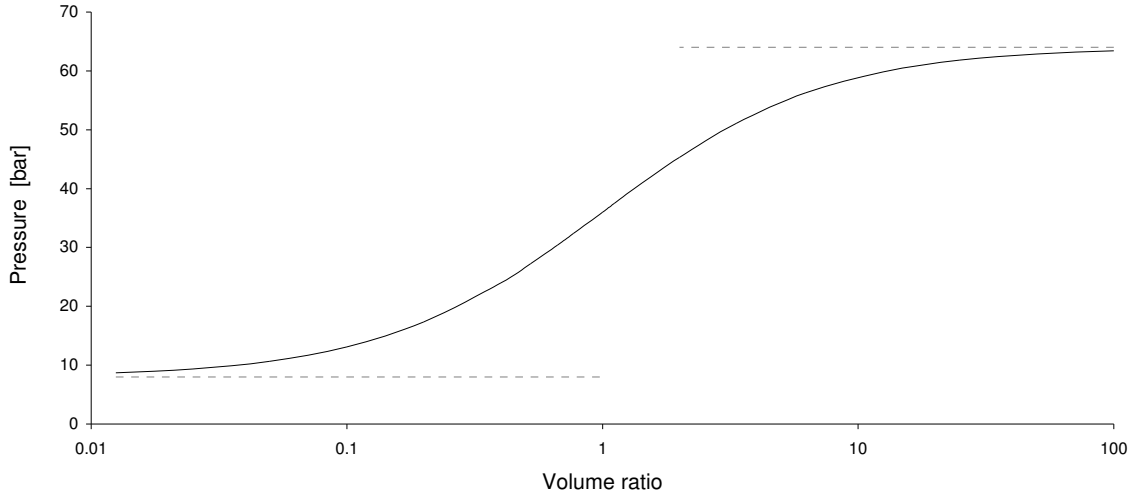

Figure 2.1 *Theoretical max pressures as a function of volume ratio. Based on complete pressure equilibrium between the two chambers prior to secondary ignition and neglible venting. (Reproduced from Lunn et al. (1996) with modifications).*

This secondary chamber also had a small connection to a tertiary camber, which in turn was connected to yet another compartment and so on. This setup is not directly analogue to the twin vessel setup, as the pressure buildup in vessel number two was vented into a third. Even though peak pressures did not qualify to be labeled pressure piling in the strict sense, the experiments had many similarities with the typical pressure-piling situation. Although somewhat unclear it also appears that ignition of the third chamber did not result in especially high pressures or rate of pressure rise. This can probably be attributed to the fast pressure rise in the second chamber which would be to fast for significant amount of gas to be transferred to the third in which no pre-compression would occur. In other words: the prospect of a pressure-piling situation repeating it self therefore seems rather unlikely. Kanzleiter's and Ficher's work also showed that the shape of the secondary compartment and the way the jet was directed into it greatly influenced the explosion violence or rate of pressure rise.

Liu and Yoshizawa (1998) conducted a series of tests with lean hydrogen mixtures in a setup similar to the one that will be used in this thesis. Their setup consisted of two interconnected vessels of 2.8 and 20.6 liters with windows that allowed for high-speed video camera and Schlieren visualization. The transfer openings ranged from 15 to 40mm. However in their experiments ignition was initiated in the smaller vessel in order to study the combustion mechanism and jet ignition. For the smallest holes, Liu et al. stated that "*because of the strong throttle effect and cooling effects, the deformed flame tip could not pass directly trough the vent,*

but became a jet of hot gasses containing a flame kernel". By the use of thermocouple wire and pressure-time history, the flow speed in the orifice was assessed and showed an approximate linear relation to the combustion rate in the secondary chamber. As transfer connection got smaller, eventually ignition was altered. Small transfer connection caused extinction of the flame and instead hot combustion products caused a delayed ignition in the secondary chamber.

With the aim to improve engine design the divided chamber bomb has frequently been used to study combustion mechanisms. The concept of the bomb, with a small ignition chamber connected to the piston cylinder, has in fact been proposed as a mean to improve engine performance. Related work conducted (Yamaguchi, Ohiwana et al. 1985) investigated the ignition characteristics in divided chamber bomb by measuring ion current, light emission, OH emission and schlieren technique. Nozzle diameter was shown to seriously affect the mechanism for secondary ignition. For nozzle diameters of about 6mm and smaller the flame jet shooting into the secondary chamber was dominated by steady stream of radical species. For higher nozzle diameters the jet contained small flame kernels and for nozzle diameter above 14 mm it was more or less intact flame that arrived in the secondary chamber. Experiments showed that the reaction mechanism was significantly affected in the orifice flow, and according to Yamaguchi, cooling caused this.

Maremonti, et al. (1999) investigated the ability of a CFD code (AutoReaGas) to model gas explosions in linked vessels. Basis for their simulation was the experiments conducted by Phylaktou et al (1993), but as previously noted the volume ratio in these tests was 1:1 and no actual pressure piling occurred. However, the code was able to take into account the effect of different ignition location (central and end ignition). The agreement between measured and calculated data was good with regard to the peak pressure but less accurate for the rate of pressure rate and flame speed. The computed values of the turbulence intensity in both chambers demonstrated that turbulence induced in the secondary vessel is a major factor affecting explosion violence. This parameter was strongly affected by the diameter of the connecting pipe. However, no quantitative comparison to experimental values was done for this parameter.

CHAPTER 3

Theory

The typical pressure-piling situation is characterized by great complexity, and insight to the phenomena necessitates a fundamental appreciation of the physical mechanisms involved. This chapter gives a brief presentation of selected theory and information on chemical aspects. The aim of this chapter is to indicate how fundamental fuel properties may affects various aspects of combustion in interconnected vessels.

3.1 Reaction chemistry

The experimental work in this thesis has been made with two types of fuel: hydrogen and methane, and the respective net reactions are given below.

$$2H_2 + O_2 \leftrightarrow 2H_2O \qquad \Delta H = -241.82\ kJmol^{-1}$$

$$CH_4 + 2O_2 \leftrightarrow CO_2 + 2H_2O \qquad \Delta H = -802.34\ kJmol^{-1}$$

The reaction mechanisms is much more complex than indicated by the equations above. A complete description of the reaction mechanism for the hydrogen-oxygen mixture uses 8 chemical spices and 19 elementary reactions as is shown in Table 3.1 (Warnatz, Maas et al. 2001). The two first reactions in Table 3.1 have special importance as these are the chain branching steeps in which one reactive species reacts with a stable species and create two reactive species. Besides the release of heat, the chemical production and termination of spices like H, OH and O (radicals) are of great importance as these are the spices responsible for carrying the chemical process through.

	Reaction						A [cm·mol·s]	b	E [Kj/mol]
1	O_2	+ H		↔	OH	+ O	$2.00 \cdot 10^{14}$	0.0	70.3
2	H_2	+ O		↔	OH	+ H	$5.06 \cdot 10^{04}$	2.67	26.3
3	H_2	+ OH		↔	H_2O	+ H	$1.00 \cdot 10^{08}$	1.6	13.8
4	OH	+ OH		↔	H_2O	+ O	$1.50 \cdot 10^{09}$	1.14	0.42
5	H	+ H	+ M*	↔	H_2	+ M*	$1.80 \cdot 10^{18}$	-1.0	0.00
6	O	+ O	+ M*	↔	O_2	+ M*	$2.90 \cdot 10^{17}$	-1.0	0.00
7	H	+ OH	+ M*	↔	H_2O	+ M*	$2.20 \cdot 10^{22}$	-2.0	0.00
8	H	+ O_2	+ M*	↔	HO_2	+ M*	$2.30 \cdot 10^{18}$	-0.8	0.00
9	HO_2	+ H		↔	OH	+ OH	$1.50 \cdot 10^{14}$	0.0	4.20
10	HO_2	+ H		↔	H_2	+ O_2	$2.50 \cdot 10^{13}$	0.0	2.90
11	HO_2	+ H		↔	H_2O	+ O	$3.00 \cdot 10^{13}$	0.0	7.20
12	HO_2	+ O		↔	OH	+ O_2	$1.80 \cdot 10^{13}$	0.0	-1.70
13	HO_2	+ OH		↔	H_2O	+ O_2	$6.00 \cdot 10^{13}$	0.0	0.00
14	HO_2	+ HO_2		↔	H_2O_2	+ O_2	$2.50 \cdot 10^{11}$	0.0	-5.20
15	OH	+ OH	+ M*	↔	H_2O_2	+ M*	$3.25 \cdot 10^{22}$	-2.0	0.00
16	H_2O_2	+ H		↔	H_2	+ HO_2	$1.70 \cdot 10^{12}$	0.0	15.7
17	H_2O_2	+ H		↔	H_2O	+ OH	$1.00 \cdot 10^{13}$	0.0	15.0
18	H_2O_2	+ O		↔	OH	+ HO_2	$2.80 \cdot 10^{13}$	0.0	26.8
19	H_2O_2	+ OH		↔	H_2O	+ HO_2	$5.40 \cdot 10^{12}$	0.0	4.20

Table 3.1 *Elementary reactions in the H_2 -O_2 system for P=1 bar and T>120 (Warnatz, Maas et al. 2001).*

Characteristic for chemical reactions is that their rate coefficients, k, depend strongly and nonlinearly on temperature. According to the modified Arrhenius law this temperature dependenc is given by:

$$k = AT^b \cdot \exp\left(-\frac{E_a}{RT}\right) \qquad (3.1)$$

Where A is a pre-exponential factor and E_a is the activation energy. T^b denotes the temperature dependence of the pre-exponential factor. These reaction rates are however not independent of their surrounding environment and in a complex mixture significant limitations of reaction kinetics may occur. Changes in pressure are known to greatly affect reaction mechanism and is a key factor in such peculiar phenomena as cool flames in hydrocarbon mixtures. Similar effects may also explain the atypical behavior of methane-air mixtures reported by Strauss and Edse (1958). High-pressure experiments (90bar) showed that the stoichiometric mixture had significantly lower burning velocity than both lean and rich mixtures. Under normal conditions the effect of pressure is much smaller but not necessarily immaterial.

In general elementary reactions, as those in Table 3.1, have their own reaction rates and respond differently to chemical and physical changes. Within a given reaction regime there is usually a set of rate limiting steeps, and as combustion proceeds the relative importance of different steps varies. As the temperature exceeds 1200K the reaction pattern becomes increasingly simpler and less fuel dependent. At this temperature, reaction number 1 in Table 3.1 is the most important in both hydrogen and hydrocarbon oxidation (Warnatz, Maas et al. 2001). When temperatures drops below 1000K molecular size and structure becomes increasingly important and reaction pattern for various hydrocarbon have less similarities (Griffiths and Barnard 1995). For lower temperatures combustion of methane spices like CH_3 and CH is especially important (Glassman 1987).

The presence of "inert species" for example nitrogen or solid surfaces pose further complications. They are generally not recognized to participate in the reaction, but may have a catalyzing role in some reactions and may affect the process as heat sinks or alter diffusivity. The replacement of nitrogen with helium in a methane-air mixture will for instance triples the burning velocity (Glassman 1987).

3.2 Diffusivity

Burning velocity is the velocity of which a flame propagates into a quiescent gas mixture and a simple expression for this quantity can be deducted from the analysis of Zeldovich and Frank-Kamenetskii (1938):

$$S_L = \sqrt{\alpha k} \tag{3.2}$$

where α denotes diffusivity (molecular diffusivity and thermal diffusivity are set equal in this model). Although equation 3.2 depends on a number of simplifications, it illustrates the basic idea of flame propagation as a diffusive processes and that the necessary gradients are sustained by the chemical reaction. The assumption of equality between molecular and thermal diffusivity are quite often invalid and for some hydrogen air mixtures the ratio of the two properties is far from unity.

Conduction of heat is described by Fourier's Law :

$$\frac{\partial q}{\partial t} = -\lambda A \frac{\partial T}{\partial x} \tag{3.3}$$

Where $\partial q/\partial t$ is the rate of heat flow trough an area A and $\partial T/\partial x$ is the temperature gradient in the direction of heat flow. λ is the thermal conductivity and is exactly defined by kinetic theory as a function of viscosity and constant volume heat capacity.

$$\lambda = \frac{5}{2}\mu c_v \tag{3.4}$$

However, the equation only applies for a monatomic ideal gas and since deriving an expression for multicomponent mixtures from kinetic theory would be of insurmountable complexity, empirical values are used. Thermal conductivity for pure hydrogen and pure methane is 0.186 $Wcm^{-1}K^{-1}$ and 0.00346 $Wcm^{-1}K^{-1}$ respectively (Perkins). Thermal diffusivity, α, is given by the thermal conductivity, density and heat capacity:

$$\alpha = \frac{\lambda}{\rho C_p} \tag{3.5}$$

Molecular diffusion flux for a component, A, is described by Fick's Law as function of the concentration gradient $\partial c_A/\partial t$ and molecular diffusivity D_{AB}

$$J_A = -D_{AB}\frac{\partial c_A}{\partial b} \tag{3.6}$$

The Chapman–Enskog equation gives the molecular diffusivity of component A into component B.

$$D_{AB} = 1.8583 \cdot 10^{-7} \cdot \frac{\sqrt{T^3\left(\frac{1}{M_A}+\frac{1}{M_B}\right)}}{p\sigma_{AB}^2\Omega_{D,AB}} \tag{3.7}$$

Where:

M_A - Molar mass of component A

M_B - Molar mass of component B

σ_{AB} - average collision diameter

$\Omega_{D,AB}$ - collision integral based on Lennard-Jones potential and can be represented as a measure on deviation from rigid sphere behavior

Equation 3.7 only applies for binary mixtures but displays how diffusivity depends on some of the basic properties of a mixture. The average collision diameter (molecular size) for hydrogen and methane is 2.9Å and 3.8Å respectively (Hirschfelder, Curtiss et al. 1954). Experimental values for diffusivity of hydrogen and methane in air is $6.1 \cdot 10^{-5}$ m^2/s and $1.9 \cdot 10^{-5}$ m^2/s respectively (concentration not known) (McCabe, Smith et al. 1993).

Determining diffusivity is greatly complicated by the fact that diffusivity depends not only on the diffusing component, but also on the mixture it diffuses into. The problem is usually approached from a different angle. Equations for multicomponent diffusion can be derived from diffusion velocities and conservation of momentum as described by (Williams 1985).

The thermal gradient generated in the reaction zone may also result in thermal diffusion, which can be defined as a diffusion of mass driven by thermal gradientis. In this process light molecules tends to be drawn towards hot regions while heavy molecules are "left behind" (Soret effect). The effect is usually neglected in combustion although it has been argued that hydrogen will be relatively strongly influenced by thermal diffusion (Williams1985, (Williams 1985)Mosbacher, Wehrmeyer et al. 2000)(note the distinction between thermal diffusivity and thermal diffusion).

Lewis number, *Le*, is the ratio of heat and mass diffusion and is used for characterising fuel mixtures.

$$Le = \frac{\alpha}{D} \tag{3.8}$$

Low Lewis number means that heat diffuses more slowly than molecules and that the latter has relative stronger influence on combustion. The inherent difficulties of assessing both thermal conductivity and molecular diffusivity obviously apply for Lewis numbers as well. The matter is further complicated by the fact that it is the diffusion of highly transient radicals that have most bearing on flame propagation. Nevertheless Lewis number is often used as a parameter in equations for laminar burning velocity (Lipatnikov and Chomiak 2002) and, as will be noted later, the Lewis number has been shown to be important for quenching in turbulent combustion.

3.3 Laminar flames

Reaction rate, thermal and molecular diffusivity are fundamentally tied to the subject of flame propagation as shown in equation (3.2). A scheme of the reaction zone showing characteristic gradients of temperature and concentrations is given in Figure 3.1.

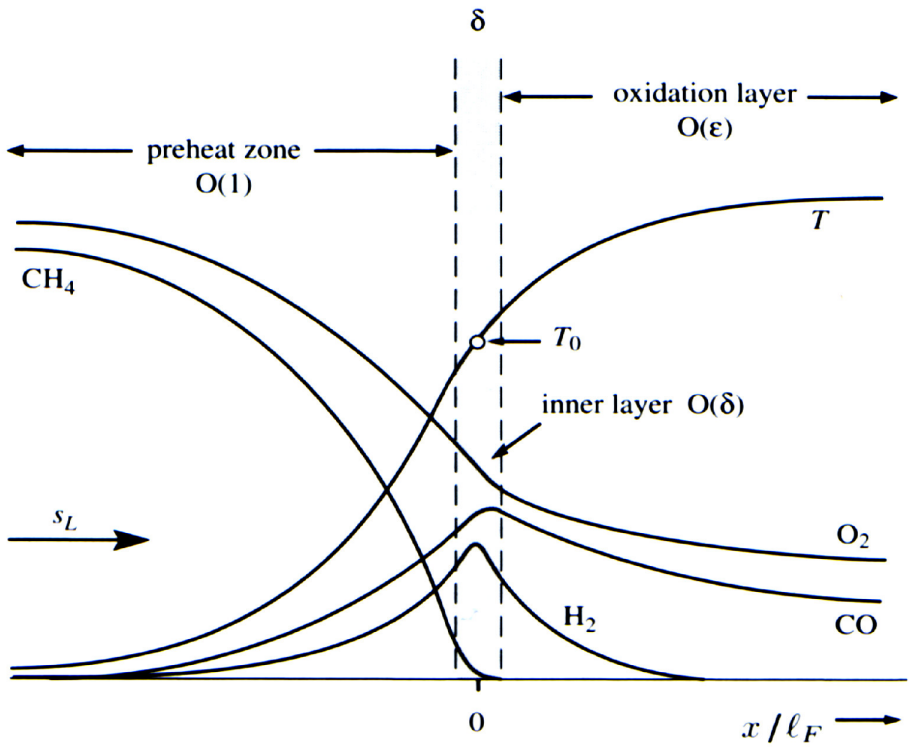

Figure 3.1 *Schematic illustration of the reaction zone for a methane-air mixture. The fuel consumption zone denoted δ is where the fuel is consumed and the radicals are depleted by chain breaking reactions. (Illustration from Peters 2000)*

There are three main branches of theories used for the description of flame propagation: thermal theory, the comprehensive theory and the diffusion theory. As the name indicates different emphasis is placed on the diffusive characteristics. The comprehensive theory, which is derived from the species conservation and energy equations, rank as the better of three and is more able to explain trends in flame propagation speeds. The expression for laminar burning velocity, S_L, for a first order reaction is given as:

$$S_L \sqrt{\frac{2\lambda_f C_{pf} A}{\rho_0 \overline{C_p^2}} \left(\frac{T_0}{T_f}\right)\left(\frac{n_r}{n_p}\right)(Le)\left(\frac{R_u T_f^2}{E_a}\right)^2 \left(\frac{e^{-E_a/R_u T_f}}{\left(T_f - T_0\right)^2}\right)} \tag{3.9}$$

However, the inherent difficulties in assessing diffusive properties and reaction rates reduce the usefulness of these models, and one is left to depend on experimental values for burning velocities. Figure 3.2 shows some experimental data for the burning velocity of hydrogen mixtures and indicates the uncertainty involved.

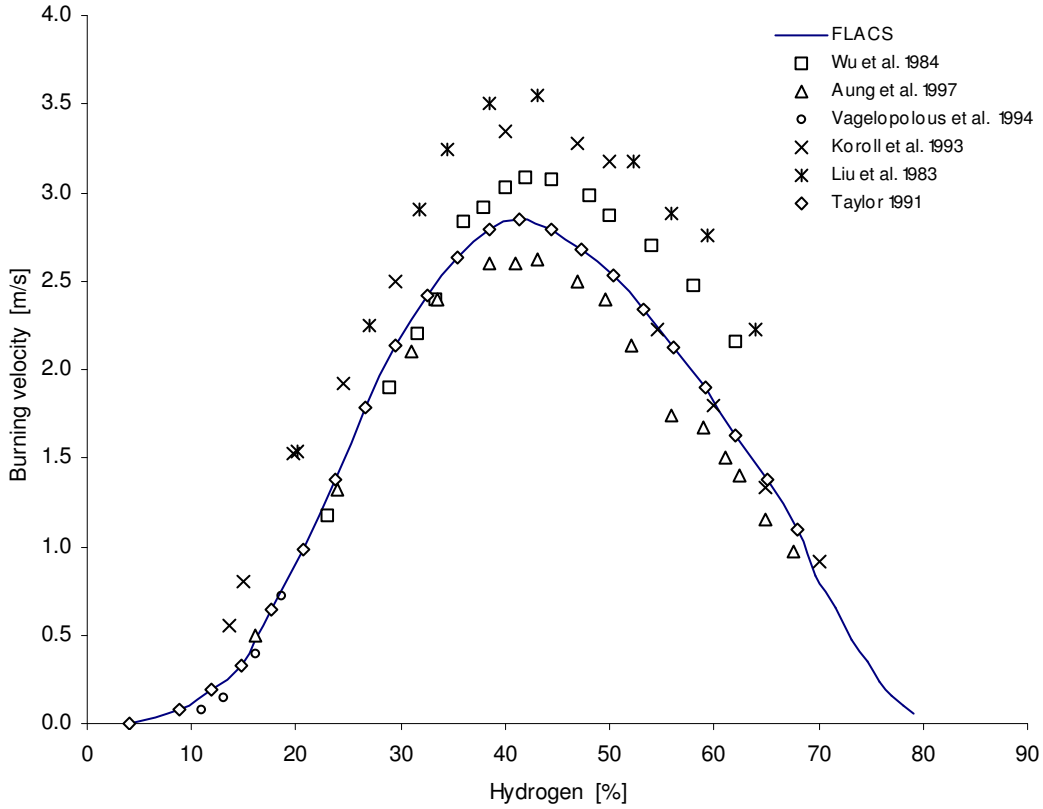

Figure 3.2 *Experimentally determined burning velocities for hydrogen/air mixtures.*

Several methods can be used to determine burning velocity from experimental pressure data and for combustion in a closed spherical vessel the following equation can be used (Skjold 2003, Dahoe 1996):

$$S_{L,ip} = \frac{1}{3p_m}\left(\frac{dp}{dt}\right)_m V_v^{1/3}\left(\frac{3}{4\pi}\right)^{1/3}\left(1+\frac{p_{ip}}{1[bar]}\right)^{-1/\kappa}\left\{1-\left(1-\frac{p_{ip}}{p_m}\right)\cdot\left(1+\frac{p_{ip}}{1[bar]}\right)^{-1/\kappa}\right\}^{-2/3} \qquad (3.10)$$

Where:

Subscript ip denotes the inflection point on the pressure curve (dt^2/d^2p)

p_m denotes measured pressure

V_v denotes vessel volume

κ denotes specific heat ratio (c_p/c_v)

Equation 3.10 is based on a few idealized assumptions (ideal gas behaviour, thin flame, fast reaction, no flame wrinkling) and only applies for central ignition.

As already indicated the burning velocity will be significantly affected by changes in temperature and to a lesser extent by changes in pressure. The increase in kinetic energy as a result of higher temperature reduces the energy needed to initiate reaction in the unburned gas and thereby enhance burning velocity. Although generally surpassed by the effect of increased temperature, elevation of pressure has the opposite effect. Laminar burning velocity, S_L, as function of T and P can be expressed by:

$$S_L = S_{L0}\left(\frac{T_R}{T_0}\right)^{\alpha}\left(\frac{p}{p_0}\right)^{\beta} \tag{3.11}$$

Where subscript *0* denotes reference state and T_R is temperature in reactants. Values for α and β are significantly affected by equivalence ratio (Metghalchi and Keck 1980) and, to a lesser degree, pressure (Shebeko, Tsarichenko et al. 1991). Table 3.2 shows some selected values for α and β.

	Methane [1]	Propane [1]	Acetylene [2]	Hydrogen [2]
α	2.0	2.13	2.0	1.26
β	-0.5	-0.17	-0.06	0.26

Table 3.2 *Empirical values for the exponents in equation (3.11) [1] (Metghalchi and Keck 1980) [2] (Milton and Keck 1984) Note how temperature and pressure dependency deviates for hydrogen and hydrocarbons.*

It should be noted that the equation and constants given apply for stoichiometric mixtures. Experiments performed by Strauss and Edse (1958), imply that values for β should be reduced for rich mixtures and increased for lean mixtures. This observation is also in agreement with the theory of diffusional stratification that is prone to occur in stoichiometrically unbalanced mixtures in which the diffusivity of the deficient component exceeds that of the excess component (Lewis 1987). This causes instability in the flame front and may result in a cellular boost of measured burning velocity.

In general, burning velocity S_L is considered to be a direct function of properties of the combustible mixture and depends neither on geometry nor flow. This is not absolutely true for the diverging flame propagation immediately after ignition. The curvature of the flame sphere results in higher diffusive losses, which in turn lowers the temperature in the reaction zone and burning velocity. The effect will rapidly diminish as the flame sphere grows and is often

neglected. Although the effect is small the critical flame diameter (or quenching diameter) indicates that methane mixtures would be relatively more affected than hydrogen. Although flame stretch is of limited importance for laminar flames its gains significant relevance as flames become turbulent.

3.4 Turbulence

Turbulence is not a feature of fluids but of fluid flows and most of the dynamics of turbulence does not depend on fluid characteristics. Although fluid properties as mass and viscosity do affect turbulence such a discussion would be outside the scope of this text.

Turbulent processes occur at different length scales and are useful parameters for characterizing turbulent structure. The largest length scale, l_L, corresponds to the geometrical dimensions of the system. The integral length scale, l_0, is the characteristic length scale of eddies containing most of the kinetic energy and is closely tied to l_L. The Kolmogorov length scale l_η denotes dimensions of the smallest turbulent structures. At the Kolmogorov length the time needed for an eddy to rotate half a revolution is equal to the diffusion time across the diameter l_η, therefore turbulent transport does not extend below l_η. The Kolmogorov length scale is defined as a function of kinematic viscosity, ν, and dissipation rate, ε.

$$l_\eta = \left(\frac{\upsilon^3}{\varepsilon} \right)^{1/4} \tag{3.12}$$

The Taylor micro scale l_λ is the ratio of time scale of large and small eddies and is associated with the dissipation of turbulent energy. k denotes kinetic energy.

$$l_\lambda{}^2 = 10\nu \frac{k}{\varepsilon} \tag{3.13}$$

The distribution of the kinetic energy among the spectrums of eddies with different diameters is described by the turbulent energy spectrum and shown in Figure 3.3. The energy spectrum has its peak at the integral length scale, l_0, and ends at the Kolmogorov length l_η scale.

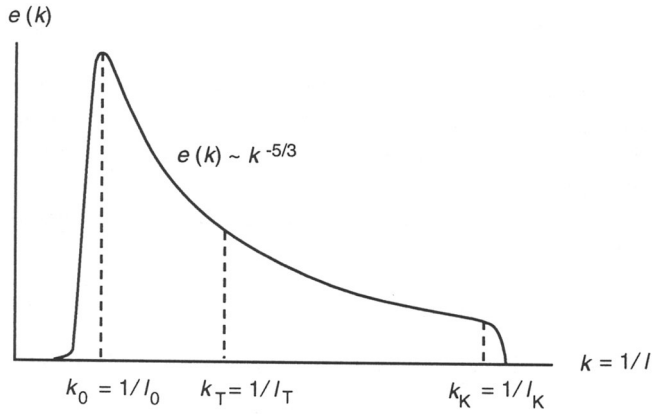

Figure 3.3 *Turbulent energy spectrum showing the energy cascade.*

Turbulent flow results when instabilities in a flow are not sufficiently damped by viscous action and the fluid at each point in the flow exhibits random fluctuations. Reynolds number can be considered as a ratio between a destabilizing momentum and a stabilizing or damping, viscous effect.

$$\mathrm{Re} = \frac{\rho u l}{\mu} \tag{3.14}$$

where u denotes velocity and l is the characteristic length of the system (diameter in tube flow) Together with the Kolmogorov length scale it can be used to define the turbulent Reynolds number, Re_t. Since Re_t is based on properties of the turbulence it is associated more closely with regimes and dynamics of turbulent motion than Re. Re_t is given as:

$$\mathrm{Re}_t = \frac{\overline{\rho}\sqrt{2k}l_0}{\overline{\mu}} = \left(\frac{l_0}{l_\eta}\right)^{4/3} \tag{3.15}$$

Where k denotes the kinetic energy.

When turbulent are initiated in a fluid it will first be present as large anisotropy eddies. Due to vortex stretching, eddies break up and fission into smaller and smaller eddies which simultaneously becomes faster and more isentropic. As eddies get smaller the strain rates increase.

The intensity of fluid fields is characterised by the root mean square, *u'*, of the velocity fluctuations. It is often expressed as a percentage of the mean velocity and may amount to 10% in very turbulent fields (McCabe, Smith et al. 1993). In practical situations the intensity usually

varies with each component of velocity and have significant spatial variations. In strict sense *u'* is only relevant for isotropic turbulence. The kinetic energy of turbulence, per unit mass, is defined as:

$$k = \frac{1}{2}\left[\overline{u^2} + \overline{v^2} + \overline{w^2}\right] \tag{3.16}$$

Characterising turbulence by such simple measures as described above have obvious limitations. Turbulence is a highly tree dimensional and time dependent phenomena and especially high spatial and transient variations must be anticipated in pressure piling situations.

3.5 Turbulent flames

Combustion regimes

Turbulent motion in a gas represents a very efficient way of transporting both heat and radical species and result in a drastic alteration of combustion pattern. A number of various diagrams have been proposed for characterization of the different combustion regimes and two of them are shown below. It should be noted that the classical Borghi diagram refers to a very ideal and academic case (single step chemistry, Le=1, spatial uniformity).

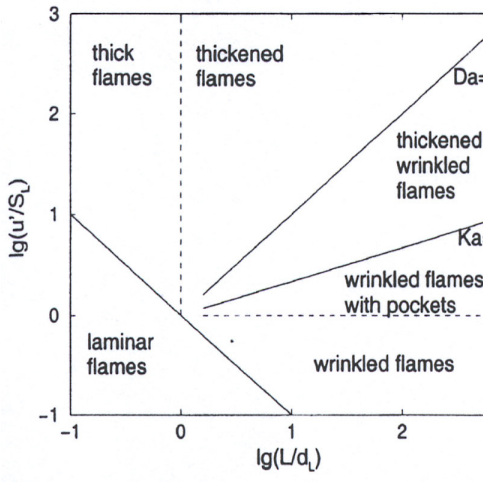

Figure 3.4 *Borghi diagram*

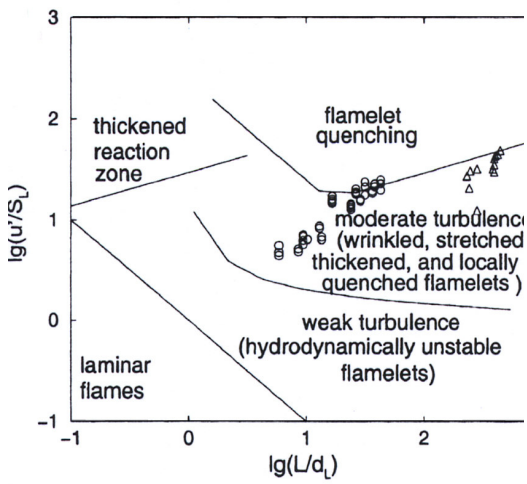

Figure 3.5 *Modified diagram: circles and triangles show results of experimental investigations of flame quenching. (Lipatnikov and Chomiak 2002)*

Two limiting regimes are emphasised in all the classical diagrams: The first is the thick flame or distributed reaction regime in which nearly all eddies are embedded in the reaction zone. In this situation the term flame front has no longer meaning. This regime is characterised by Damköhler number, *Da*, less than unity.

$$Da = \frac{t_0}{t_L} = \frac{l_0 S_L}{u' \delta_L} \tag{3.17}$$

Here t_0 denotes integral timescale, and t_L timescale of laminar flame (often referred to as chemical time scale). The other criteria used is the Karlovitz number:

$$Ka = \frac{t_c}{t_\eta} = \frac{\delta_L u_\eta}{S_L l_\eta} \tag{3.18}$$

where u_η is the Kolmogorov velocity. According to Borghi and Destriau (1998) the system can be described as a locally laminar flame imbedded in a turbulent flow when flame thickness is less than the Kolmogorov length (Ka <1). In between these limits lies the wrinkled-thickened flame regime in which a fraction of eddies are imbedded in the reaction zone. It has been stressed that limits given is not precise boundaries and that a turbulent premixed flame will not be represented by a single point in the diagram, but rather as a zone that may cross boundaries.

The right diagram in Figure 3.5 is an attempt to incorporate more recent development in turbulent combustion theory together with experimental data (Lipatnikov and Chomiak 2002). At least three different mechanisms have been emphasised in the characterisation of turbulent flames:

i. At low turbulence intensity ($u' < S_L$) the laminar flamelets are believed to be significantly affected by hydrodynamic instability (mixing caused by acceleration of fluids with diverging density) (Kobay 1996).
ii. At higher turbulence intensity ($u' > S_L$) eddies penetrates into the preheating zone of the flamelets. The zone thickens as heat and mass transfer inside it intensifies, and combustion rate increases (Peters1996). Such penetration is only possible if the preheating zone thickness is larger than the smallest eddies (Kolmogorov length scale). The process is complicated by the fact that the eddies are rapidly dissipated by the increased viscosity in the preheating zone and that their survival depends on their kinetic energy.

iii. A third mechanism is the stretching of flamelets by turbulent eddies. The stretching can change the local combustion rate and eventually cause quenching. Local flamelet quenching is assumed to be of importance if $Ka \approx 1$ and $Ka=16$ or $Re_t = 250$. These values have been proposed as possible quenching criteria and are represented by the right upper line in Figure 3.5 (Poinot1990).

The two latter mechanisms are upheld as the significant ones in the moderate turbulence regime in Figure 3.5. In more realistic, non-adiabatic and non-equidiffusive flames the existence of the thick flame regime (ideal reactor) is somewhat questionable due to the likelihood of quenching (Lipatnikov and Chomiak 2002).

Turbulent burning velocity

The turbulent burning velocity S_t, has been shown to be a phenomenological meaningful quantity as various experimental investigations indicate the same qualitative trends:

- S_t increases with rms turbulent velocity u'
- S_t and dS_t/du' increases for higher values of the laminar burning velocity
- S_t increase with pressure (even if the effect on laminar burning velocity is the opposite)

Turbulent flame propagation is a poorly understood function of many properties relating both to the turbulent flow field and to the reacting medium. Based on experimental data and theoretical analysis, a simple expression of turbulent flames can be given in terms of a global turbulent burning velocity (Veynante and Vervisch 2002).

$$S_T = S_L + S_L \alpha \left(\frac{u'}{S_L} \right)^n \tag{3.19}$$

where α and n are model constants. Such simple relations do not reflect the complexity involved and will have limited validity. More sophisticated models frequently uses parameters such as dimensional groups (Re Da Ka), integral length scale of turbulence, l_i, and molecular viscosity, μ, (Lipatnikov and Chomiak 2002).

The expression used for turbulent burning velocity in the FLACS code (Arntzen 1998) is given as:

$$S_T = \min(S_{T1}, S_{T2}) \tag{3.20}$$

where:

$$S_{T1} = 1.8 S_L^{0.784} u'^{0.412} l_i^{0.196} \nu^{-0.196} \tag{3.21}$$

$$S_{T2} = 0.96 S_L^{0.284} u'^{0.912} l_i^{0.196} \nu^{-0.196} + S_L \tag{3.22}$$

v denotes kinematic viscosity and is proportional to pressure.

The turbulent burning velocity has been documented to be strongly dependent on Lewis number (Abdel-Gayed, Bradley et al. 1984; Bradley 1992). Bradley proposed the following expression for S_T as a function of Lewis number and the Karlovitz stretch factor, K:

$$S_T = 0.88 u' (LeK)^{-0.3} \tag{3.23}$$

Where K is given as

$$K = \left(\frac{u'}{l_\lambda}\right)\left(\frac{\delta_L}{S_L}\right) \tag{3.24}$$

Figure 3.6 shows plots of turbulent burning velocity versus turbulence intensity for different fuels and equivalence ratios. Some skepticism should be exercised when considering the figure for hydrogen: As fluid properties change significantly with hydrogen content, “fan speed” is not necessarily a precise measure for the turbulence intensity. In spite of this, mixtures with low Lewis numbers appear to have higher burning velocity and are less prone to quench. Extra attention should be given to Figure 3.6 as the trends seen are expected to be relevant in pressure piling situations.

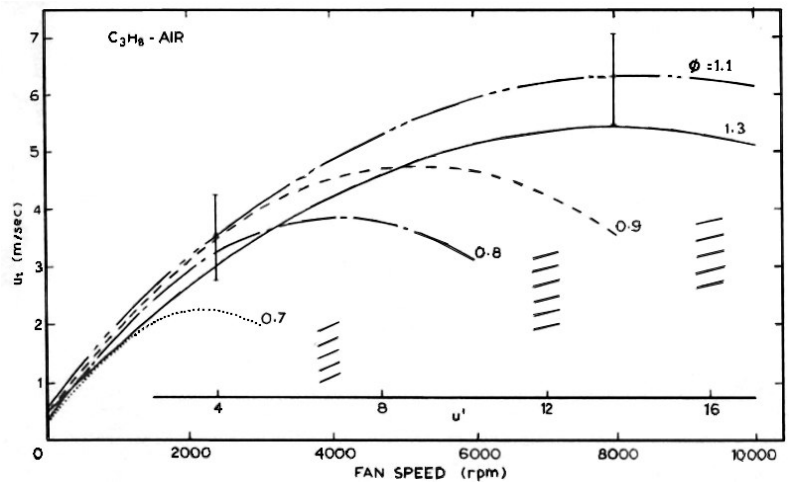

φ	Le
1.3	0.85
1.1	0.88
0.9	1.97
0.8	1.98
0.7	2.03

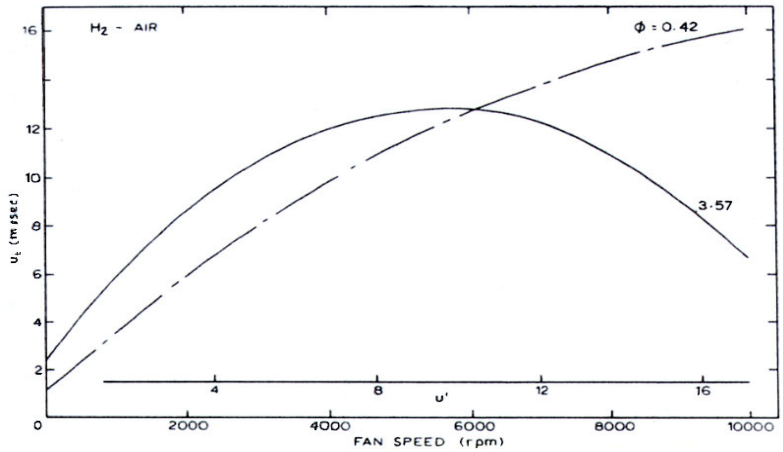

φ	Le
3.57	4.71
0.42	0.70

Figure 3.6 *Top: propane air turbulent burning velocities (u_t=S_T) of different equivalence ratios. Shading shows quenching regions. Bottom: hydrogen-air no quenching. Illustration from Abdel-Gayed, Bradley et al. (1984).*

The effect of pressure on turbulent burning velocity has been experimentally investigated by Kobayashi, Tamura et al. (1996) and their results are shown in Figure 3.7. The effect of pressure on S_t is included in equation (3.21) and (3.22) as the kinematic viscosity is about proportional to pressure. The simple dependency on pressure is however questionable as it has been reported that the pressure dependency varies with fuel type and equivalence ratio (Kobayashi, Kawabata et al. 1998).

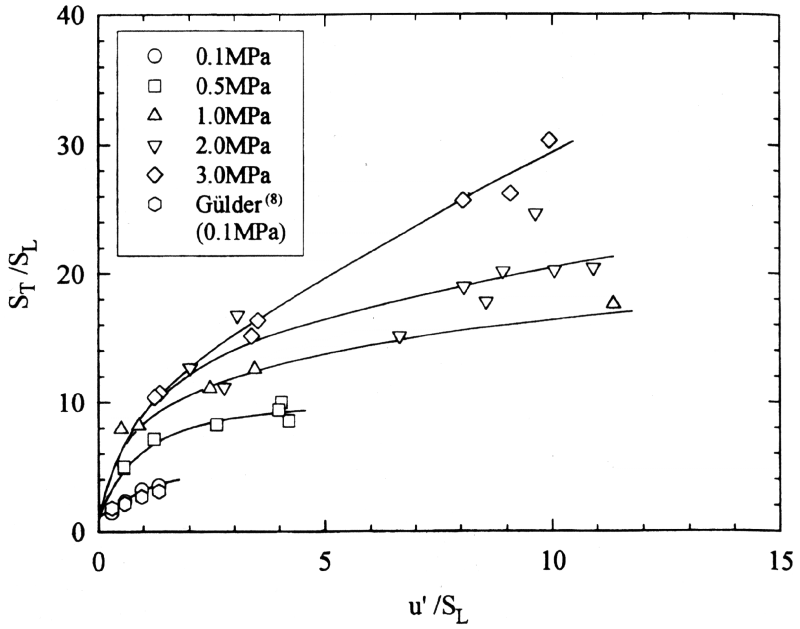

Figure 3.7 *Pressure dependency of turbulent burning velocity for methane (Kobayashi, Tamura et al. 1996)*

3.6 Orifice flow

Orifice flow is one of the key factors in pressure piling. For small pressure differences between the chambers, velocity will moderate and flow can be characterized by the Bernoulli equation. For compressible fluids the density will decrease as velocity increases and for flow with mach number, M, greater than 0.3 the Bernoulli equation is no longer adequate (Nørsterud 1997). For higher mach numbers flow (without combustion) is described by the following equations:

Conservation of mass:
$$\rho_1 u_1 = \rho_2 u_2 \tag{3.25}$$

Conservation of momentum:
$$\rho_1 u_1^2 + p_1 = \rho_2 u_2^2 + p_2 + K_f / F \tag{3.26}$$

Conservation of energy:
$$\frac{1}{2}u_1^2 + H_1 = \frac{1}{2}u_2^2 + H_2 + q \tag{3.27}$$

Second law of thermodynamics
$$S_1 - S_2 = C_p \ell n \frac{T_2}{T_2} - R \ell n \frac{p_1}{p_2} \tag{3.28}$$

Equation of state
$$\frac{p_1}{\rho_1 T_1} = \frac{p_2}{\rho_2 T_2} \tag{3.29}$$

$$C_p = \frac{\kappa}{\kappa - 1} R \tag{3.30}$$

Where the term K_f/F is the friction force per contact area and q denotes heat loss. S is the entropy and κ, the specific heat ratio. This system of equations is indeterminate, but an analytical expression for the friction force can be derived with a few assumptions (Nørsterud 1997). Such an approach is not likely to be valid for the orifice flow between the chambers and the quantity of heat loss trough radiation and convection/conduction is also unknown. Disregarding heat loss and friction an expression for the sound of speed can be added and allow for a unique solution.

$$c^2 = \kappa RT \tag{3.31}$$

For isentropic conditions, sonic flow (M=1) will occur at a given pressure ratio:

$$\frac{p}{p_0} \geq \left(1 + \frac{\kappa - 1}{2} M^2\right)^{-\frac{\kappa}{\kappa - 1}} \tag{3.32}$$

In practical terms this means that flow will be sonic for most mixtures at a pressure ratio of about 0.5. Mass velocity, G, is given by the following equation (McCabe, 1993):

$$G = u\rho = \sqrt{\frac{2\kappa\rho_0 p_0}{\kappa - 1}} \left(\frac{p}{p_0}\right)^{1/\kappa} \cdot \sqrt{1 - \left(\frac{p}{p_0}\right)^{1-1/\kappa}} \tag{3.33}$$

For flow trough an orifice, an empirical expression for the rate mass transfer, m_t, is given by

$$\dot{m}_t = A \cdot C_D \sqrt{\kappa \left(\frac{2}{\kappa + 1}\right)^{\frac{\kappa+1}{\kappa-1}}} \cdot \frac{p_0}{\sqrt{RT/M}} \tag{3.34}$$

Where A is the cross sectional area of the orifice, C_D is an empirical discharge coefficient and M is the molecular weight. The magnitude of C_D varies with Reynolds number and the ratio between the diameters of orifice and vessel/tube Figure 3.8. Table 3.3 gives ratios of specific heat and sound of speed for some mixtures.

		H_2	CH_4	Air	H_2O	CO_2
Speed of sound, c	[m/s]	1294	185	340	423	873
Specific heat ratio, κ		1.41	1.32	1.40	1.33	1.30
Gas constant, R	[$m^2/(s^2K)$]	4124	518	287	461	189

Table 3.3 *Sound of speed and specific heat ratio for different gases (White 1994).*

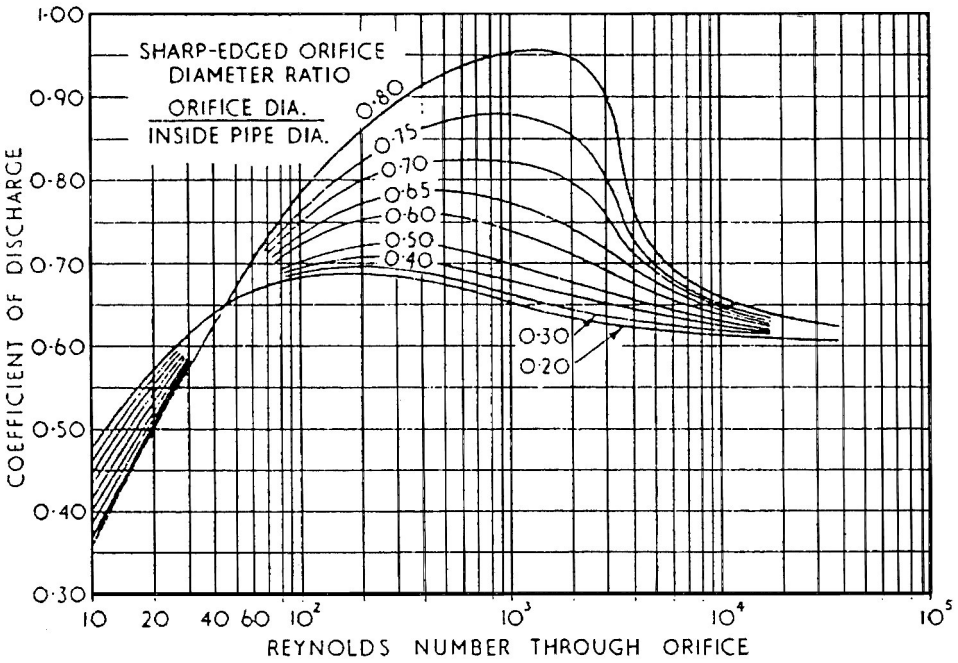

Figure 3.8 *Discharge coefficients for orifices (Coulson and Richardson 1957).*

Based on the above equations and with reference to the double-compartmented vessel, the following aspects should be emphasised:

- In flammable mixtures of air and methane the former constitute 85-95%, hence the sound of speed will be close to that of pure air. However, rich mixtures of hydrogen/air will have a significantly higher speed of sound and with reference to equation (3.32) hydrogen will flow with much higher velocity at the critical pressure difference.
- For mixtures at the lower flammability concentrations, the critical flow velocity would not differ much as air would constitute about 95% in both mixtures.

As combustion take place in the secondary chamber and pressure rise, the flow will be reversed. However the flowing gas will now contain a significant amount of combustion products, which will tend to reduce the critical flow velocity (see values for R in tab). The increased temperature will have the opposite effect as indicated by equation (3.31). Increase in temperature will also increase viscosity and thereby friction.

3.7 Heat loss

In explosion scenarios loss of energy trough the flame surface is usually low compared to the energy liberated within it, hence heat loss trough radiation is often neglected. With decreasing explosion scale the surface to volume ratio becomes less favourable and radiation becomes increasingly important.

Radiation from a reacting gas is generated by to separate mechanisms (Lewis. B. von Elbe 1987):

- In a high temperature gas the high energy level will cause spontaneous shifts in quantum states resulting in radiation of specific wavelengths. This mechanism is associated with thermal equilibrium and is given by the Stefan-Boltzmann law

$$W = \frac{dq}{dA} = \sigma T_g^4 \varepsilon_g \tag{3.35}$$

  Where, W is the radiating power, dq is the rate of energy transfer from the gas to the surrounding, A is the radiating surface, σ is the universal Stefan-Boltzmann constant, T_g is the gas temperature and ε_g is gas emissivity.
- The second mechanism, chemiluminescence radiation, is radiation emitted by active molecules formed in elementary reactions that is present in greater concentration than what would correspond to equilibrium.

Radiation from burning hydrogen mixtures is mainly caused by the thermal equilibrium mechanism whereas hydrocarbon also will have significant contribution from chemiluminescence (Griffiths and Barnard 1995). Heat loss trough convection/conduction will be affective from the time of flame arrival at the wall and will grow with increasing contact area. Condensation of water at vessel walls is a third mechanism for removal of heat from the gas mixture. The effects of the two latter mechanisms are very difficult to assess.

3.8 Detonations

The possible transition from deflagration to detonation is highly dependent on the scale of the explosion and is not likely in small-scale situations. As size of the geometries increase detonations may become part of the pressure-piling scenario. This is especially likely for gases

such as hydrogen and acetylene. Detonation cell size reflects the reactivity of the gas and determines whether detonations may occur. Some values are given in Table 3.4.

	Hydrogen	Methane	Propane	Acetylene
Detonation cell size [1] [mm]	10	300	50	3
Detonation velocity [2] [m/s]	2821	2146	2600	2716

Table 3.4 *Detonation characteristics for some stoichiometric mixture. (293K, 1 bar). [1]Sheperd, Melhem et al. (1991) [2]Lewis (1987).*

Detonation characteristics is limited by geometrical conditions and for a detonation to occur in a tube the diameter must be larger than one third of the cell size. For transfer of detonation from a tube into a larger vessel the minimum tube diameter is about 13 times the cell size (Bjerkved, Bakke et al. 1993). Detonations are not deemed as relevant for the experimental setup used in this study, but for large-scale situation detonations may become relevant in pressure piling situations.

CHAPTER 4

Experimental setup

The basic equipment used in this study can be divided into the following four categories: explosion vessels, gas mixing and filling system, measure and logging system and ignition system.

4.1 Explosion vessel

Explosion vessels were made of two or more short steel pipes with flange collars. Between these two pieces an exchangeable perforated aluminum disc with gaskets could be fitted. Flanging the two remaining pipe openings then gave a double-compartmented closed vessel as seen in Figure 4.1 Dimensions of chambers or "pipes" are given in Table 4.1.

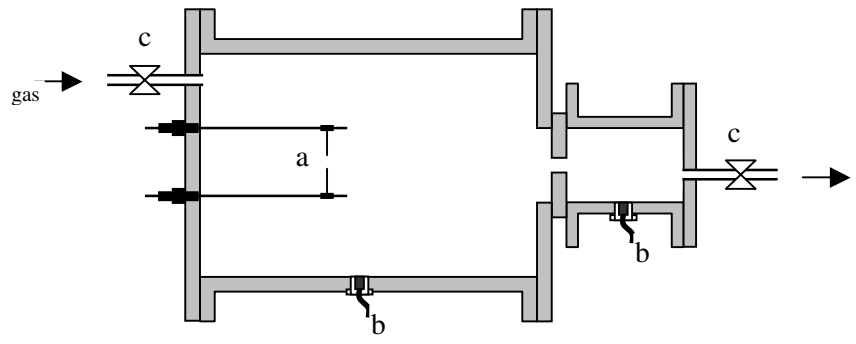

Figure 4.1 *Explosion vessels with spark electrode (a), pressure transducers (b) and valves (c).*

Chambers	Diameter [cm]	Length [cm]	Volume [litre]
secondary	10,0	10,0	0,79
small	10,0	15,0	1,15
medium	14,7	20,0	3,39
large	30	45	31.81

Table 4.1 Tube dimensions

The transfer opening between the chambers could be adjusted between 2 and 40 mm by exchanging aluminum discs. Table 4.2 lists the various orifice diameters used. A few tests were also made with alterations of shape and number of orifices. Figure 4.2 shows some selected orifices.

Diameter [mm]	2,0	4,0	5,6	8,0	11,3	16,0	20,0	25,0	30,0	40,0
Cross sectional area [mm^2]	3,1	12,6	24,6	50,3	100,3	201,1	314,2	490,9	706,9	1256

Table 4.2 Hole diameters and cross sectional area.

Figure 4.2 *A selection of some of the orifices used. The aluminum disk in the lower left corner has a small piece of metal mounted 10 mm away from the orifice opening to redirect the flow in a radial manner. Number of orifices in the discs is 1, 7 and 19.*

In general two types of vessels configurations were used. The majority of tests were conducted with vessel similar to the one displayed in Figure 4.3 with a length to diameter ratio of 1.33-1.5 (primary chamber). In addition, tests were also done in vessels with long and narrow primary chamber (Figure 4.4). Such vessel configurations were expected to be more prone to pressure, but also be more affected by turbulence and cooling in primary chamber.

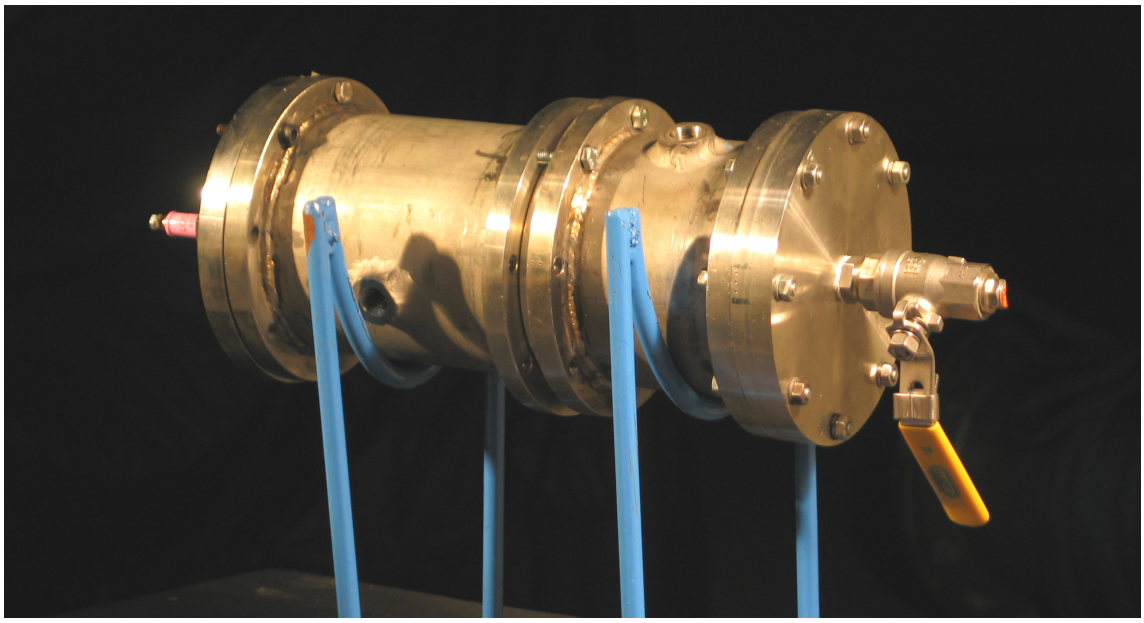

Figure 4.3 *1.94-liter vessel with small length to diameter ratio in primary chamber (1.5).*

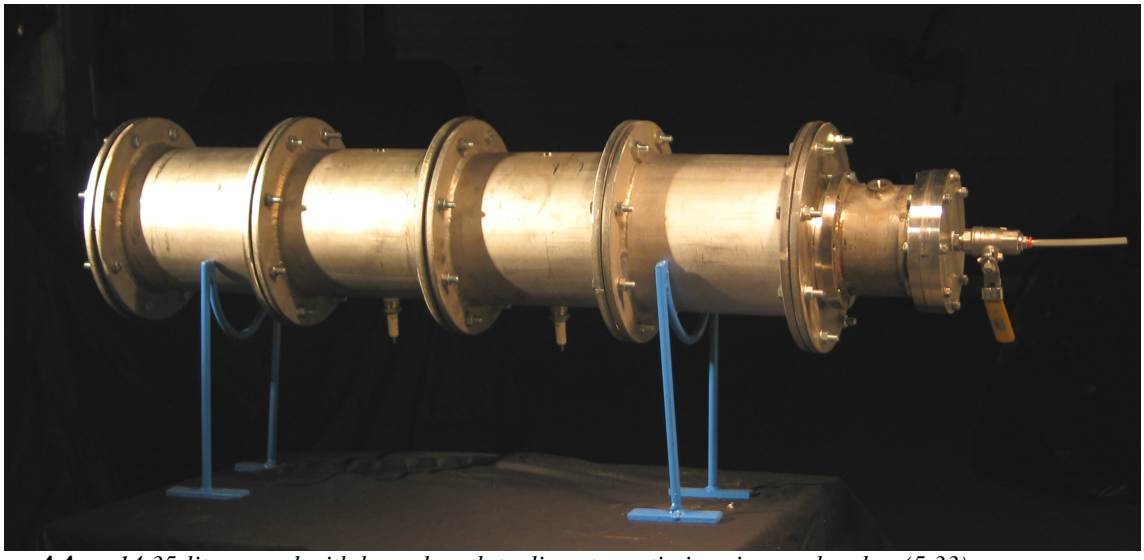

Figure 4.4 *14.35-liter vessel with large length to diameter ratio in primary chamber (5.33).*

4.2 Gas mixing and filling system

The gas mixing system consisted of a mixing panel, a small mixing tank, a gas analyser with pump, two high-pressure pneumatic valves, two electro-pneumatic valves, as well as a large number of various fittings and hoses. The setup is shown in Figure 4.5.

Gas mixing

To ensure desired mixture each gas was directed trough the mixing panel where pressure and flow for the respective gases could be adjusted. The gas was then directed to a small mixing tank to ensure proper mixing before injection to the explosion vessel. Exact adjustments of gas level were difficult and generally quite time consuming due to a significant time delay between adjustment and detection. For this reason explosion test with various mixture fraction was done with somewhat random intervals in gas concentration.

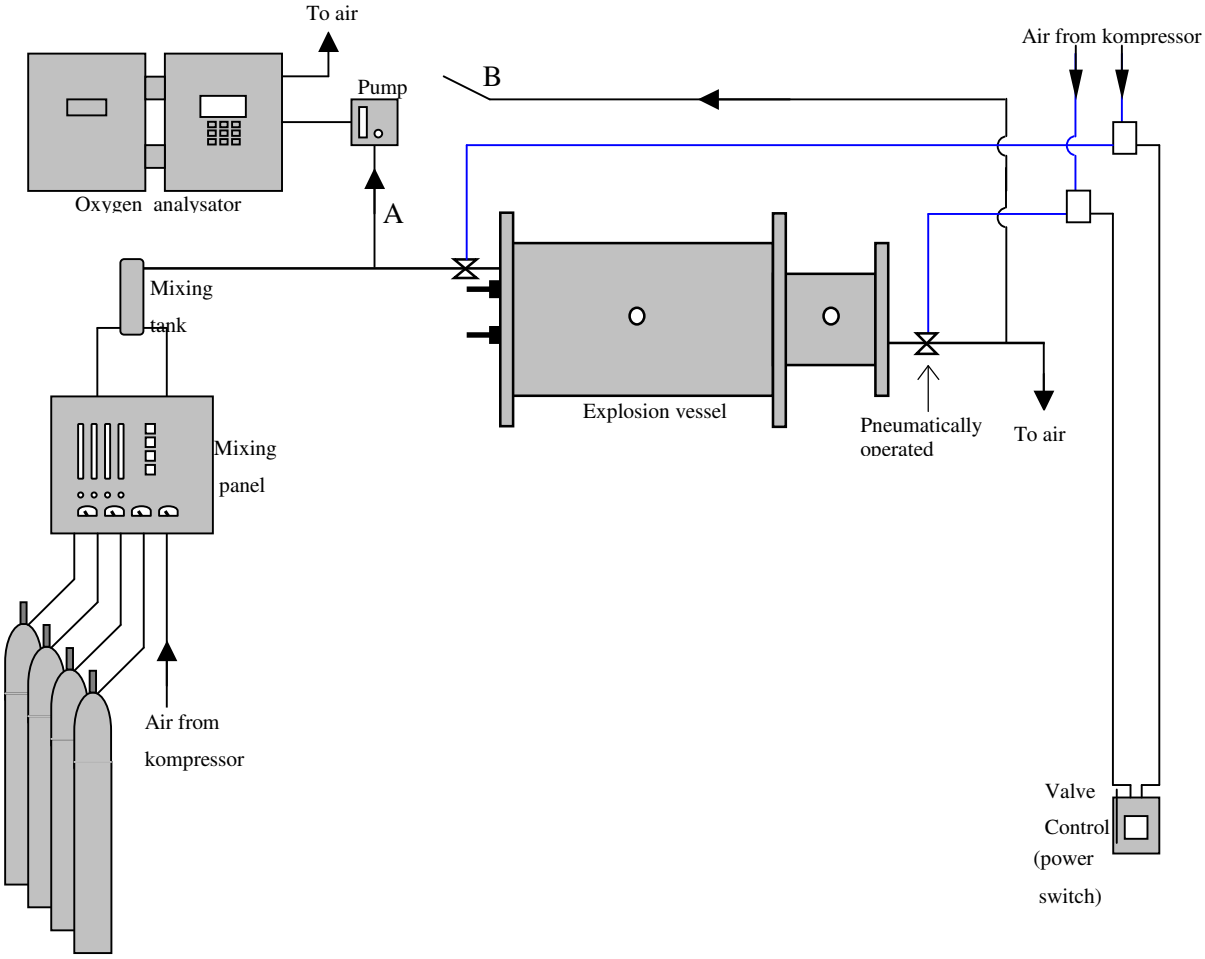

Figure 4.5 *System for gas filling and valve control. The blue line indicates pressurized air used to control pneumatic valves.*

Gas measurement

Prior to vessel entry a small portion of the gas was directed to the gas analyser. After stable readings were achieved the hose marked A was disconnected from the analyser and hose B connected. As gas flushed trough the explosion vessel the gas measurements would eventually become identical to the one made prior to vessel entry and ensured a homogen and well-defined gas mixture.

Gas Analyser

Two types of gas analyser were used: The oxygen analyser Servomex 1100A was used to indirectly measure hydrogen content. For hydrogen the indirect measurements work well in part because of the wide flammability range of hydrogen which correspond to oxygen content ranging from 4.2 to 19.9 percent. The oxygen analyser utilizes the paramagnetic susceptibility of oxygen and provides high accuracy measurements. Calibration was done with a certified gas containing 14,60 % oxygen and pure nitrogen (0% oxygen).

Measurements of methane content were done with the Hartman & Braun Uras 10 E infrared light adsorption analyser. This analyser utilizes methane's wavelength specific adsorption of infrared light and represents a less accurate measuring method than the one described above.
Calibration was done with a certified gas containing 10,00 % methane and pure nitrogen (0% methane).

Valves and valve operation

Flow in and out of the explosion vessel was controlled with to set of valves each consisting of a pneumatic high-pressure valve which was controlled by a 3-ports electro pneumatic valve. The valves could then be simultaneously operated by a power switch as seen in Figure 4.5. Due to the laborious process of demounting and mounting the various vessels and attached equipment, these valves were eventually exchanged with two manually operated ball valves.

4.3 Ignition system

Initial ignition system consisted of a custom made spark generator with control unit and two Lodge sparkplugs with straight metal rods (Figure 4.6). Sparkplugs were modified in order to facilitate the adjustment of spark location and spark gap (see Figure 4.1). By connecting the oscilloscope to the ignition control unit, ignition and logging could then be initiated simultaneously.

Serious problems were encountered with the spark generator, which eventually had to be replaced. The replacement could not be connected to the oscilloscope and consequently simultaneous initiation of ignition and logging was no longer possible.

4.4 Measure and logging system

The measure and logging system consisted of two piezo-electric pressure transducers (Kistler 701A), two charge amplifiers, oscilloscope and PC (Figure 4.6).

The piezo electric pressure transducer relies on a small crystal, which generates a small electrostatic charge when exposed to pressure. Charge leakage will occur to the charge amplifier when this is activated and may also occur if the sockets are contaminated (dust). Hence handling and operation was done with outmost caution to minimizing these effects.

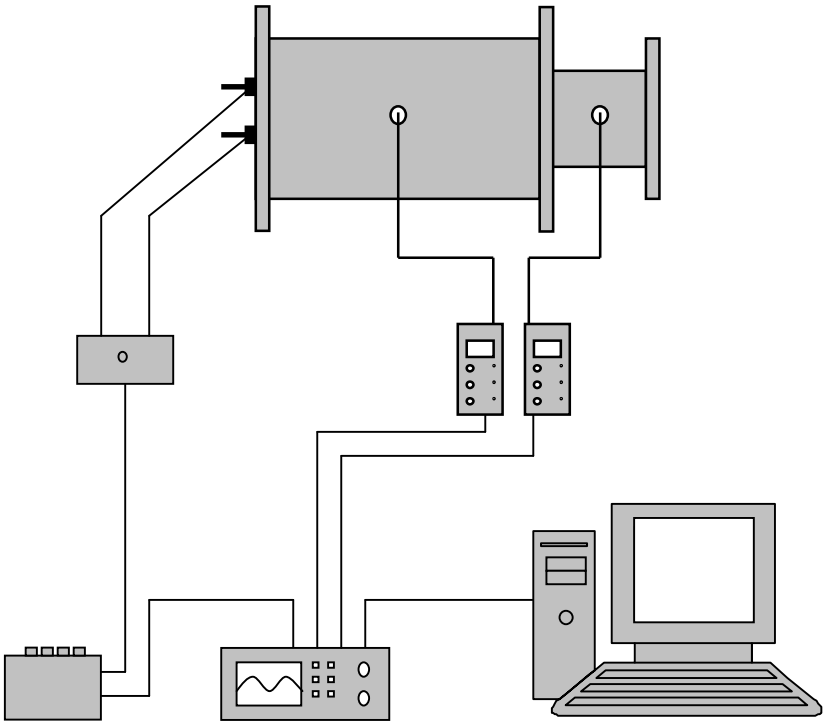

Figure 4.6 *Explosion vessel with ignition system and measurement/logging system.*

Depending on charge produced by the transducer and the transient character of each test, charge amplifier and oscilloscope had to be adjusted accordingly. The large difference in time needed to reach peak pressure in different gas mixtures gave corresponding differences in sampling frequency. This introduced some uncertainty regarding the values of peak pressure and treatment of recorded data (see section 4.6).

4.5 Experimental procedure

Methane and oxygen analysers were calibrated before each test session according to the instruction manuals. Test preparation consisted of a thorough flushing of the explosion vessel with subsequent gas measurements and eventually closing of the valves. The manual valves had to be closed in proper order to assure atmospheric pressure in the vessel. To avoid any effect of initial turbulence the mixture was given at least 30 seconds to settle before charge amplifiers were activated and ignition induced. To avoid any drift the charge amplifiers were activated immediately prior to ignition and deactivated as soon as possible afterwards. Depending on how fast combustion would take place, time scale on the oscilloscope was adjusted accordingly.

4.6 Representation of data

The pressure curves for different tests were often not directly comparable and a number of tests showed large local variation or “messy” curves. In general, these variations were related to situation with fast combustion and thereby to high sampling frequency. Increased variations was also seen in experiments were significant pressure piling occurred. Such variations may very well be a correct representation of the combustion process. However, in practical situation the focus of interest would be the pressure load received by the geometry and for the sake of comparison, treatment of the raw data was necessitated.

The smooth pressure curves for the relatively slow burning methane mixtures (low sampling frequency) were generally used directly. For hydrogen most pressure curves had to be smoothened which was done by the method of “ moving average”. The argument for using this simple technique was that it represented a less laborious way of retrieving peak pressure for hundreds of tests. Pressure values attained using curve integration and least square polynomial

fit showed very small deviations to those found using moving average. The differences were less than 2 % and moving average generally gave more conservative values.

For each data series, samplings were averaged in periods of 10-50 depending on sampling frequency and the nature of the pressure curves. Values from the smoothened curve were then sorted in descending order and the highest value was taken as peak pressure. As a quality check variation in the top ten values was evaluated: large variation in these values indicated insufficient smoothening, which then had to be redone. Accuracy of peak pressures was frequently controlled by plotting the small segment of the data series in which peak pressure was located. This would exclude the possible misrepresentation caused by harmonic oscillation. (Harmonic variation would produce small variations in the sorted values, but might still not represent the peak pressure).

Values for the various expression is determined by the procedure presented above.

P_s – peak pressure in single chamber vessel
p_1 – peak pressure in the primary chamber
p_2 – peak pressure in the secondary chamber
p_{diff} – pressure difference between the two chambers: p_1 and p_2
p_p – pressure difference between peak pressure in the secondary chamber(p_2) and the peak pressure achieved in a single chamber bomb (p_s) under similar conditions.

p_p is used as an attempt to make a quantitative measure for pressure piling and a positive p_p would then indicate pressure piling as defined in the introduction. This measure has some limitations and the problems are essentially related to the comparison of to vessels with different volume to surface characteristics. Ideally, comparison should be between vessels with identical surface to volume ratios. As will be seen later heat loss and possibly other surface related factors may be significant and in these situations the value of p_p as a comparative measure is reduced. In general the importance of vessel characteristics is more important for the slower burning mixtures and for these situations evaluation of both p_p and p_{diff} might give a better picture. p_{diff} may be interpreted as a rough measure of the dynamic character of the explosion.

4.7 Sources of error

Gas analyzer

Calibration of the oxygen analyser was done with a certified span gas containing 14,60 % oxygen and pure nitrogen (0% oxygen) which correspond to a stoichiometric hydrogen mixture and 100% hydrogen respectively. Measurements close to these values would have the highest accuracy and as gas mixture depart from these values accuracy would be somewhat lower. For mixtures far from the reference point, accuracy depend on the linearity between the to points or the extrapolation toward lean mixtures. Alternatively; how well the analyser calibrates for non-linearity.

Changes in flow rate effects accuracy and a change from 0 to 200 mL will introduce an error <0,1 % (Servomex manual). Adjustment of flow was done with a flow meter that actually measures the momentum of the moving gas particles rather than volume flow. Due to variation in specific gravity between oxygen and hydrogen the flow rate measured on the flow meter had to be increased as hydrogen content went from 5 to 75%. In general the flow was not changed for every interval and was on some occasions not changed at all. This is assumed to be the most significant error in hydrogen measurements. In any case the error would be much lower than 0,1% and probably significantly less than 0,05% for oxygen. How this affect the hydrogen measure is uncertain as the Servomex instruction manual gives no information on how or if the given error (0,1%) depend on the oxygen content of the sample. However, with a fixed value (worst case) the estimated error from this source would not exceed 0,25% for hydrogen.

Pressure measurements

As previously described, sampling frequency and more importantly, the smoothening and general treatment of data is probably one of the most significant sources of error.

Operational errors

Operational errors are obviously also a possible source of error. Insufficient flushing would in the case of methane have considerable effect, as the presence of CO_2 would affect combustion. Improper operation of the valves may result in an elevated pressure prior to ignition and cause elevated explosion pressure.

Resonance effects

In general the fast burning mixtures showed considerable local variation often of periodic character. Such effects could have been caused by resonance effect in the geometry, the

measurement system or by the combustion itself. The latter effect has been reported to occur in closed vessel (Lewis and von Elbe 1987) and is related to the very rapid combustion of the gas close to the vessel wall. As earlier noted, the last portion of the gas will be compressed prior to its rapid combustion. In the process gas will be accelerated to very high velocities and small pressure waves is set up. The amplitudes are reported to increase with burning velocity and are in agreement with the current experiment. Audible vibrations usually occurred with hydrogen and are expected to be associated to the rapid flow of gas trough the orifice. Whether or not the small variations seen in the pressure curves are correct representation of the process remains uncertain.

Condensed water

After a few tests water will typically condense on the inside of the vessel walls and may represents a significant source of error. Water may evaporate from the warm vessel walls during gas filling and the subsequent period of turbulence settling, altering the gas composition. Water in the gas mixture may affect reaction mechanisms and heat capacity, whereas a small portion of the water at the vessel walls may evaporate during the explosion. It is generally assumed that the explosions will be to rapid for significant amounts of water to evaporate.

CHAPTER 5

Experimental results

5.1 Preliminary tests

5.1.1 Single chamber -hydrogen

The first series of tests were conducted in a 1.15 litre single chamber vessel (0.1m in diameter and 0.15m long) with the ignition point located close to the vessel centre. The purpose of these tests was to provide a basis for comparing experimental pressure readings with corresponding values for adiabatic combustion. Discrepancy between these values would then indicate the relative importance of unknown quantities such as heat loss, the effect of condensed water at the vessel walls, incomplete combustion etc. Figure 5.1 shows calculated and experimental peak pressures for a 1.15 litre single vessel.

By fitting a polynomial trend line to the experimental values, as seen in Figure 5.1, an expression for the pressure as function of gas concentration was acquired. In later experiments with pressure piling this expression could be used to calculate single chamber pressure and a reference point high pressures in pressure piling situations.

From Figure 5.1 it should be noted that the difference between the experimental and calculated pressure values changes with fuel ratio and that the differences for rich mixtures are more than twice as large as for the lean mixtures. Evaluation of the time history for these tests shows that the rich mixture burn considerably faster than the lean one, which uses twice as long time to reach peak pressure (Figure 5.2). Presumably, the short combustion time for the rich mixture would allow less heat to escape and only give a small pressure reduction. Obviously this effect cannot be important as the richer mixtures produce relatively lower pressures.

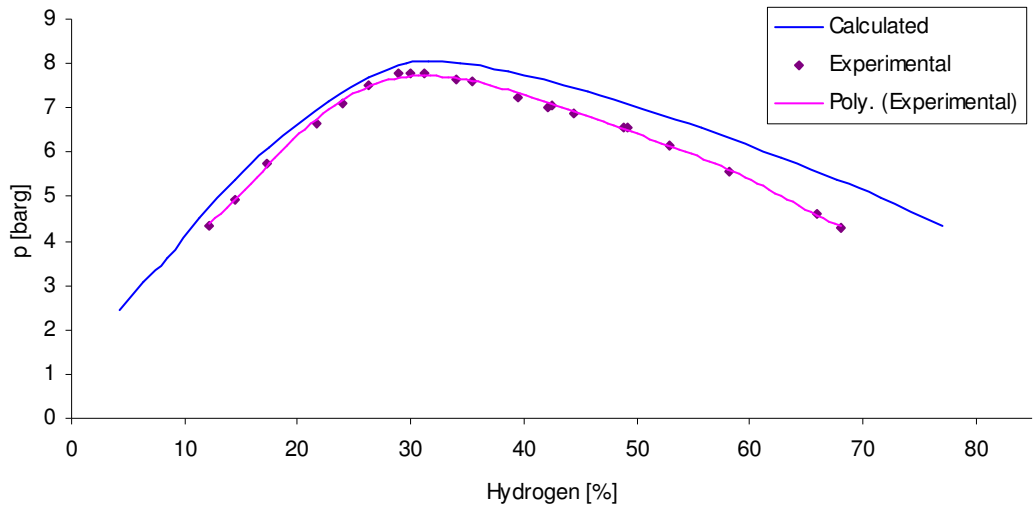

Figure 5.1 *Calculated and experimental peak pressures for various hydrogen concentrations. Values for adiabatic combustion were found by using the chemical calculator GasEq.*

A possible cause for the trend seen in Figure 5.1 could be a systematic under prediction of hydrogen content. However during experiments the oxygen analyser was frequently calibrated with two gases corresponding to stoichiometric equivalent mixture and 100% hydrogen (0% O_2) and significant misrepresentation seems unlikely.

Calculations of adiabatic pressure (GasEq) show that the presence of H_2O in the mixture will have a larger pressure reducing effect for lean mixtures. Water content of 5% gives a pressure reduction of about 4.5% for lean mixtures (15% H_2) and a 2.3% pressure reduction for rich mixtures (60% H_2).

Pressure history for three selected mixtures are shown in Figure 5.2. Time between flame contact with the vessel wall (the inflection point) and peak pressure varies considerably between the mixtures. During this time span the vessel walls will interfere with the reaction pattern both chemically and thermally and reduce peak pressure. From Chapter 3 one might recall that inert components (as the vessel walls) are involved in several chain terminating processes. The extent to which such a process may occur will be highly dependent on the level of contact between the gas molecules (or radicals) and solid surface. Even though the gas will be compressed toward the end of the combustion process, only a very small portion of the molecules will be within the

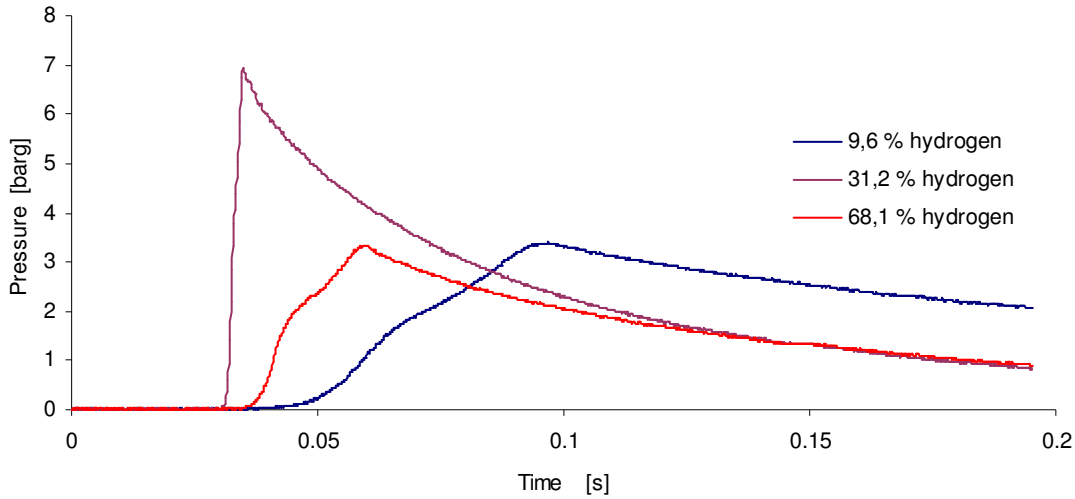

Figure 5.2 *Time pressure history for three selected hydrogen concentrations*

diffusive range of the vessel walls. As previously noted, the diffusive range will be higher in a rich hydrogen mixture (see equation 3.7), but it is questionable if effect will have a large impact.

None of the factors discussed above seem to present a satisfying explain to the large discrepancies seen in Figure 5.1. The diverging trend will not have much significance of the experimental part of this study. However, in the subsequent attempts to simulate pressure piling it may be of greater importance.

As noted there are considerable differences between mixtures with regard to chemically bound energy and reaction rate. Figure 5.2 show time histories for three selected mixtures. By the use of Equation 3.10, laminar burning velocity for stoichiometric mixture was calculated to approximately 2.7m/s.

The tests discussed above were all conducted in a vessel 15 cm long and 10 cm in diameter and ignition took place in the centre of the vessel. Consequently, the flame would have little time to interact with the vessel walls before peak pressure was achieved. For long and narrow vessel heat loss will be greater both because of the larger surface to volume ratio and the longer contact time between flame and vessel walls before peak pressure is reached. Ignition point close to the vessel wall will have similar effect.

In order to present some information about the magnitude of such effects, a few more tests were conducted in an oblong vessel with a diameter of 0.15m and 0.8m long (13.6litre). Ignition point was 2cm from one end. Results from these tests are shown in Figure 5.3 together with the

corresponding values for the 15x10 cm vessel. The surface to volume ratio for these two vessels was 27.2 and 4 respectively. As seen in the figure, the oblong vessel gives consistently lower pressures (3.5-5 %). Stoichiometric mixtures give about 0,5 bar lower pressure whereas lean and rich mixtures seem to be slightly less affected.

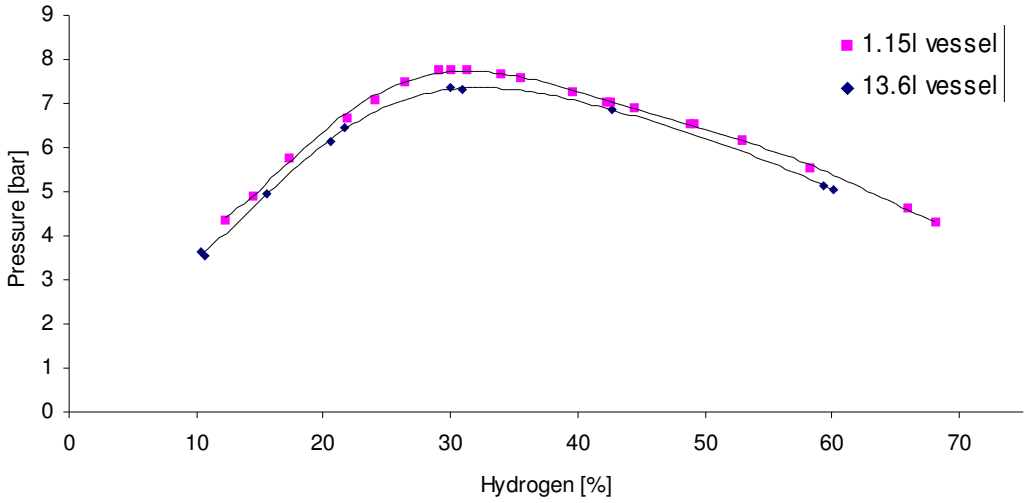

Figure 5.3 *Experimental peak pressures for various vessel shapes.*

5.1.2 Single chamber –methane

Single chamber tests with methane showed large deviations to the calculated values (Figure 5.4). Compared to the hydrogen mixtures, heat loss will typically be larger in a methane mixture for several reasons. Due to the larger time span between ignition and peak pressure, heat loss mechanisms will be effective for a long period of time. Calculations of laminar burning velocity (Equation 3.10) give a rather low value of 0.25m/s and this low value indicate that heat loss and contact with the vessel walls have a strong effect. Due to the difficulty of assessing some of the quantities used in the equation the calculation is rather imprecise.

Radiative losses will also be larger for a methane mixture as the emissivity of some of the chemical spices involved will be larger than those found in hydrogen combustion. Heat loss trough radiation will also be a quicker process than conduction and convection as it will be effective immediately after ignition whereas conduction (to the vessel walls) is only significant in the final stage. According to (Glassman 1987) the reaction mechanism of methane combustion is generally more affected by cooling.

Comparison of pressures in the 1.15 litre and 13.6 litre vessels shows that the latter give 4.5 to 6 percent lower pressures. This is slightly higher than the corresponding values for hydrogen (3.5-5%) and indicates that heat loss is more significant in the methane experiments.

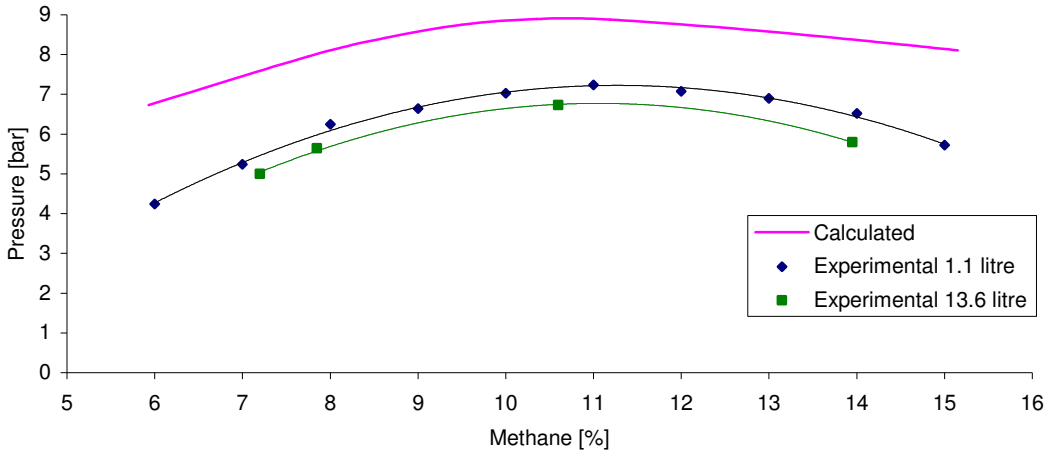

Figure 5.4 *Calculated and experimental peak pressures for various methane concentrations*

5.1.3 Consecutive tests - deviations

The reproducibility of explosion experiment is sometimes quite low, - especially for large and complex geometries where deviations can be as large as 30-40 % (Bjerkved, Bakke et al. 1993). For well-defined and small-scale set-ups the reproducibility would be much higher. However, deviations found for one geometry and fuel mixture, cannot generally be assumed to be representative for other tests. Typically one would expect the reproducibility to be lower for rich and lean mixtures where small errors in concentration measurements can pose significant misrepresentation of burning velocity (due to the steeper gradient). Lower reproducibility would also be expected for the larger geometries and possibly also for more reactive fuels as such conditions would represent a more violent and dynamic combustion process.

A series of experiments were done in order to assess the uncertainty associated with the pressure measurements. About a dozen experiments with stoichiometric mixtures were conducted in the 1,15 litre single camber vessel and gave a standard deviation of 1%. Ten identical tests in the 4,18 litre double compartment vessel gave standard deviations of about 1% for the secondary chamber and 2% for the primary chamber.

5.2 Survey tests: gas mixture, orifice size and volume ratio

In these test the objective was to "map" any pressure piling behaviour over a wider range of parameters. Experiments were carried on beyond the point were pressure piling was expected to occur, in order to get a broader perspective. A large number of tests were done with varying orifice diameter, fuel mixture and volume ratio, to see how these parameters affected peak pressure. Three different volume ratios were used. The secondary chamber, which was the same in all tests, was mounted on three different chambers. All chambers were cylindrical and had similar length to diameter ratio. In each set-up ignition took place near the centre of the largest vessel to ensure that the flame front would develop with the least possible interference from the vessel walls. Orifices where varied from 2mm to 40mm depending on mixture and scale. For the small transfer opening quenching would typically occur, preventing secondary ignition and resulting in a negative pressure difference between the chambers. Except for the largest set-up, fuel mixture was varied between upper and lower flammability limits or to the degree where secondary ignition could be achieved.

Fuel	Fuel content	Orifice diameters	Vessel volume	Volume ratio
H_2	9-70%	2-15 mm	1.94 l	1,49
CH_4	6-14%	2-15 mm	1.94 l	1,49
H_2	9-70%	5,6-20 mm	4.18 l	4,29
CH_4	6-14%	5,6-20 mm	4.18 l	4,29
H_2	29.6 %	8-40 mm	32.6 l	40,25
CH_4	10. 0 %	4-25 mm	32.6 l	40,25

Table 5.1 *Schematic overview of test variables.*

5.2.1 Fuel content

Methane

Figure 5.5 present a typical plot of peak pressure versus methane content. Due to the small volume ratio in this experiment the level of pressure piling is limited. As seen in the figure, dependence on burning velocity (as a function of fuel content) is not very pronounced. Peak pressure and pressure difference is almost independent of mixtures within a limited range. Mixtures with 8% and 11,5 % methane have approximately the same burning velocity, which is slightly less than half of the 10,5% mixture. Still the mixtures tend to respond very similar.

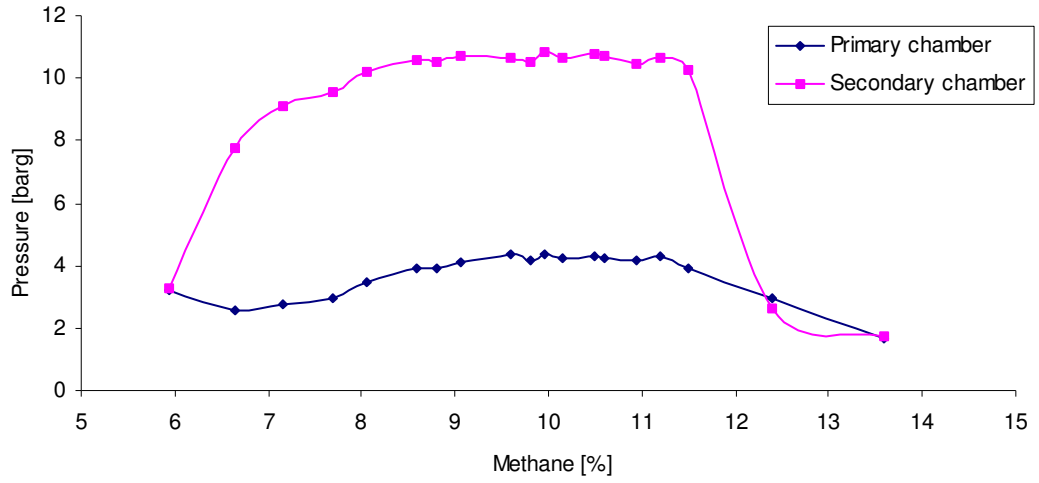

Figure 5.5 *Peak pressures for primary and secondary chamber with methane as fuel. Data from 1,94 liter vessel, volume ratio: 1,49, orifice diameter: 5,6mm. Lines has been added to the plots to better illustrate the pattern.*

This seems to be in agreement with the use of the parameter B used by (Abdullin, Babkin et al. 1988) which roughly can be described as the ratio between outflow of chemically bound energy and heat release trough combustion. That is, for the slow burning mixtures more gas will flow into the secondary mixture before ignition and thereby compensate for the lower energy content in the transferred gas.

The laminar burning velocities is only relevant in the primary chamber and to the degree turbulent burning velocity is seen as a function laminar burning velocity. According to (Bray, Champion et al. 1996) the turbulent reaction is very sensitive to equivalence ratio, and a rich or lean mixture will be more affected by shear and strain caused by turbulence. However, any pronounced effect of quenching was not identified in the methane experiments.

The general trend seen in Figure 5.5 was characteristic for the majority of the methane experiments. As Orifice diameter was made larger, the pressure difference got smaller and peak pressure in secondary chamber became increasingly sensitive to fuel mixture. Orifice diameter below 5.6mm gave no ignition in secondary chamber.

Hydrogen

Similar experiments with hydrogen gave generally low peak pressures, and the highest value measured in all tests, was about 8,5 bar. Since the laminar burning velocity of hydrogen is roughly 6 times that of methane, the time needed for the flame to arrive at the orifice is much shorter. In the current geometry, the short distance, and thereby the small time span between primary and secondary ignition did not allow for a significant amount of gas to flow into the secondary chamber. Consequently the level of pressure piling was severely reduced.
Pressure differences between the two chambers were in general very low except for small ranges of lean and rich mixtures. The general trend seen in Figure 5.6 with increasing pressure differences toward rich and lean mixture was more or less observed for all orifice sizes below 15 mm. (see appendix). Figure 5.7 show level of pressure piling.

Slow primary combustion would allow more gas to flow into the secondary chamber but as seen in the methane experiments this effect is probably diminished by the lower energy content in the transferred gas.

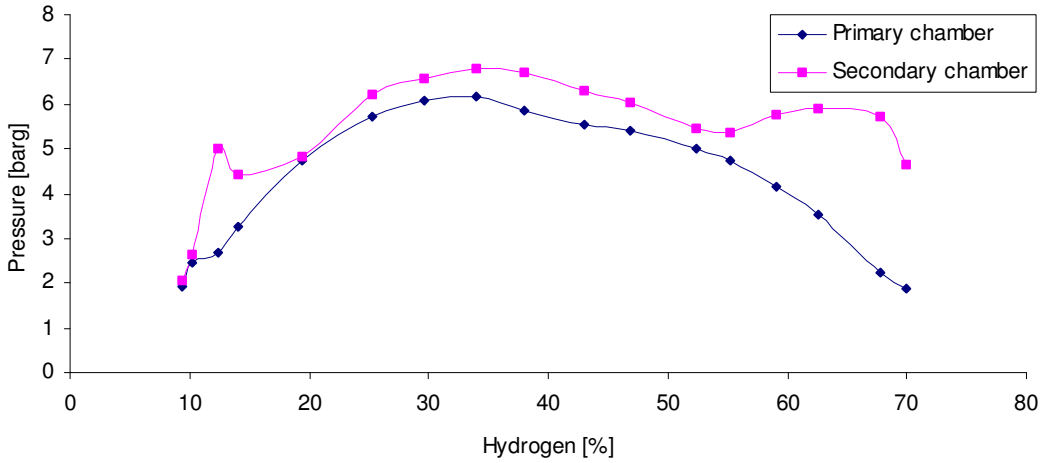

Figure 5.6 *Peak pressures for primary and secondary chamber (Hydrogen, 1.94 litre vessel, volume ratio: 1:1,49,* orifice *diameter 8mm).*

An explanation for the trend seen in Figure 5.6, with higher level of pressure piling for lean and rich mixtures, can be sought in the burning velocity's dependence on turbulence intensity. Turbulent burning velocity of rich mixtures have a negative response to strong turbulence (Abdel-Gayed, Bradley et al. 1984) (se also Figure 3.6). Due to the pressure differences

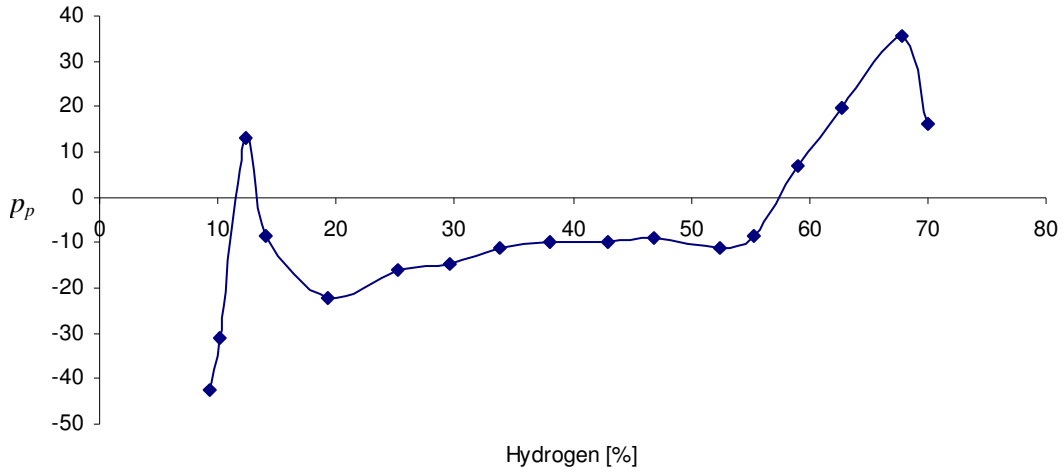

Figure 5.7 *Pressure piling. Pressure difference between max pressure in secondary chamber and corresponding max pressure for single chamber experiments. Values have been normalized by single chamber values and plotted as percentage overpressure. Positive values indicate pressure piling as defined in chapter 1.*

between chambers, the gas will flow with the speed of sound (se equation 3.32) resulting in very high turbulence intensity. With reference to the speed of sound in different gas mixtures (Table 1.1), hydrogen mixtures, and especially rich hydrogen mixtures, will have higher turbulence intensity than mixtures with methane/air.

The turbulence generated by the rapid in-rush of gas will have high spatial variations. A brief peep at the FLACS simulation results (Chapter 6) confirms these expectations and to illustrate this a picture from FLACS simulations has been included here. Figure5.8 shows turbulence level, *u*', at the time of flame transfer into the secondary chamber. Turbulence reaches a level of about 80 m/s in the central core of the jet and roughly half the volume has values of 20 m/s or above. The turbulence level predicted by FLACS corresponds to the far right side of Figure 3.5, or a situation in which the lean mixture burns much faster than the rich one. Under these conditions, rich mixtures are likely to quench.

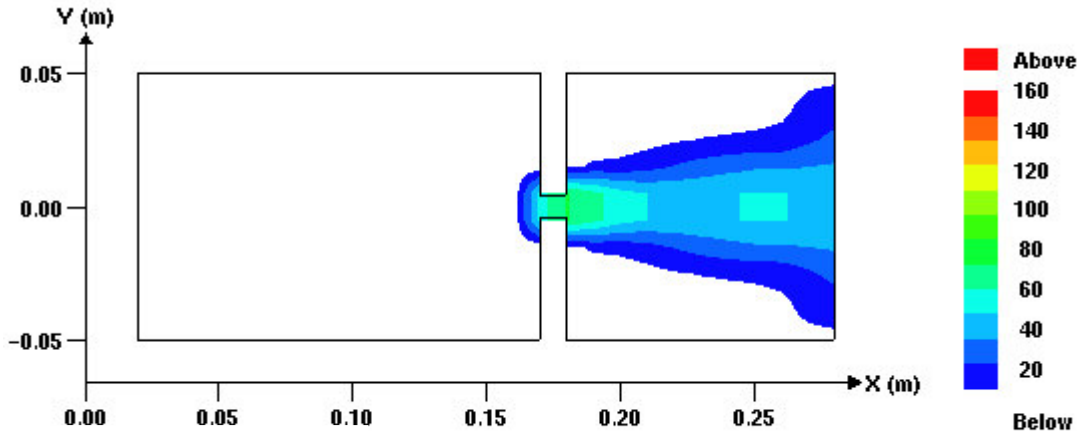

Figure 5.8 *Turbulence level, u',(m/s) in the secondary chamber at the time of secondary ignition (t=8ms)*

For the lean mixture it would be a situation in which the mixture burned relatively slowly (laminar) in the primary chamber and very fast in the secondary chamber, or in other words: optimal conditions for pressure piling. This neatly explains the first peak in Figure 5.7.

For rich mixtures the situation would be opposite: A relatively fast combustion in the primary chamber followed by a relatively slow turbulent combustion in the secondary chamber. Apparently this ought to result in a low level of pressure piling which is obviously not consistent with the experiments (Figure 5.6). In spite of these unfavourable conditions for pressure piling, it is the rich mixtures that give the highest p_p values (Figure 5.7). With reference to the flow equations in chapter 3.6, it is apparent that the transfer of chemical energy between the two chambers also depends on the flow characteristics of the gas mixture.

Based on the idealized equation for mass velocity (3.22 and repeated below), a simple calculation may be used to indicate the magnitude of these effects. For the sake of simplicity the pressure is set to two bar in the primary chamber and 1 bar in the secondary chamber. Assuming a linear relation between the κ-values and the gas composition, the mass velocity has been calculated for to mixtures corresponding to the two peaks in Figure 5.7.

$$G = u\rho = \sqrt{\frac{2\kappa\rho_0 p_0}{\kappa - 1}}\left(\frac{p}{p_0}\right)^{1/\kappa} \cdot \sqrt{1 - \left(\frac{p}{p_0}\right)^{1-1/\kappa}} \qquad (5.1)$$

Due to the higher density of the lean mixture, mass transfer will be larger for this mixture whereas the transfer of chemically bounded energy will be larger for the rich mixture. Between the two mixtures, the combustion enthalpy of the transferred gas differs in the ratio 1:1.6 with the latter value corresponding to the rich mixture. Under otherwise equal conditions, flow properties of the rich mixture results in higher energy density in the secondary chamber.

Although flow characteristics of the mixtures undoubtedly is an important factor, a closer look at the pressure time history for some of these mixtures reveals what quenching in the secondary chamber is by far the most important factor. Figure 5.9 show pressure time history of two selected mixtures with highly diverging level of pressure piling.

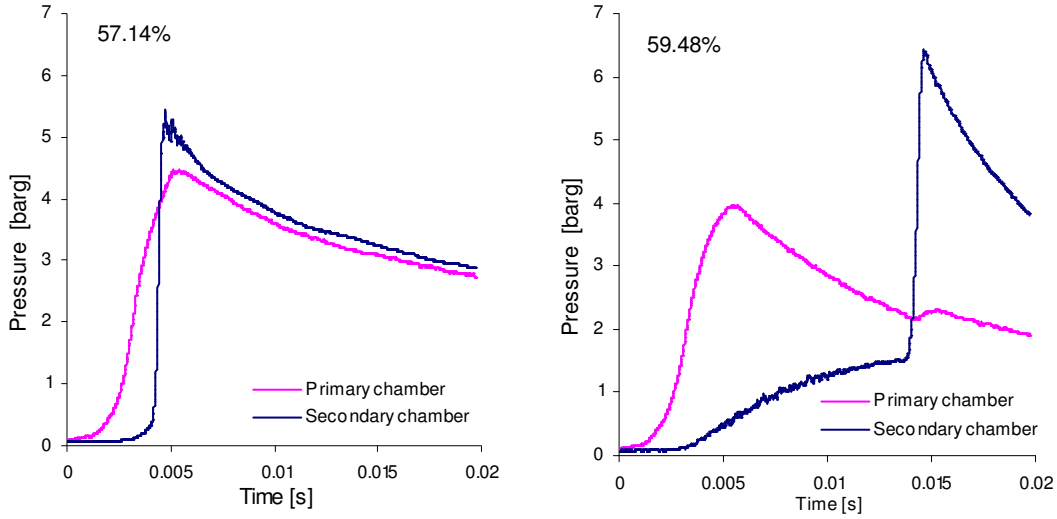

Figure 5.9 *Pressure time history for two selected mixtures. 1.94l vessel 5,6mm orifice, hydrogen.*

As hydrogen content rises, the mixture becomes increasingly sensible to quenching and at some point the turbulence level will inhibit secondary ignition. Eventually, ignition takes place in the secondary chamber after a delay during which pressure and energy density has risen. Delayed ignition caused by warm combustion products is well documented by several authors (Wolfard and Bruszak 1960; Phillips 1963; Yamaguchi, Ohiwana et al. 1985; Larsen 1998). As shown by (Larsen 1998), jets of moderate velocity will reignite a short distance away from its source causing only a very short ignition delay. This effect is probably present in the majority of the current experiments. For rich hydrogen mixtures flow velocity may be extremely high and turbulence intensity may cause quenching in the whole chamber. This would constitute a qualitative difference in the combustion process as indicated in Figure 5.9. Gas will continue to

flow into the secondary chamber and ignition will not occur before turbulence level drops below some threshold value. As pressure rises and hot combustion products accumulates in the secondary chamber viscosity of the mixture rises rapidly and contributes to a damping the turbulent motion.

5.2.2 Orifice size

Methane

Since orifice regulates flow in and out of the secondary chamber, it plays a crucial role in pressure piling (Brown 1959). The effect of changing orifice diameter can be seen in Figure 5.10. It is the 5,6mm orifice that gives the maximal pressure difference regardless of size of the primary chamber. This is of course caused by the fact that the secondary chamber is the same in all tests, and that outflow from this chamber controls peak pressure. For 4mm holes quenching occurred in all geometries. For large-scale experiments orifice diameters would increase accordingly, and the problem with quenching would not occur. In this situation it would most likely also be a regime in which inflow to the secondary chamber would be the limiting factor.

Evaluation of the pressure time history for tests with different orifices shows that combustion in primary chamber is significantly affected by orifice size. With a small orifice the combustion in primary chamber proceeds almost like in the single chamber and is not significantly affected by what goes on in the secondary chamber. Large orifices results in early secondary ignition with a subsequent reversal in flow direction. The crossing of the two pressure curves in Figure 5.11 indicates the time of flow reversal. Agitation of the gas in the primary chamber accelerates the combustion process and altogether the course of the whole explosion proceeds more rapidly.

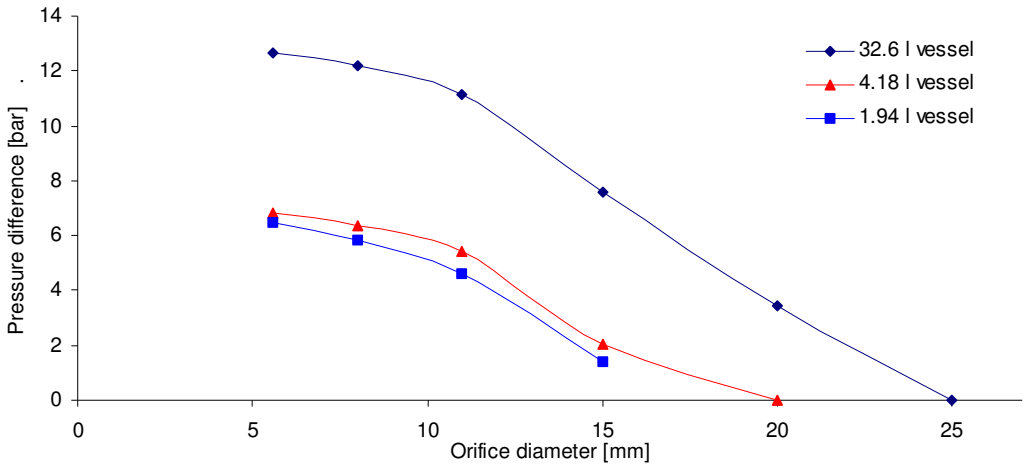

Figure 5.10 *Pressure difference as function of orifice diameter for stoichiometric equivalent methane mixtures.*

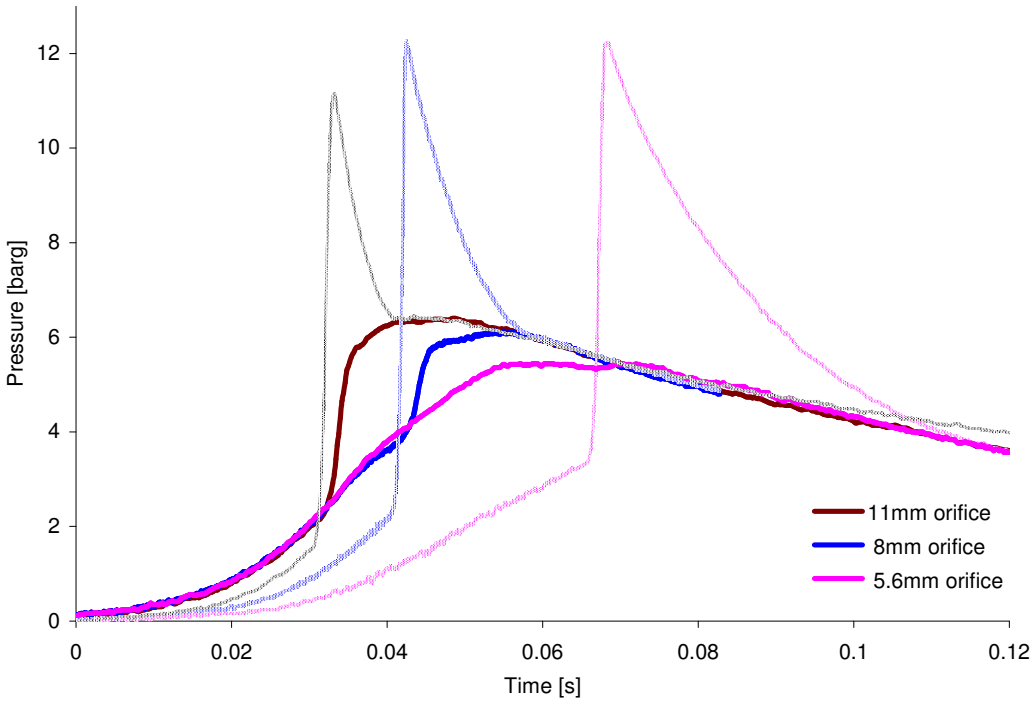

Figure 5.11 *Pressure-time history for three tests with different orifice sizes. Thick lines represent pressure in primary chamber and thin lines in secondary chamber. 4.18 litre vessel. Fuel: methane.*

Hydrogen

Figure 5.12 shows pressure difference as function of orifice diameter. In general the pressure piling in the strict meaning did not occur in the two smallest geometries and the values given in Figure 5.12 are perhaps less representative for the actual level of pressure piling. However all vessel show a similar trend with the curves having a pronounced maximum value. Compared to similar data for methane this indicates that both flow into and out of the secondary camber are limiting factors.

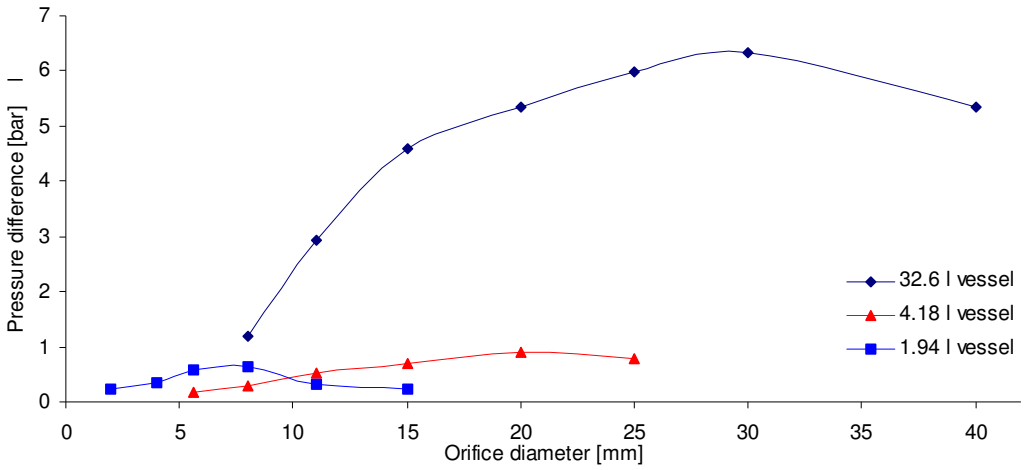

Figure 5.12 *Pressure difference as function of orifice diameter. Fuel: Hydrogen, stoichiometric equivalent mixture.*

5.2.3 Volume ratio

Methane

Figure 5.13 shows the effect of volume ratio on maximum pressure in secondary chamber, and as expected there is a dramatic rise in maximum pressure with increasing volume ratio.

In order to provide more plots in Figure 5.13, an extra test series was conducted in a 7.57 litre vessel. The length to diameter ratio for this vessel was 2.6, which is about twice the value of the other vessels configurations. Due to geometrical confinement of the flame sphere this vessel had a slightly lower rate of pressure rise in primary chamber that should give a slightly lower maximum pressure. The error caused by vessel shape is expected to be quite small compared to the effect of volume ratio. Tests conducted in this vessel are marked with transparent colours in Figure 5.13.

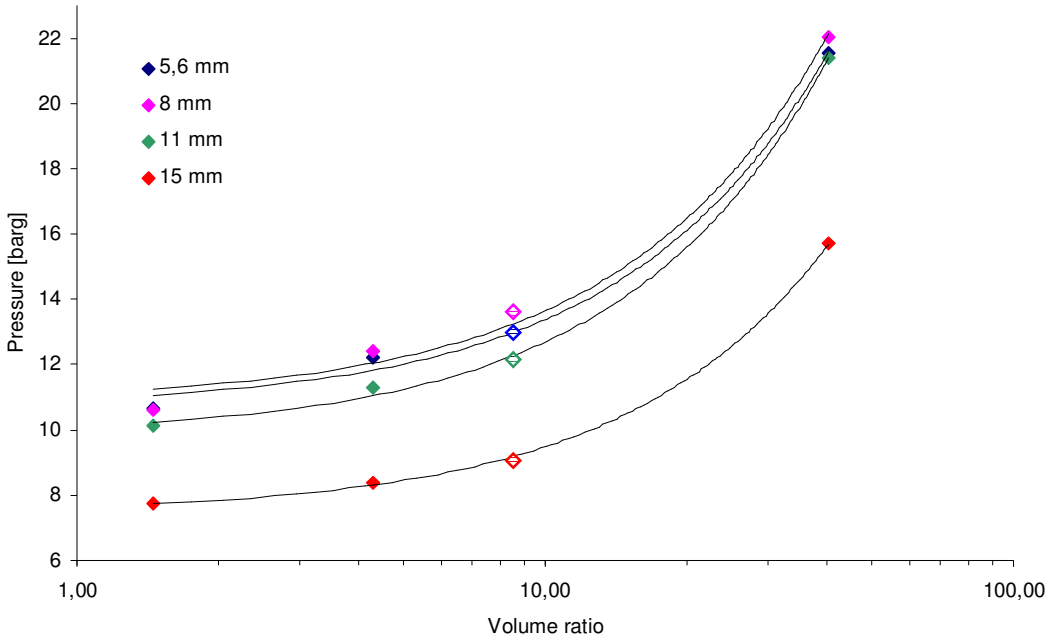

Figure 5.13 *Maximum pressure in secondary chamber. Fuel: Methane.*

The explanation for the strong dependency of volume ratio is twofold: First the larger scale of the primary chamber result in a longer time gap between primary and secondary ignition, and during this time gap more chemically bound energy will be transferred to the secondary chamber. Secondly the higher volume ratio will in it self result in higher compression of the gas in the secondary chamber. This effect was discussed in chapter 2 and presented in Figure 2.1. Figure 2.1 is based on a few very coarse simplifications, such as late secondary ignition and complete pressure equilibrium prior to secondary ignition. For this reason the pressure levels indicated in Figure 2.1 are obviously erroneous but the general trend should be more or less correct: For very small volume ratios, maximum explosion pressure must asymptotically approach single chamber explosions. For very high volume ratios, preignition pressure would be equivalent to single chamber vessel and with a very small orifice, secondary pressure would roughly be eight times as high. Consequently maximum pressures should asymptotically approach a value of about 64 bar.

Hydrogen

Figure 5.14 shows maximum explosion pressure versus volume ratios of stoichiometric equivalent hydrogen mixtures. Compared to Figure 5.13, the trend lines in Figure 5.14 converges toward the same pressure for low volume ratios. Due to a quicker secondary ignition, the level of pressure piling is reduced and hence pressures converge. With reference to Figure 2.1 the curve segments for hydrogen (Figure 5.14) would be located further to the left than the curve segments for methane (Figure 5.13).

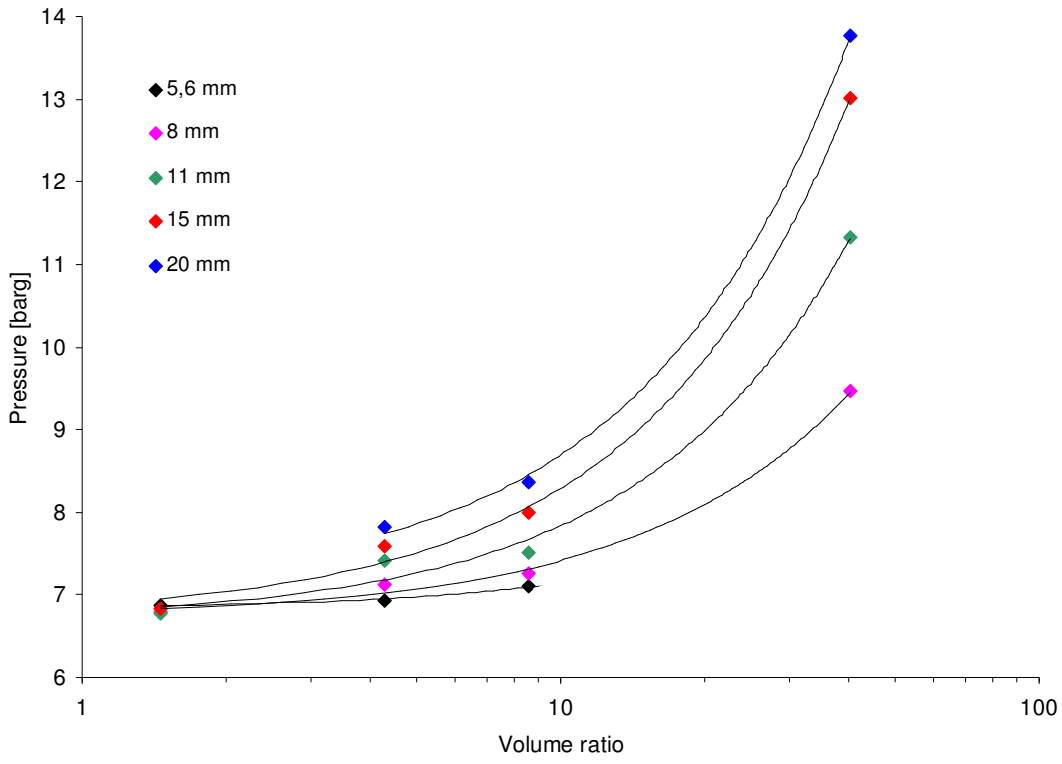

Figure 5.14 *Maximum pressure in secondary chamber. Fuel: Hydrogen.*

5.3 Oblong vessel tests

The experiments discussed in Chapter 5.2 referred to tests in which the primary chamber had low length to diameter ratio and ignition took place close to the vessel centre. Short distance between ignition point and orifice meant little time for transfer of energy between the chambers and relatively low explosion pressures. For the tests that will be discussed in this chapter, the

intention has been to reduce this effect. Testing has been carried out with oblong vessels and ignition point as far from the orifice as possible. Diameter of the primary chamber was 15 cm and the length was varied between 40 an 80 cm. The secondary chamber has been the same as in the tests above (0,79 litre). Within the limits of the current test apparatus, these tests are assumed to represent worst-case situations.

5.3.1 Gas concentration and vessel length

Methane

Figure 5.15 shows maximum explosion pressures for the two vessels. Difference in maximum pressure for the two geometries is moderate. Investigation of pressure curves shows small pressure differences between the two chambers at the time of secondary ignition. For the longest vessel, the time gap between primary and secondary ignition is long and assures almost complete pressure equilibrium between two chambers. Longer distance between ignition point

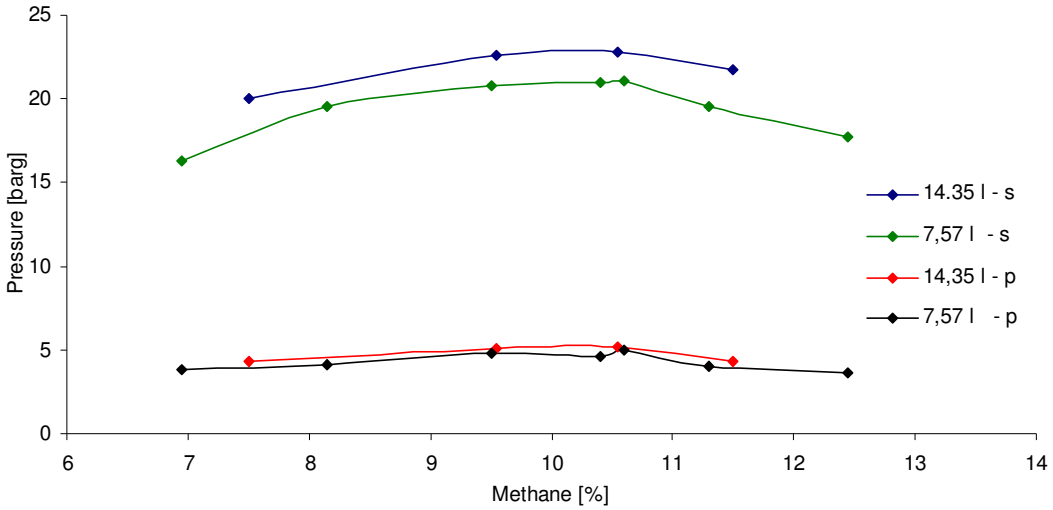

Figure 5.15 *Peak pressures for primary and secondary chamber (Methane, orifice diameter: 8mm).*

and orifice would not result in higher pressures and this " time span" would not be a limiting factor. For the longest vessel, the factor deciding maximum pressure is outflow from the secondary chamber.

For the short vessels the pressure curves show small pressure differences between primary and secondary pressure. Prior to secondary ignition, a smaller amount of chemically bound energy is transferred to the secondary chamber and consequently peak pressure is slightly lower.

However, the differences are very small and indicate that the "time span" factor is limited also for the shorter vessel. Figure 5.16 show examples of pressure curves for two selected mixtures. From the figure it should be noted that the time the flame front uses to reach the orifice is not twice as long for the long vessel even though the actual distance is. Both volume expansion and turbulence will affect primary combustion and flame propagation in primary chamber is not entirely laminar in these tests.

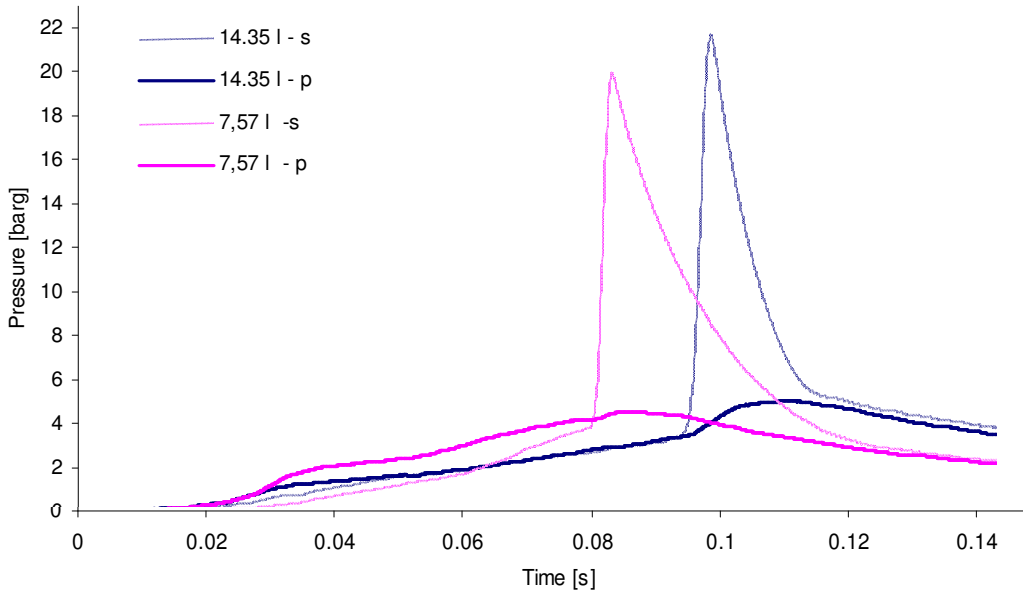

Figure 5.16 *Pressure curves for two different vessel lengths.*

Hydrogen

Figure 5.17 shows maximum pressure for oblong vessel tests with hydrogen. The pattern seen in the figure, with higher pressure piling tendency for rich and lean mixtures, have some resemblances with result presented in Chapter 5.2 (Figure 5.6). Investigation of pressure curves show that quenching does not occur in the current tests.

Examination of the pressure curves indicate that the relative high maximum pressures for lean mixtures are caused by a slow combustion in primary chamber and a rapid combustion in the secondary chamber. Or in other words: a high ratio between turbulent and laminar burning velocity.

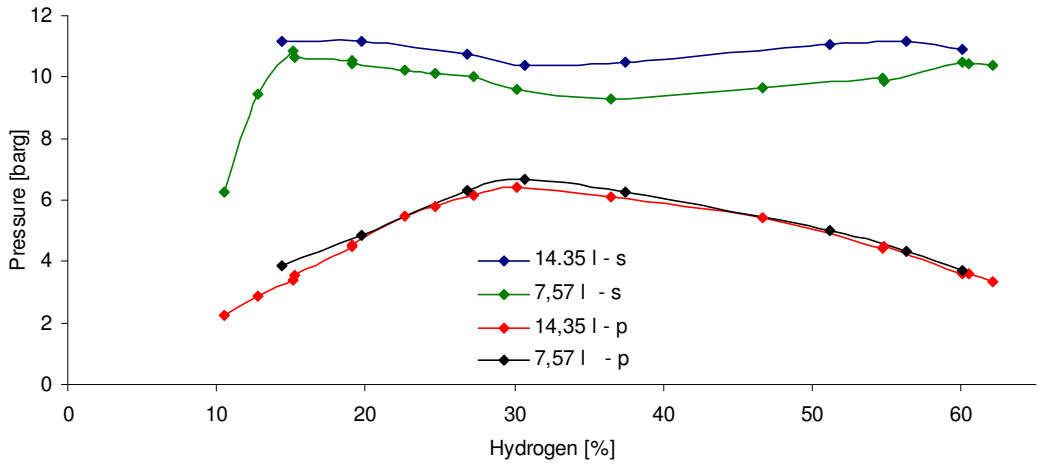

Figure 5.17 *Peak pressures for primary and secondary chamber (Hydrogen, orifice diameter: 8mm).*

Level of pressure piling is also high in rich mixtures, which is caused by the flow properties of the mixture. Pressure curves for a rich and lean mixture is presented in Figure 5.18 and shows that secondary ignition takes place much quicker in the rich mixture. Still, pressures in the secondary chambers at the time of secondary ignition are almost the same in the two tests. Or in other words almost equal amounts of gas are transferred into the secondary chamber but the time in which it happens differs with a factor of almost two.

As seen from the two upper curves in Figure 5.17, there is only a moderate difference in maximum pressure between the two vessels. Flame propagation is enhanced by gas expansion and interactions with the wall (turbulence), and the time the flame needs to burn through the

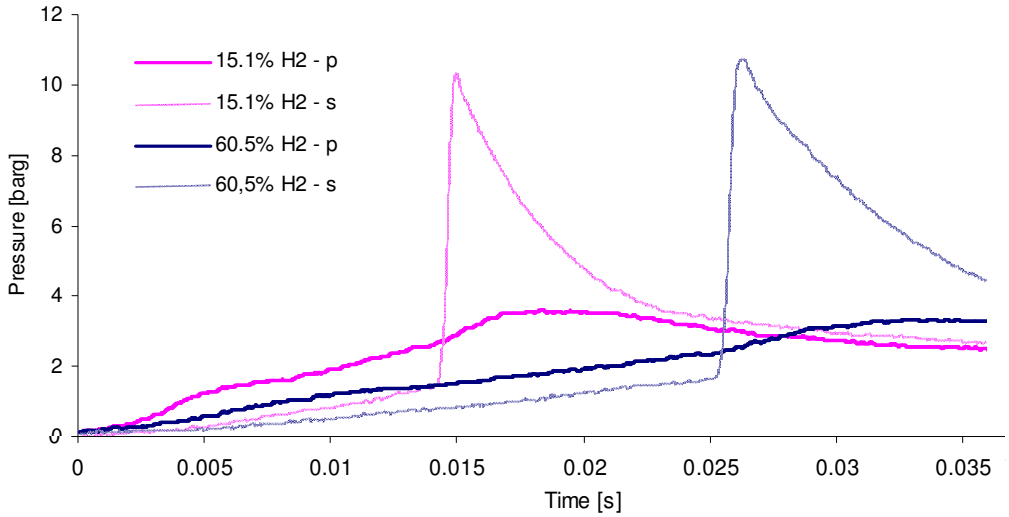

Figure 5.18 *Pressure curves for two different mixtures. (7,57 l vessel, orifice diameter: 8mm).*

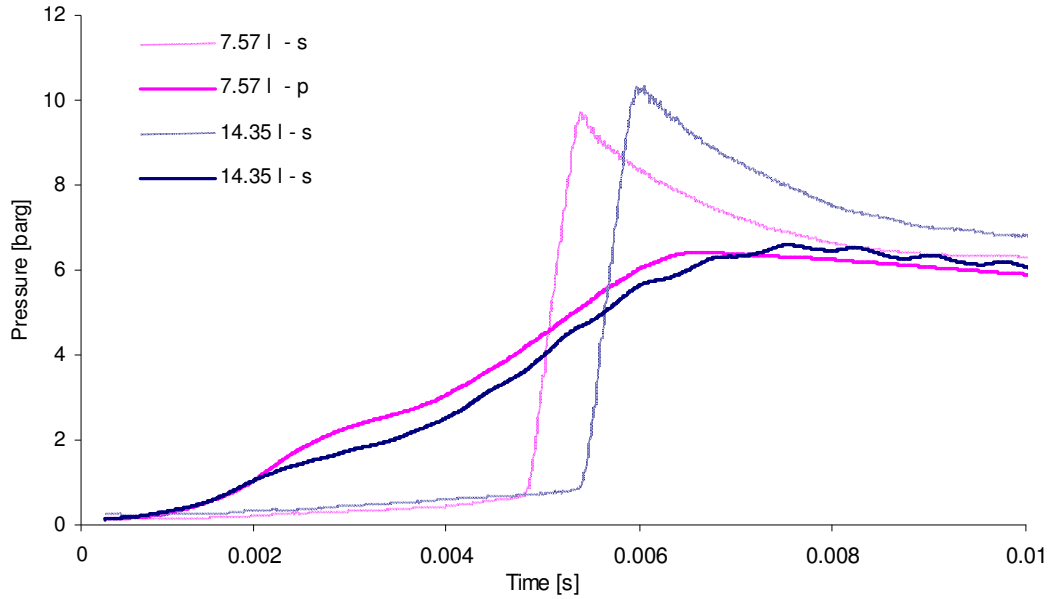

Figure 5.19 *Maximum pressure in secondary chamber. Fuel: Hydrogen.*

primary chamber is not directly proportional to its length. As can be seen in Figure 5.19, rate of pressure rate in primary chamber differs slightly in the initial phase. After a about 0,05 seconds a bump on the pressure curves indicate that the flame ball is confined by the outer walls of the vessel. After about 10 milliseconds the rate of pressure rise is slightly higher in the longest vessel and indicates a higher combustion rate due to more turbulence or flame wrinkling. Adding more length to the Primary chamber would enhance this effect giving only slightly less time for pressure to build up in the secondary chamber. Even if the chamber was made very long, pressure equilibrium between the to chambers might not occur, and consequently the level of pressure piling would be limited. Making the tube radically wider would reduce flam acceleration due to the wall but would also give a higher rate of pressure rise since there would be less geometrical confinement.

Altogether this indicates that it will be very difficult to find a geometry in which pressure equilibrium between the chambers can be achieved. Hence there would be more difficult to achieve a high level of pressure piling. Obviously pressure equilibrium could be achieved with a larger orifice but larger orifice would also mean more efficient back venting. For high pressures to occur in the secondary chamber with large vent opening (orifice) into the premier chamber, the combustion rate would have to be extremely fast. But as already discussed quenching mechanisms bound the rate of fuel consumption in turbulent combustion. At some point there will be a limit to how fast secondary combustion can become. If this limit is met before pressure

equilibrium can be achieved, the level of pressure piling will be reduced. Or in other words: it will not be possible to reach the "optimal "conditions for pressure piling.

5.3.2 Orifice size

Methane

A series of tests with different orifice size was also conducted for the oblong vessel and the result is shown in Figure 5.20. The curve for the 7,57 litre vessel is very similar to the corresponding plots for vessels with lower length to diameter ratio (Figure 5.10). The "flattening" of the curve for small orifices indicate that in flow to the second chamber is a

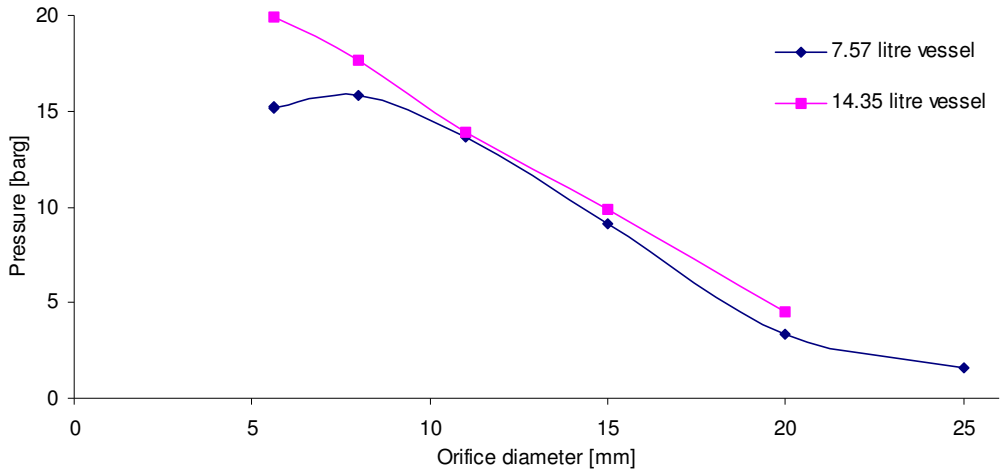

Figure 5.20 *Pressure difference as function of orifice diameter for stoichiometric equivalent methane mixtures.*

limiting factor. For the long vessel (14.35 litre) more time is available to reach pressure equilibrium resulting in higher level of compression in the secondary chamber. Consequently, maximum pressure with the smallest orifice is significantly higher for the long vessel.

Hydrogen

Figure 5.21 shows pressure difference as function of orifice diameter for stoichiometric equivalent hydrogen mixtures. The curves indicate that optimal orifice diameter for pressure piling is about 25 mm for the 7.57 litre vessel and a little less for the 14.35 litre vessel. Explosion pressure in the two vessels differs significantly and evaluation of the pressure time

curves show that the higher pressures in the longest vessel is caused by a higher level of pre compression in secondary chamber prior to flame arrival.

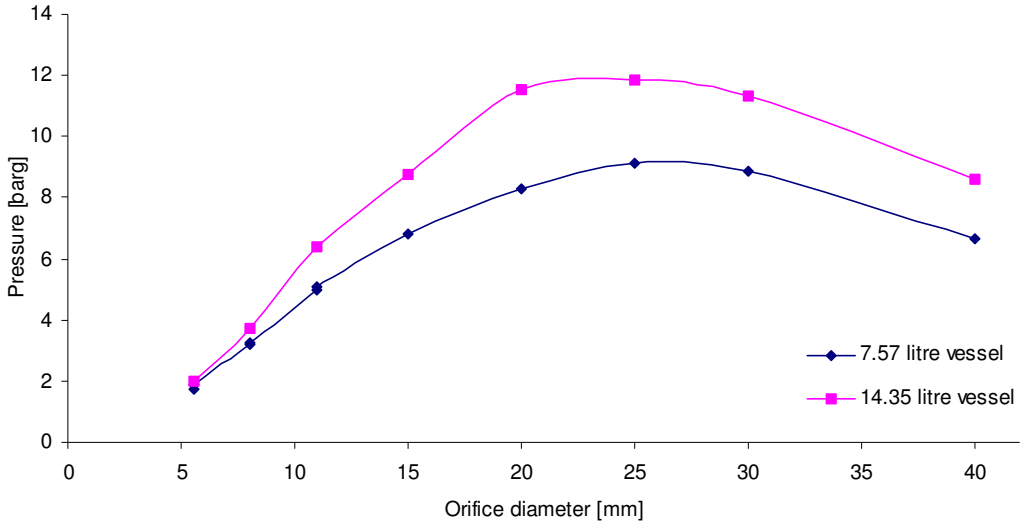

Figure 5.21 *Pressure difference as function of orifice diameter for stoichiometric equivalent hydrogen mixtures.*

5.3.3 Number of orifices

Several tests series were carried out to see if multiple of orifices had any effect on level of pressure piling. The purpose of these tests was to investigate the effect of altered flow pattern and the spatial distribution of turbulence in the secondary chamber. As commented in Chapter 3, turbulent burning velocity is frequently seen as a function of turbulent length scale. Turbulent length scale is tied to the geometrical dimension of the system, and by altering orifice dimension, the turbulent length scale in the jet would also be altered.

All tests in this chapter were conducted in the 14.35 litre oblong vessel as this vessel configuration had a record of giving the highest level of pressure piling.

Methane

Figure 5.22 shows maximum pressure in secondary chamber as function of the cross sectional area of the orifice. As can be seen in the figure, tests with 7 orifices give consistently lower pressures. Comparing test only on basis of the cross-sectional area of orifices is obviously somewhat misleading as flow resistance between the two chambers is not purely a function of

this quantity. Flow resistance will be higher for many small orifices than for a single large orifice since a larger portion of the gas will be flowing closer to the orifice walls. If this argument is valid it means that the blue curve in Figure 5.22 should be shifted leftward to represent a lower "effective orifice area ", and the differences between the two curves would be less.

Regrettably the curves in Figure 5.22 does not show a defined maximum and it is therefore difficult to draw any conclusions about how or if flow pattern and turbulence distribution affects pressure in the secondary chamber.

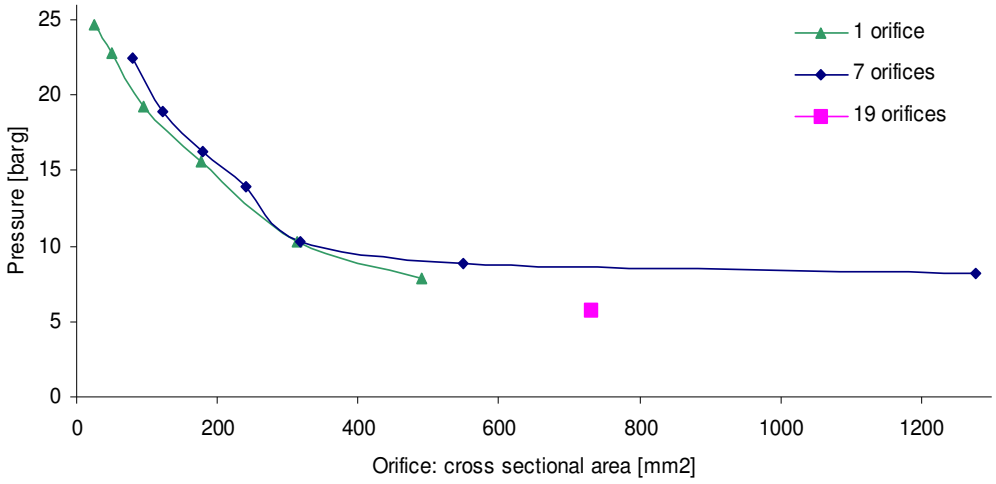

Figure 5.22 *Maximum pressure in secondary chamber as function of the cross sectional area of the orifice.*

Hydrogen

The curves in Figure 5.23 do show defined maximum values and the tests with numerous orifices generally give lower pressures. Investigation of the pressure curves does not present any satisfactory explanation for the pattern. The intention behind this test was in part to look for any indication that the turbulent burning velocity had been changed. Exchanging one large orifice with several small will presumably alter the turbulent length scale in the secondary chamber and thereby turbulent burning velocity (see equation 3.20 and 3.21). Evidently, the precision level in the current experiments was too low to register any such effect.

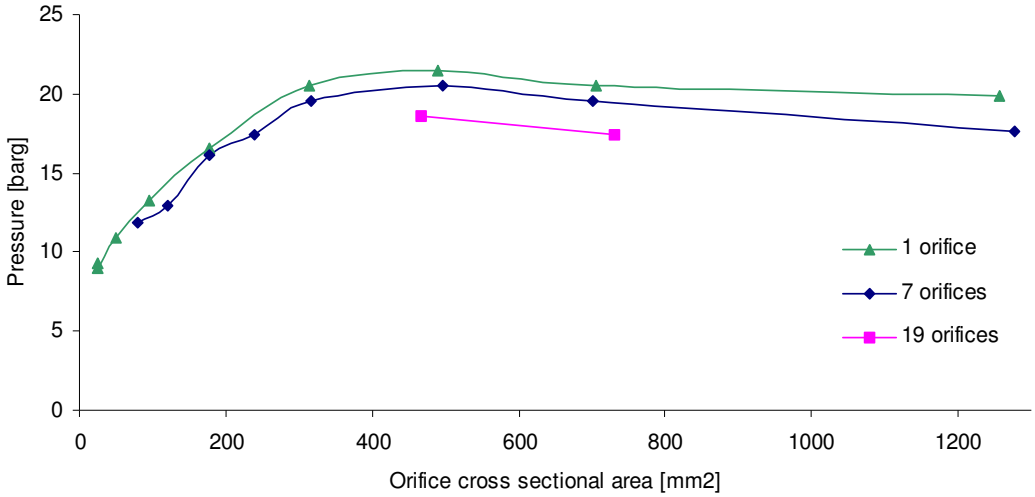

Figure 5.23 *Maximum pressure in secondary chamber as function of the cross sectional area of the orifice.*

Test in the oblong vessels and especially in the long one, result in quite messy pressure curves. These explosions can be characterized as highly dynamic and it is believed that spatial pressure variations may occur in the secondary chamber. Local elevation of pressure might occur when small eddies burn to fast for the pressure to be evenly distributed in the secondary chamber. Such an argument would indicate that local gas expansion might approach the speed of sound, which seems somewhat questionable. (Although as seen in Figure 1.1 burning velocity can become very high towards the late stage of closed bomb experiments). Although it does present an explanation for the messy curves, this argument seems somewhat speculative. Nevertheless, to enable comparison, the messy curves must be smoothened and the smoothening operation may affect different test slightly different. From the pressure curves it may look like the multiple orifice tests are slightly less messy, indicating a more uniform pressure distribution. Consequently the explanation for the differences seen in Figure 5.23 may partly be caused by the smoothening operation.

5.3.4 Shape of orifice

A few more tests were conducted to further investigate the effect of altered flow pattern in secondary chamber. Several tests were carried out with convex orifices. In addition to this a small metal disk was mounted about 1centimeter away from the orifice opening in the secondary chamber. The purpose of this disc was to diverge the jet and possibly cause more

uniform turbulence intensity and more efficient secondary ignition. However none of these tests gave significantly higher pressure in the secondary chamber. Consequently shape of orifice seems to have no impact on pressure piling.

CHAPTER 6

FLACS simulations

Predicting explosion pressures in pressure piling situations is a highly challenging task even for the most sophisticated CFD code. The predictive capability of such codes depends largely on the accuracy of which various parameters can be represented. Laminar burning velocity, turbulent burning velocity, turbulent flow field, flow characteristics of the medium and the orifice must all be modelled with high level of precision if success are to be achieved.

6.1 Single chamber simulations

Figure 6.1 show simulated and experimental values for single chamber (1.15litre) explosion with hydrogen as fuel. In the FLACS version used, the ability to simulate heat loss is limited to heat loss through radiation. Pink curve in Figure 6.1 show simulated explosion with heat loss and blue curve show adiabatic pressure. Obviously, heat loss trough radiation, as modelled in FLACS, does not have significant impact on peak pressure for hydrogen combustion. The small effect must be attributed to the short time span in which heat can escape, and the low emissivity of the chemical species involved. Corresponding figure for Methane (Figure 6.2) show that heat loss through radiation is considerable, especially for rich mixtures. In experiments, radiation will be much larger for rich mixtures due to the formation of soot, which have high emissivity. Soot formation is not incorporated into FLACS, and in simulations, the increased radiative losses in rich mixtures is associated with higher content of methane.

Although heat loss as modelled in FLACS, has moderate impact on peak pressure, Figure 6.3 and Figure 6.4 indicate that the heat loss in the later stage of combustion is fairly well represented (In Figure 6.3 and Figure 6.4: note the gradients of the after peak pressure has been reached).

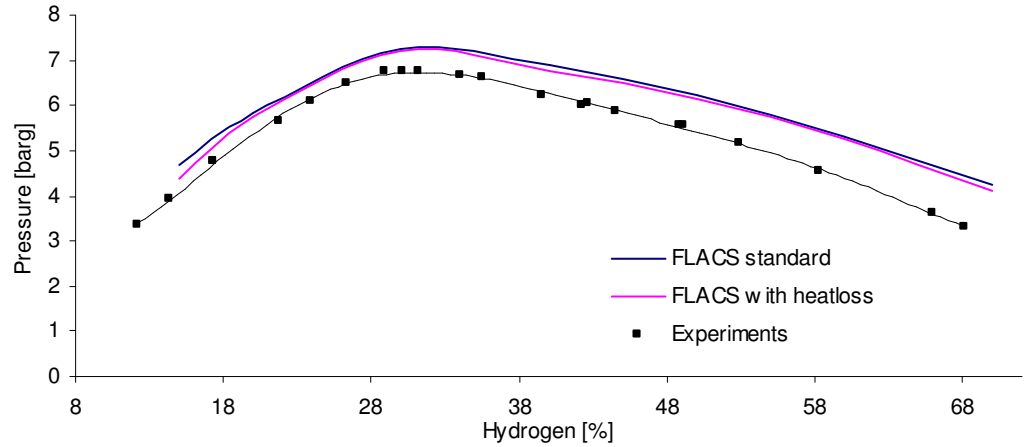

Figure 6.1 *Simulated and experimental explosion pressure in single chamber vessel: hydrogen.*

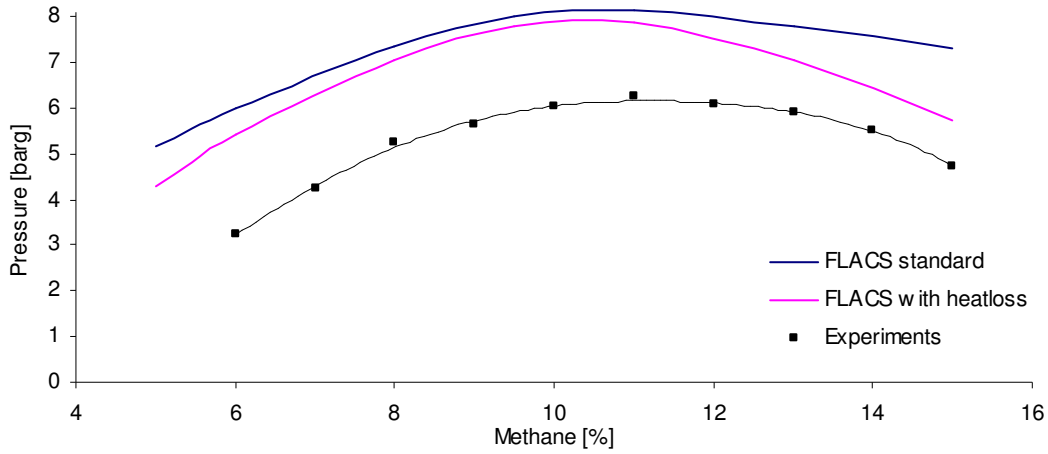

Figure 6.2 *Simulated and experimental explosion pressure in single chamber vessel: methane.*

Comparison of pressure curves from simulations and experiments show large differences in the rate of pressure rise. Figure 6.3 and Figure 6.4 show experimental and simulated pressure curves for methane and hydrogen. Calculation of flame velocity by equation 3.10 gives approximate values for laminar burning velocity of about 5.5m/s for hydrogen and 0.7m/s for methane (stoichiometric equivalent mixtures), while experimental values (Chapter 5) are approximately 2.7m/s and 0.25m/s. Consequently both calculations and experiments indicate that FLACS over predicts burning velocity in explosion of this scale. A closer look at the simulation results show that FLACS wrongly predicts a significant turbulence level inside the flame sphere. This results in a too high burning velocity and a too early flame arrival in the secondary chamber. Due to the short time span, the amount of gas transferred to the secondary chamber will be to small and thereby causes FLACS to under predict the peak pressures.

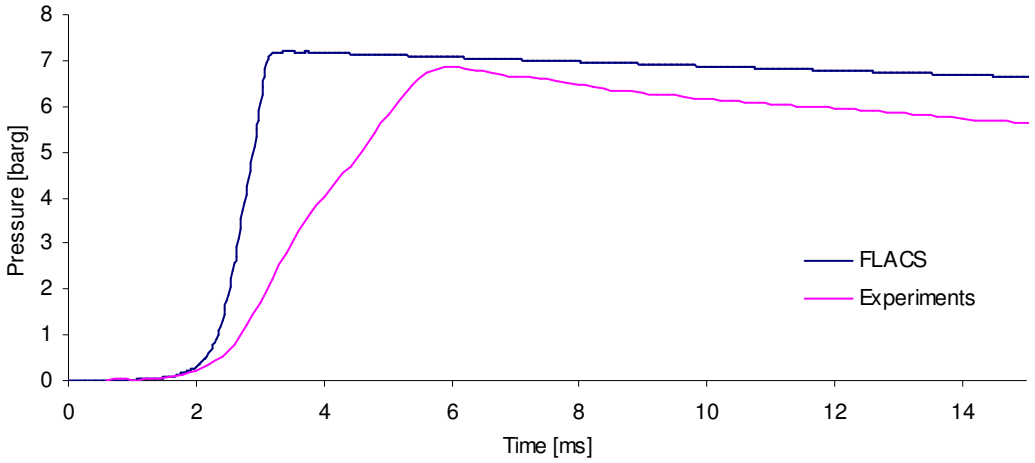

Figure 6.3 *Simulated (blue) and experimental (pink) pressure curves for single chamber explosion with hydrogen.*

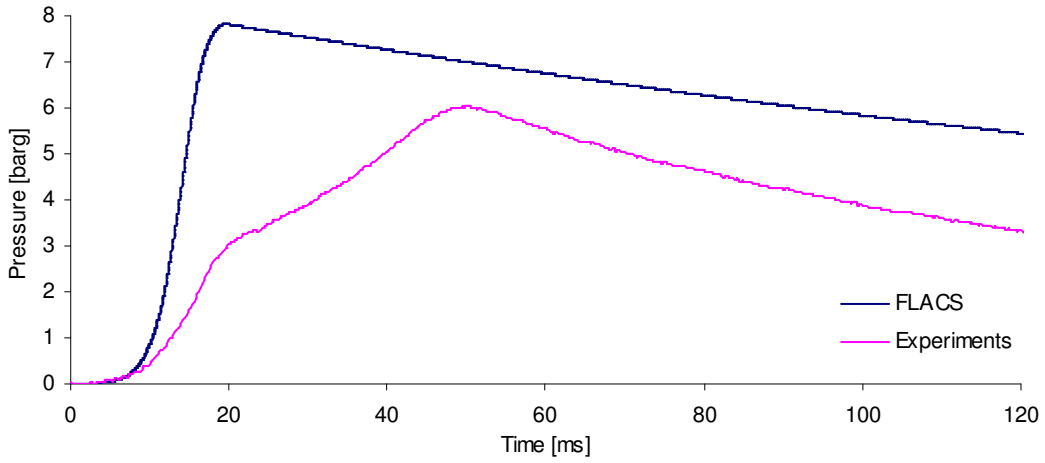

Figure 6.4 *Simulated (blue) and experimental (pink) pressure curves for single chamber explosion with methane.*

6.2 Grid dependency

Grid dependency is a known problem in computational fluid dynamics and time dependent processes such as burning velocity will typically be affected. In pressure piling situations grid dependency will tend to reduce the predictive capabilities of CFD-codes.

In the current study, grid dependency was assessed by repeating simulations with various grid cell sizes. Grid cells were varied from 5-20 mm and grid cells of 5mm gave the fastest combustion. Grid dependency was given a superficial treatment due to lack of time. A wider

investigation of grid dependency in pressure piling situations may be a way to improve the precision level of FLACS. However such a strategy could be founded in a set of well-defined guidelines (ie. criteria's for choosing grid size).

In large geometries with small orifices it is tempting to use grid refinement in the orifice area. Simulations showed that grid refinement, which distorts the grid cells, resulted in quicker flame transfer to the secondary chamber and reduced peak pressure. Consequently grid refinement should not be used these situations.

6.3 Double chamber simulations

Simulations have been conducted for selected range of experiments and reveals that FLACS tend to under predict peak pressure in secondary chamber. Figure 6.5 show results from experiments and simulations with various orifice sizes in the large setup (32.6l).

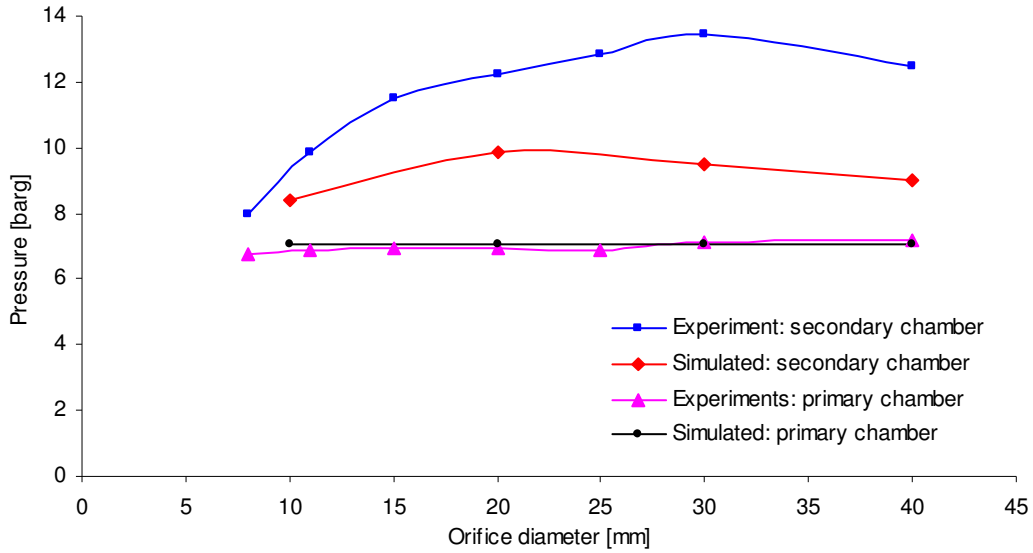

Figure 6.5 *Simulated and experimental results from explosion in large vessel (32.6l) with varying orifice diameter. Fuel: stoichiometric equivalent hydrogen/air.*

Comparison of pressure curves from FLACS and experiments are very similar although peak pressure in secondary chamber diverges. Simulated and experimental pressure curves are shown in Figure 6.6 and Figure 6.7. As noted in Chapter 4 exact logging of ignition time was not possible (due to failure of spark generator) and a correction of start time has been made for Figure 6.7. Consequently only qualitative comparison should be made between the two figures.

Figure 6.6 and 6.7 indicate that rate of pressure rise in secondary chamber is lower in the simulations. This can either be caused by a too slow turbulent combustion in secondary chamber, or a more efficient back venting of pressure ("large orifice"). As seen in Chapter 3 viscous forces and wall friction have a limiting effect on flow close to solid objects (ie. walls in orifice). FLACS does not handle effects like friction or skin drag and this may result in an over prediction of mass flow between the two chambers. This would result in a more rapid accumulation of gas in secondary chamber prior to flame entry and thereby counter the effect of too fast combustion in primary chamber. Over prediction of mass flow would also work the other way and constitute more effective venting of peak pressure in the secondary chamber.

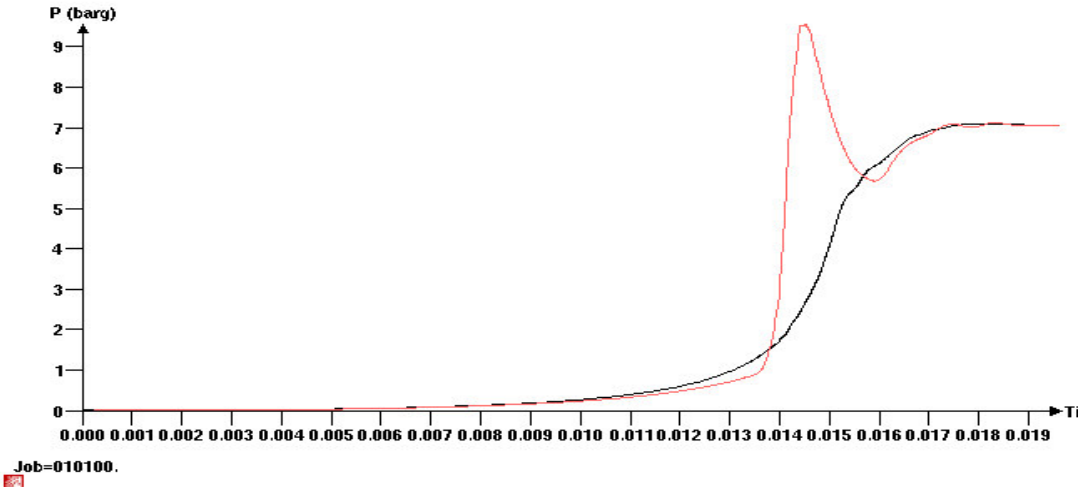

Figure 6.6 *Simulated pressure curves: 32.6l vessel, 30 mm orifice diameter, stoichiometric equivalent hydrogen/air mixture. Red curve show pressure in secondary chamber.*

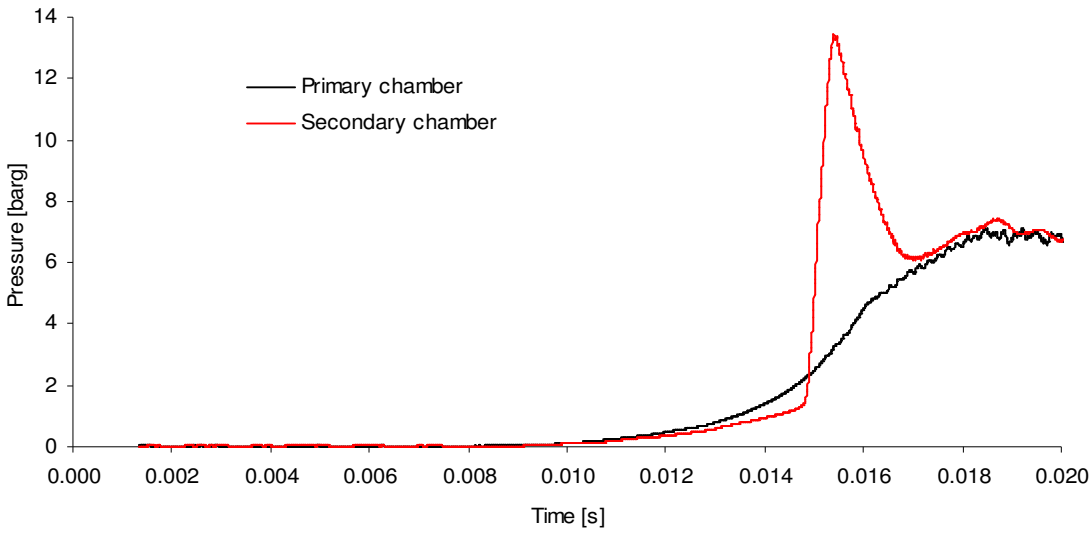

Figure 6.7 *Pressure curve from experiments: 32.6l vessel, 30 mm orifice diameter, stoichiometric equivalent hydrogen/air mixture.*

Simulation of pressure piling with methane as fuel showed similar trends as with hydrogen. That is: a consistent under prediction of peak pressure in secondary chamber. A few exceptions for this general pattern occurred for some very lean methane mixtures where FLACS gave high pressures in the secondary chamber. Figure 6.8 show percentage overpressure in secondary chamber compared to singe chamber values, $p_{p.}$ The pattern seen was representative for all geometries. As the figure show, mixtures close to upper and lower flammability limit tend to give higher levels of pressure piling. This trend was also seen in the experiments.

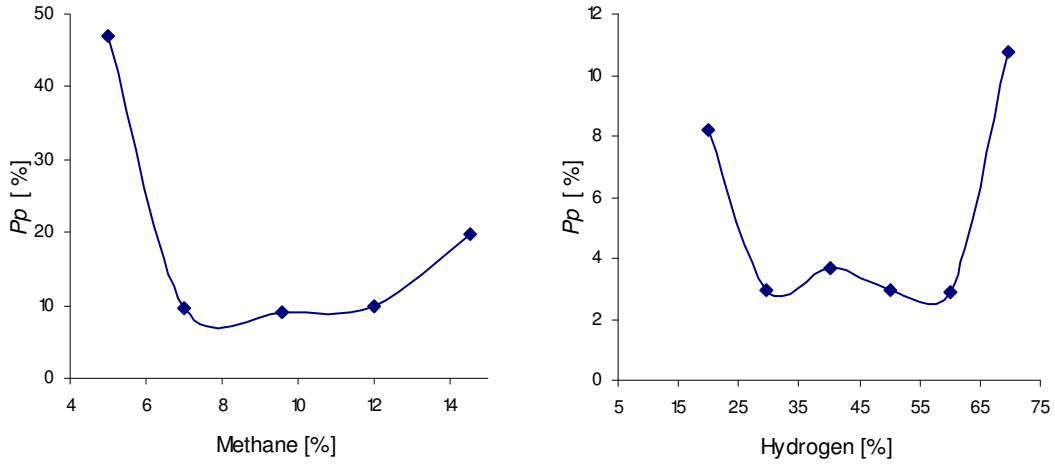

Figure 6.8 *Simulated level of pressure piling, p_p, for 4.18l vessel. 5,6 mm orifice.*

6.4 Turbulence level

As noted in Chapter 5.2.1, rich and lean hydrogen mixtures have very different flow characteristics. This will not only affect the flow rate through the orifice, but also the turbulence level in the secondary chamber. Plots of turbulence for two selected hydrogen mixtures are shown in Figure 6.9. The hydrogen content is 20 % and 60% respectively. The plots are taken at the time of flame arrival at the secondary chamber and correspond to the time of maximum turbulence. As can be seen in the figure, level turbulence is notably higher in the rich mixture. The experimental results in Chapter 5.2.1 showed that rich mixtures were more prone to quenching and that the effect was related to quenching properties of the mixtures (i.e. Figure 3.6). With reference to Figure 6.9 it seems like the higher quenching tendency for rich mixtures also is caused by the flow properties of the mixture itself.

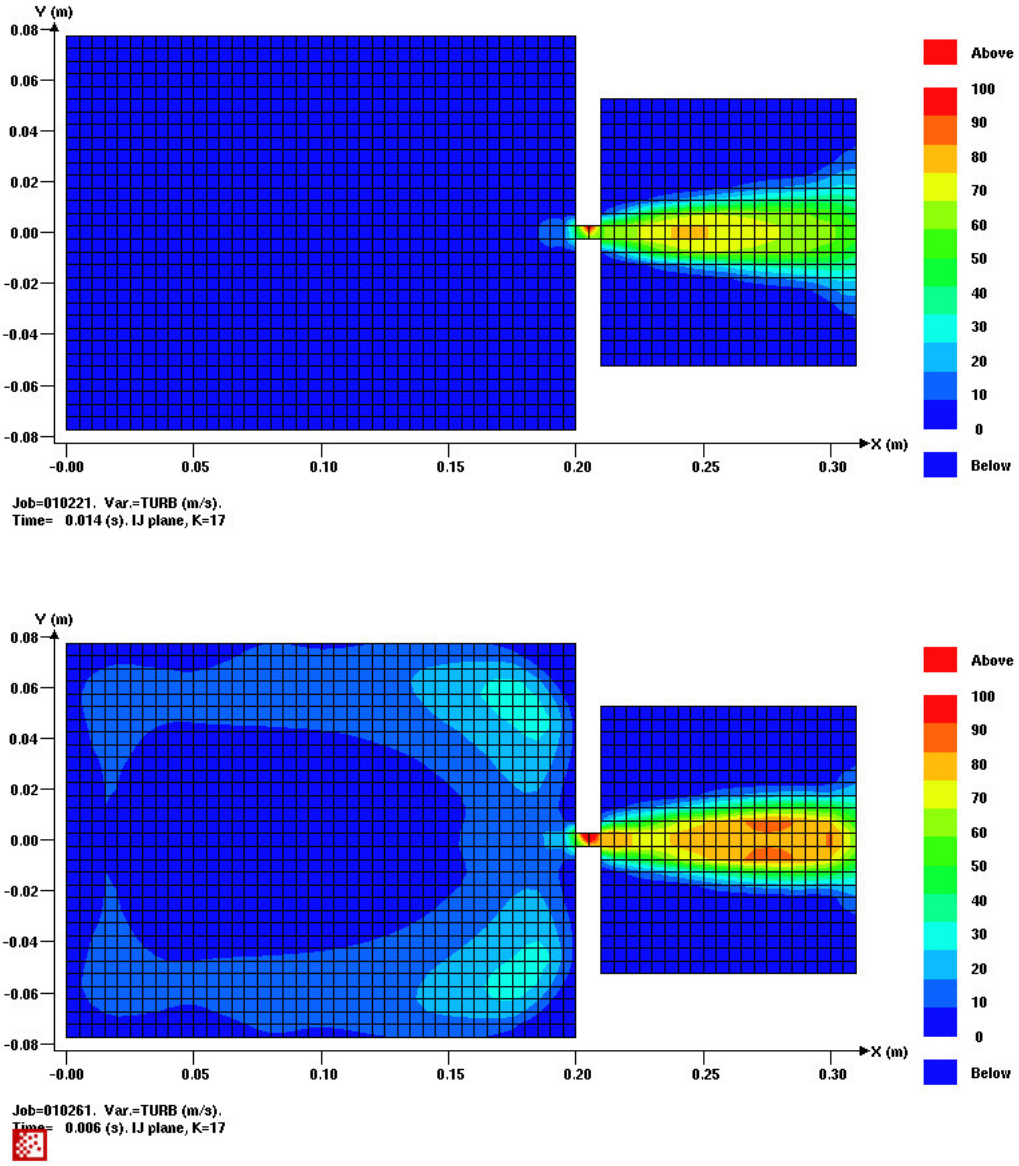

Figure 6.9 *FLACS-plots of turbulence for lean (top) and rich (bottom) mixture.*

CHAPTER 7

Conclusions

Pressure piling is a highly dynamic and complex process. This thesis has attempted to describe and document this very complex matter with very simple methods, i.e. by measuring pressure. Although pressure is the only way to quantify pressure piling, measurement of this single variable has obvious limitations when trying to establish the relevance of some of the underlying physical mechanisms.

One of the initial questions asked was whether a fast burning mixture like hydrogen would be more prone to pressure piling than common hydrocarbon gases. Based on the current work it is difficult to make robust conclusions, but results from experiments imply the same trends:

- In nearly all conducted experiments, methane gave higher peak pressure in secondary chamber than hydrogen. The main reason for this is that methane has a slow laminar burning velocity that causes late ignition in the secondary chamber and high peak pressure. Due to of hydrogen's high (laminar) burning velocity, less time is available for pre compression of the secondary chamber and consequently peak pressures are lower for this gas. This trend is expected to be valid for all geometries resembling the ones used in the experiment, but might not be invalid for large-scale situations.

- For methane, maximum pressure occurs when there is a high "level " of separation or small openings between to distinct volumes. Hydrogen typically gives the highest pressures in more open geometries with less defined volumes.

- For methane, the level of pressure piling is largely independent on fuel mixture. This effect is associated with the ratio of heat released trough combustion and transfer of chemical energy in fluid flow. For methane this ratio does not seem to be much affected by fuel content (equivalence ratio).

The tendency of pressure piling in hydrogen explosions shows some dependency on fuel content:

- Lean hydrogen mixtures appear to be more prone to pressure piling than stoichiometric mixtures. Lean hydrogen mixtures have (like methane mixtures) a relatively low laminar burning velocity and a relatively high turbulent burning velocity. This translates into a late ignition in secondary chamber and an effective compression of the gas therein. Subsequent combustion of this gas is fast and gives high peak pressure.

- For some geometries, rich hydrogen mixtures are more prone to pressure piling than stoichiometric mixtures and the effect is caused by two separate effects:
  -Higher tendency of rich mixtures to quench, which can result in more inflow of reactants into secondary chamber delayed ignition in this chamber.
  -Flow properties of rich mixtures (higher sound velocity) which results in a high transport rate of chemically bound energy.

It should be emphasised that these dependencies on hydrogen content are very geometry dependent. However the points above also serve as exemplification of the following general conclusion:

- Any circumstantial effect or fluid, chemical or geometrical characteristic that tend to delay secondary ignition will also have a tendency to increase peak pressure.

Naturally this conclusion will depend on geometry and will not apply for very slow burning mixtures.

Simulations with the CFD code FLACS has shown that the code predicts the most significant trends in respect to fuel mixtures and geometry. It is also clear that FLACS tend to under predict peak pressure and that this is related to over prediction burning velocity in the laminar regime. This effect is suspected to depend on scale and may not be valid for large-scale simulations.

References

Abdel-Gayed, R. G., D. Bradley, et al. (1984). "Lewis number effects on turbulent burning velocity." Twentieth Symposium on Combustion / The combustion Institute: 505-512.

Abdullin, R. K., V. Babkin, S , et al. (1988). "Combustion of gas in connected vessels." Combustion explosion and shockwaves 24(2): 123-132.

Arntzen, B. J. (1998). Modeling of turbulence and combustion for simulation of gas explosions in complex geometries. Institutt for mekanikk, thermo- og fluiddynamikk. Trondheim, Norges teknisk-naturvitenskapelige universitet.

Baker, W. E., P. A. Cox, et al. (1983). Explosion hazards and evaluation, Elsevier Sientific Publishing Company.

Bartknecht, W. (1981). Explosion: Course, Prevention, Protection. Berlin, Springer-Verlag.

Beyer, M. a. r. t. b. L., Ø. (1997). "Über den Zunddurchslag explodierender Gasgemiche an Gehäusen der Zündschutzart " Druckfeste Kapselung"." Fortschr. -Ber. VDI Reiche21 Nr 228. Dusseldorf:VDI Verlag.

Beyling, E. (1906). ""Tests for Determining the Safety of Specially Protected Electric Motors and Apparatus Against Explosion from Firedamp" (translated)." Gluckauf 42: 129-138.

Bjerkved, D., J. R. Bakke, et al. (1993). Gas Explosion Handbook. Bergen, Christian Michelsen Research AS.

Borghi, R. and M. Destriau (1998). Combustion and Flames. Paris, Editions Technip.

Bradley, D. (1992). "How fast can we burn?" Twenty-Fourth Symposium on Combustion / The combustion Institute: 247-262.

Brown, T. J. A. (1959). Pressurepiling in compartmented vessels. Technical Report D/T 109, The British electrical and allied industrial research association.

Coulson and Richardson (1957). Chemical engineering.

Gaseq http://www.c.morley.ukgateway.net/.

Glassman, I. (1987). Combustion. London, Academic Press Inc.

Gleim, E. J. and J. F. Marcy (1952). A study to determine factors causing pressure piling in testing explosion-proof enclosures. Report of investigations 4904, U S Bureau of Mines.

Grice, C. S. W. and R. V. Wheeler (1929). "Firedamp Explosions within Closed Vessels "Pressure Piling"." Safety in mines Research Board paper no 49.

Griffiths, J. F. and J. A. Barnard (1995). Flame and combustion. Glasgow, Blacie Academic & Proffesional.

Hirschfelder, J. O., C. F. Curtiss, et al. (1954). Molecular Theory of Gases and Liquids. New York, Wiley.

Jost, W. (1946). Explosions and combustion processes in gases. London, McGraw-Hill book company inc.

Kanzleiter, T. F. and K. O. Ficher (1994). "Multicompartment Hydrogen Deflagration Experiments and Model Development." Nuclear Engineering and Design 146(1-3): 417-426.

Kobayashi, H., Y. Kawabata, et al. (1998). "Experimental study on general correlation of turbulent burningvelocity at high pressure." Twenty-sixth Symposium on Combustion / The combustion Institute 1: 941-948.

Kobayashi, H., T. Tamura, et al. (1996). "Burningvelocity of turbulent premixed flames in a high pressure environment." Twenty-sixth Symposium on Combustion / The combustion Institute 1: 389-396.

Koroll, G. W., R. K. Kumar, et al. (1993). "Burning Velocities of Hydrogen-Air Mixtures." Combustion and Flame 94: 330-340.

Kutcha, J. M. (1985). " Investigation of fire and explosion accidents in the chemical mining and fuel related industry." US Bureau Of Mines Bulletin.

Larsen, Ø. (1998). A Study of Critical Dimensiones of Holes for Transmission of Gas Explosions and Development & Testing of a Schlieren System for Studying Jets of Hot Combustion Products. Department of Physics, The University of Bergen.

Lewis, B. and G. von Elbe (1987). Combustion, Flames and Explosions of gases. Orlando, Academic Press Inc.

Lipatnikov, A. N. and J. Chomiak (2002). "Turbulent flame speed and thickness: phenomenology, evaluation, and application in multi-dimensional simulations." Progress in Energy and Combustion Science 28: 1-74.

Liu, D. D. S. and R. MacFairlane (1983). "Laminar Burning Velocities of Hydrogen-Air and Hydrogen-Air-Steam Flames." Combustion and Flame.

Liu, F. and Y. Yoshizawa (1998). "Combustion and Flow of Premixed Lean Hydrogen /air Mixtures in the Connected Compartments." International Journal of Hydrogen Energy 23(5): 373-379.

Lunn, G. A., P. Holbrow, et al. (1996). "Dust Explosions in Totally Enclosed Interconnected Vessel Systems." Journal of Loss Prevention in the Process Industries 9(1): 45-58.

Maremont, M., G. Russo, et al. (1999). "Numerical simulation of gas explosions in linked vessels." Journal of loss prevention in the process industries 12(3): 189-194.

McCabe, W. L., J. C. Smith, et al. (1993). Unit Operations of Chemical Engineering, McGraw-Hill.

Metghalchi, M. and J. C. Keck (1980). "Laminar burning velocity of propane air mixtures at high temperatures and pressure." Combustion and Flames 38: 143-154.

Milton, B. E. and J. C. Keck (1984). "Laminar burning velocity in stoichiometric hydrogen and hydrocarbon mixtures." Combustion and Flames 58: p13-22.

Mosbacher, D. M., J. A. Wehrmeyer, et al. (2000). "Experimental and numerical investigation of premixed tubular flames." 29th International Symposium on Combustion / The Combustion Institute submitted.

Nørsterud, H. (1997). Gassdynamikk. Institutt for mekanikk, thermo- og fluiddynamikk. Tronheim, Norges teknisk- naturvitenskapelige universitet.

Perkins, R. A. NBSIR 84-3006: hydrogen, methane, ethane, and propane.

Peters, N. (2000). Turbulent Combustion. Cambridge, University Press.

Phillips, H. (1963). "On the Transmission of an Explosion through a Gap Smaller Than the Qeunching Distance." Combustion and Flames 7: 129-135.

Phylaktaou, H. and G. E. Andrews (1993). "Gas Explosions in Linked Vessels." Journal of Loss Prevention in the Process Industries 6(1): 15-19.

Poinsot, T., D. Veynante, et al. (1990). "Diagrams of Premixed Turbulent Combustion Based on Direct Simulation." Twenty-Third Symposium on Combustion /The Combustion Institute: 613-619.

Shebeko, Y. N., S. G. Tsarichenko, et al. (1991). Phys. Combust. Explos. 27: 52-56.

Sheperd, J. E., G. A. Melhem, et al. (1991). Unconfined Vapor Cloud Explosions: A New Perspective". International Conference and Workshop on Modeling and Mitigating the Consequences of Accidental Releases of Hazardous Materials. CCPS of AIChE, New Orleans.

Singh, J. (1984). "Gas Explosions in Compartmented Vessels: Pressure Piling." Chem. Eng Res 62.

Singh, J. (1993). "Gas Explosions in Inter-connected Vessels: Pressure Piling." I Chem E Symposium Series No134: 194-212.

Strauss, W. A. and R. Edse (1958). "Burning Velocity Measurements by the Constant-pressure Bomb Method." Seventh Symposium on Combustion / The combustion Institute: 377-385.

Vagelopoulos, C. M., F. N. Egolfopoulos, et al. (1994). "Futher Consideration on the Determination of Laminar Flame Speeds with Counterflow Twin-flame Technique." Twentyfifth Symposium on Combustion / The combustion Institute: 1341-1347.

Veynante, D. and L. Vervisch (2002). "Turbulent Combustion Modeling." Progress in Energy and Combustion Science 28: 193-266.

Warnatz, J., U. Maas, et al. (2001). Combustion. Berlin, Springer-Verlag.

White, F. M. (1994). Fluid Mechanics, McGraw-Hill, Inc.

Williams, F. A. (1985). Combustion Theory. Menlo park, California, The Benjamin/Cummings Publishing Company, Inc.

Wolfard, H. G. and A. E. Bruszak (1960). "The Passage of Explosions through Narrow Cylindrical Channels." Combustion and Flames 4: 149-159.

Wu, C. K. and C. K. Law (1984). "On the Determination of Laminar Flame Speeds from Streched Flames." Twentieth Symposium on Combustion /The combustion Institute: 1941-1949.

Yamaguchi, S., N. Ohiwana, et al. (1985). "Ignition and Burning Process in a Divided Chamber Bomb." Combustion and Flames 59: 177-187.

Appendix

Pressure data The following pages show the peak pressure data for selected test series.

-Pink color refer to secondary chamber

-Unless othervise specified : ignition takes place one vessel diameter awvay from the end of the vessel

Hydrogen:

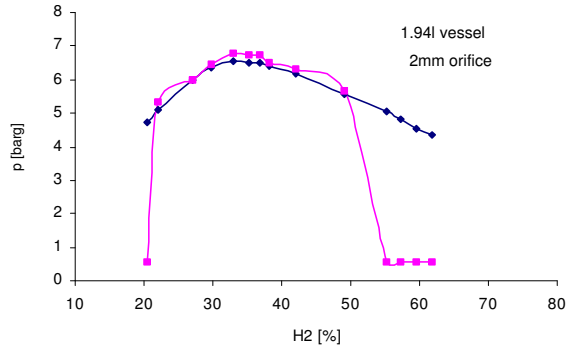

H2	61,71	59,62	57,28	55,28	49,19	42,14	38,09	36,90
p1	4,37	4,56	4,82	5,04	5,57	6,16	6,40	6,50
p2	0,54	0,56	0,56	0,56	5,66	6,32	6,51	6,72

H2	32,86	29,76	27,00	22,14	20,52			
p1	6,56	6,37	6,00	5,12	4,74			
p2	6,80	6,46	5,98	5,33	0,56			

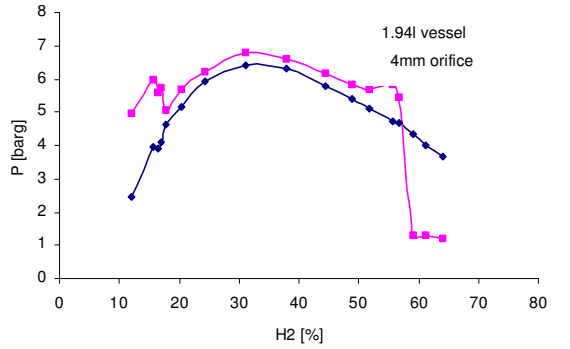

H2	12,00	15,71	16,47	17,05	17,90	20,28	24,28	31,14
p1	2,48	3,94	3,92	4,08	4,62	5,15	5,90	6,43
p2	4,96	6,00	5,57	5,71	5,07	5,66	6,22	6,78

H2	37,95	44,33	48,81	51,86	55,57	56,67	59,00	61,09
p1	6,30	5,76	5,38	5,12	4,72	4,69	4,34	4,02
p2	6,61	6,19	5,82	5,68	5,82	5,44	1,30	1,28

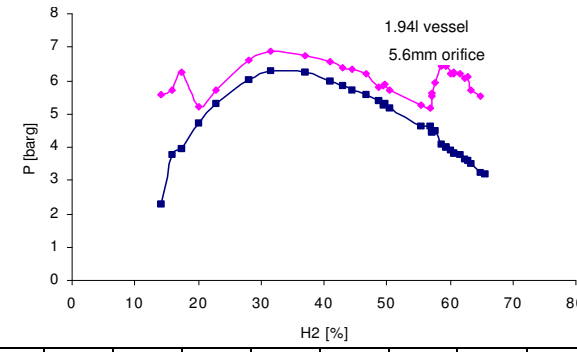

H2	14,28	15,81	17,28	20,14	22,90	28,00	31,62	36,90
p1	2,28	3,76	3,96	4,70	5,29	6,04	6,29	6,26
p2	5,58	5,70	6,24	5,22	5,70	6,59	6,88	6,74

H2	41,09	43,09	44,48	46,81	48,81	49,43	49,81	50,43
p1	5,96	5,82	5,70	5,58	5,38	5,26	5,30	5,18
p2	6,58	6,36	6,34	6,22	5,78	5,86	5,87	5,69

H2	55,33	56,90	57,14	57,24	57,71	58,57	59,28	59,48
p1	4,63	4,62	4,43	4,45	4,50	4,08	4,02	4,00
p2	5,26	5,15	5,51	5,62	5,95	6,43	6,47	6,42

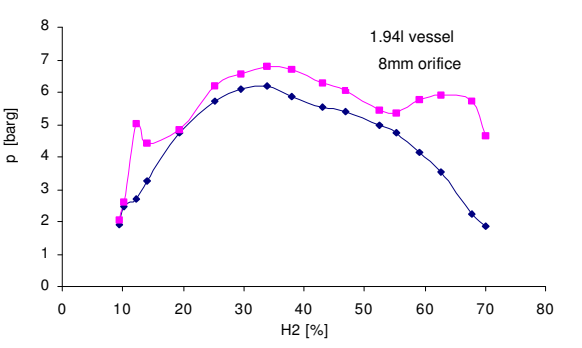

H2	9,38	10,14	12,33	14,09	19,33	25,28	29,62	33,90
p1	1,93	2,48	2,70	3,25	4,73	5,73	6,10	6,16
p2	2,06	2,62	5,01	4,41	4,84	6,19	6,55	6,80

h2	43,00	46,86	52,38	55,24	59,05	62,67	67,76	69,95
p1	5,52	5,40	4,99	4,73	4,14	3,53	2,23	1,87
p2	6,30	6,05	5,46	5,35	5,78	5,89	5,70	4,64

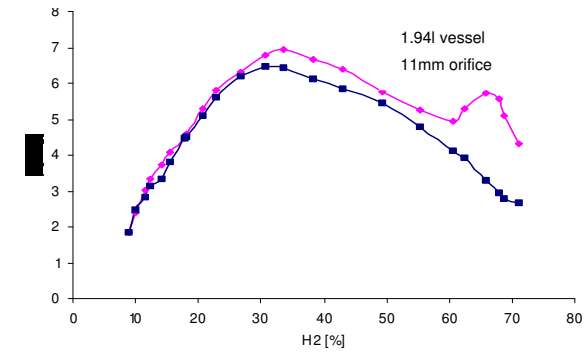

H2	8,95	10,00	11,66	12,33	14,28	15,38	17,86	18,05
p1	1,85	2,46	2,83	3,12	3,35	3,80	4,48	4,52
p2	1,84	2,40	3,02	3,34	3,71	4,09	4,48	4,59

H2	20,62	22,90	26,76	30,62	33,67	38,28	43,09	49,19
p1	5,10	5,59	6,21	6,45	6,44	6,14	5,82	5,43
p2	5,31	5,81	6,31	6,78	6,95	6,66	6,38	5,77

H2	55,24	60,67	62,48	65,71	67,81	68,71	71,00	
p1	4,78	4,12	3,94	3,31	2,92	2,79	2,67	

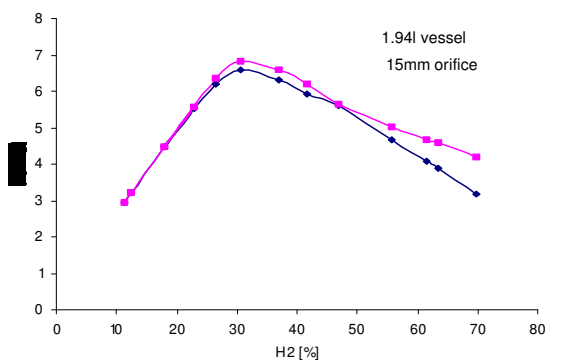

H2	11,38	12,38	22,95	17,90	26,47	30,67	36,95	41,67
p1	2,93	3,21	5,53	4,45	6,18	6,59	6,33	5,94
p2	2,94	3,23	5,55	4,49	6,37	6,83	6,60	6,21

H2	46,86	55,81	61,38	63,38	69,76			
p1	5,59	4,69	4,09	3,89	3,19			
p2	5,65	5,03	4,65	4,59	4,19			

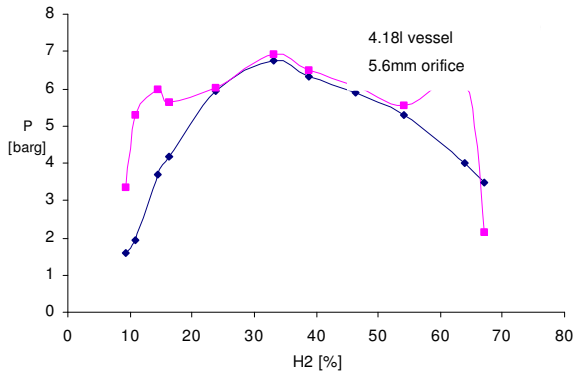

H2	9,28	11,00	14,43	16,28	23,76	33,19	38,86	46,28
p1	1,60	1,92	3,68	4,17	5,93	6,74	6,34	5,88
p2	3,36	5,28	6,00	5,63	6,04	6,93	6,50	6,05

H2	64,05	67,14						
p1	3,99	3,49						
p2	6,16	2,16						

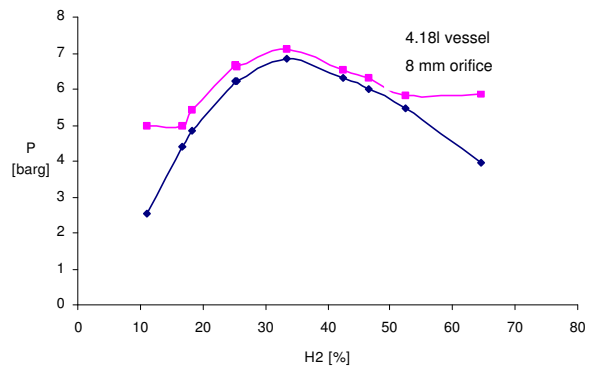

H2	9,14	10,95	16,62	18,33	25,28	25,38	33,33	42,52
p1	1,86	2,55	4,41	4,85	6,21	6,24	6,84	6,32
p2	1,69	4,98	4,98	5,40	6,68	6,64	7,13	6,55

H2	52,52	64,67						
p1	5,46	3,94						
p2	5,80	5,89						

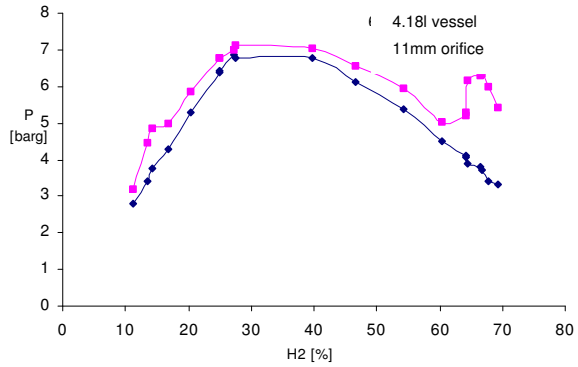

H2	9,28	11,00	14,43	16,28	23,76	33,19	38,86	46,28
p1	1,60	1,92	3,68	4,17	5,93	6,74	6,34	5,88
p2	3,36	5,28	6,00	5,63	6,04	6,93	6,50	6,05

H2	9,28	11,00	14,43	16,28	23,76	33,19	38,86	46,28
p1	1,60	1,92	3,68	4,17	5,93	6.74	6.34	5.88
p2	3,36	5,28	6,00	5,63	6,04	6L vessel 20 mm orifice		

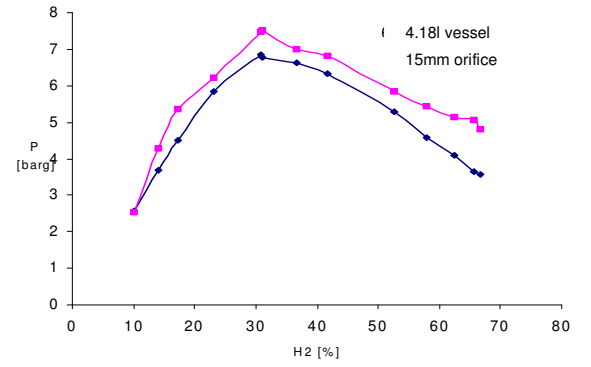

H2	10,14	14,05	17,33	23,19	30,76	31,05	36,71	41,81
p1	2,55	3,69	4,49	5,83	6,85	6,77	6,63	6,31
p2	2,54	4,26	5,34	6,22	7,49	7,40	6,80	6,80

H2	58,00	62,33	65,52	66,67				
p1	4,57	4,10	3,64	3,58				
p2	5,42	5,14	5,05	4,81				

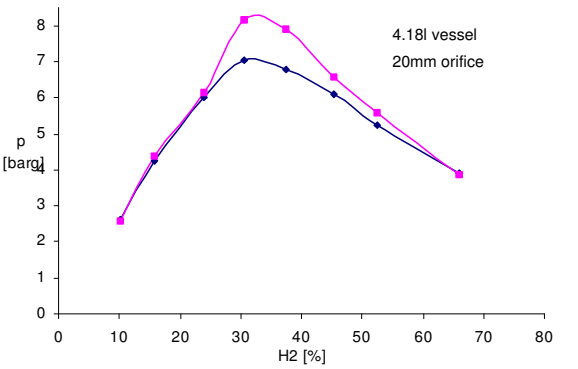

H2	10,28	15,90	24,05	30,47	37,33	45,33	52,48	66,0
p1	2,64	4,24	6,00	7,04	6,78	6,09	5,22	3,89
p2	2,56	4,40	6,13	8,144	7,88	6,58	5,56	3,84

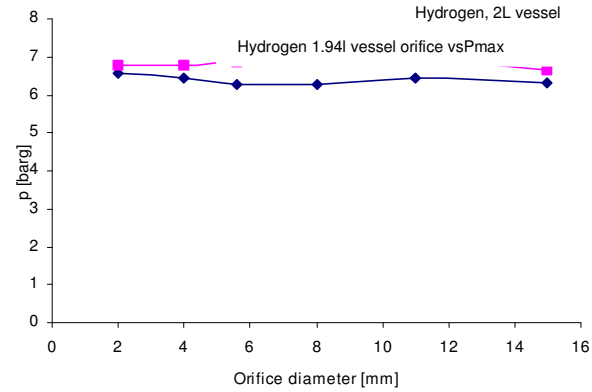

Orifice	2	4	5,6	8	11	15	
p1	6,56	6,43	6,29	6,26	6,44	6,33	
p2	6,80	6,78	6,88	6,90	6,95	6,66	

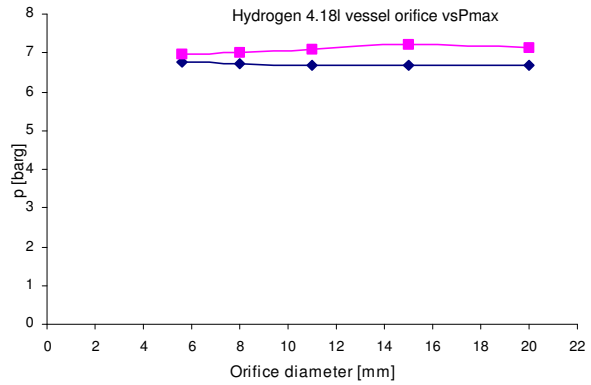

Orifice	5,6	8	11	15	20	25	
p1	6,75	6,74	6,68	6,67	6,69	6,67	
p2	6,98	7,03	7,08	7,20	7,13	6,63	

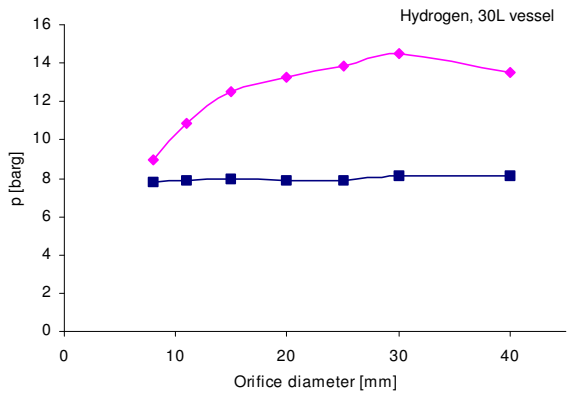

Orifice	8	11	15	20	25	30	40
p1	8,26	8,39	8,42	8,41	8,36	8,64	8,66
p2	9,46	11,33	13,01	13,76	14,34	14,98	13,99

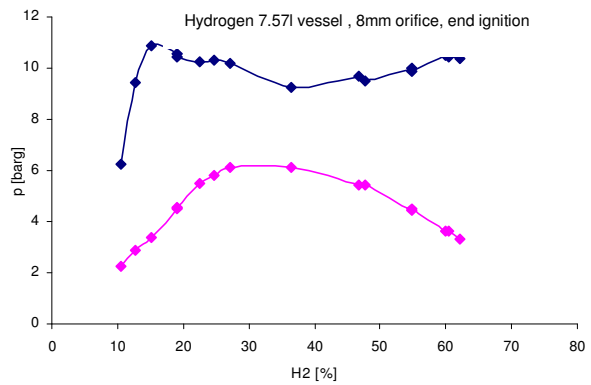

H2	10,47	12,71	15,09	19,09	19,09	22,62	24,71	27,24
p1	2,24	2,88	3,40	4,51	4,56	5,50	5,81	6,14
p2	6,24	9,44	10,87	10,55	10,43	10,22	10,32	10,20

H2	36,43	46,62	47,62	54,71	54,76	60,05	60,48	62,14
p1	6,11	5,44	5,41	4,448	4,49	3,6	3,62	3,33
p2	9,27	9,67	9,52	9,984	9,86	10,5	10,46	10,37

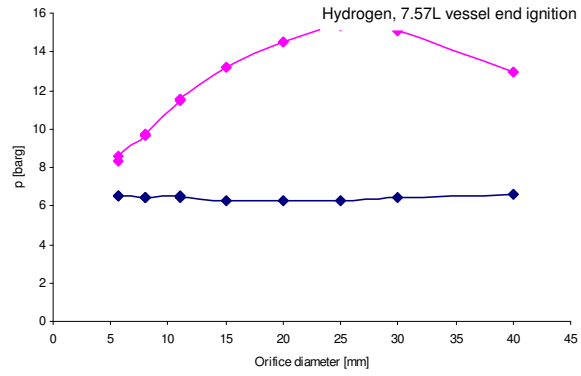

Orifice	5,6	5,6	8	8	11	11	15
p1	6,49	6,49	6,42	6,43	6,51	6,42	6,28
p2	8,33	8,58	9,62	9,69	11,47	11,53	13,18

Orifice	20	25	30	40			
p1	6,23	6,24	6,45	6,57			
p2	14,52	15,35	15,12	12,97			

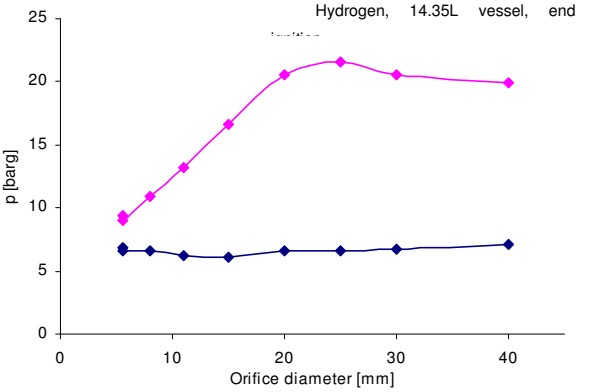

Orifice	5,6	5,6	8	11	15	20	25
p1	6,88	6,63	6,66	6,20	6,15	6,61	6,54
p2	9,34	8,97	10,88	13,23	16,57	20,51	21,63

Orifice	30	40					
p1	6,70	7,12					
p2	20,56	19,90					

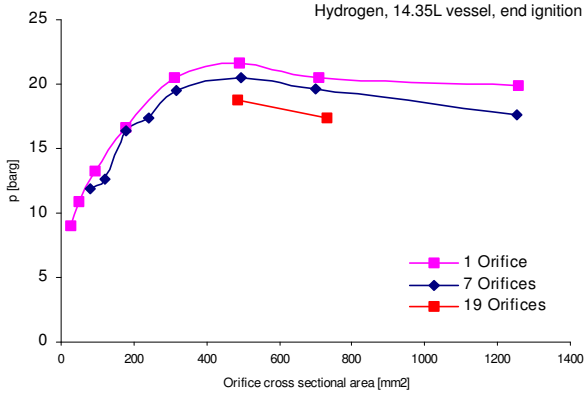

Orifice (1)	5,6	8,0	11,0	15,0	20,0	25,0	30,0	40,0
P1	6,63	6,66	6,20	6,15	6,61	6,54	6,70	7,12
P2	8,97	10,88	13,23	16,57	20,51	21,63	20,56	19,90
Area	24,60	50,3	95,0	176,7	314,2	490,9	706,9	1256

Orifice (7)	3,8	4,7	5,7	15,0	20,0	25,0	30,0	40,0
p1	6,66	6,38	6,48	6,15	6,61	6,54	6,70	7,12
p2	11,87	12,63	16,33	16,57	20,51	21,63	20,56	19,90
Areal	79,3	121,4	178,5	176,7	314,2	490,9	706,9	1256

Methane

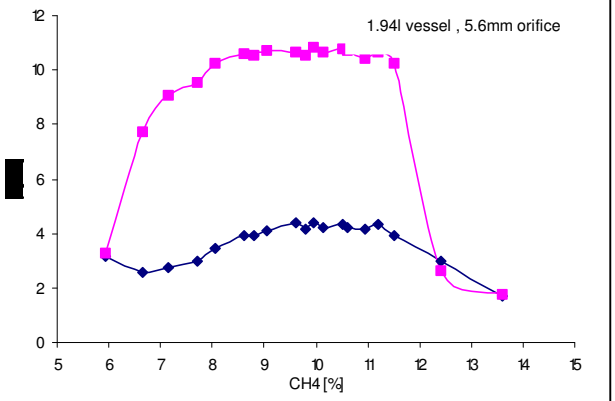

CH4	5,95	6,65	7,15	7,70	8,05	8,60	8,80	9,05
p1	3,18	2,56	2,74	2,96	3,44	3,92	3,94	4,11
p2	3,30	7,74	9,09	9,55	10,22	10,57	10,51	10,70

CH4	9,60	9,80	9,95	10,15	10,50	10,60	10,95	11,20
p1	4,39	4,18	4,37	4,24	4,32	4,24	4,16	4,32
p2	10,68	10,53	10,82	10,65	10,77	10,70	10,45	10,68

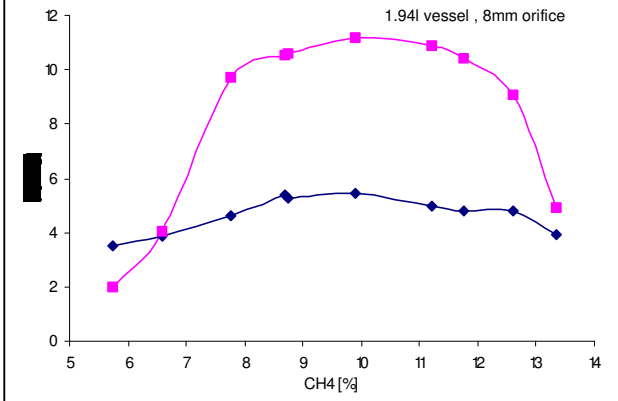

CH4	5,75	6,60	7,75	8,70	8,75	9,90	11,20	11,75
p1	3,53	3,88	4,648	5,41	5,28	5,44	4,98	4,80
p2	1,99	4,02	9,696	10,51	10,62	11,15	10,88	10,40

CH4	12,60	13,35						
p1	4,80	3,93						
p2	9,06	4,91						

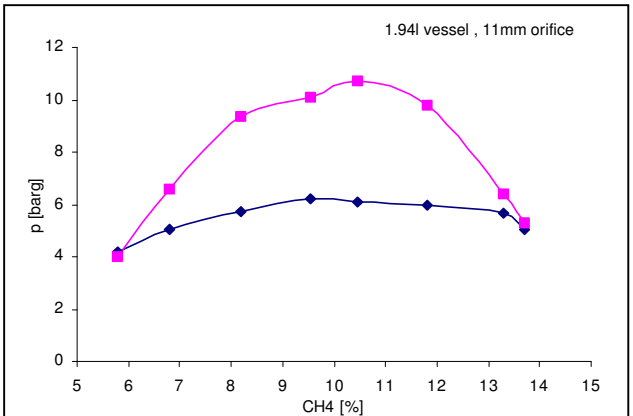

CH4	5,80	6,80	8,20	9,55	10,45	11,80	13,30	13,70
P1	4,16	5,04	5,73	6,24	6,09	6,00	5,68	5,04
P2	4,01	6,56	9,37	10,11	10,70	9,78	6,40	5,28

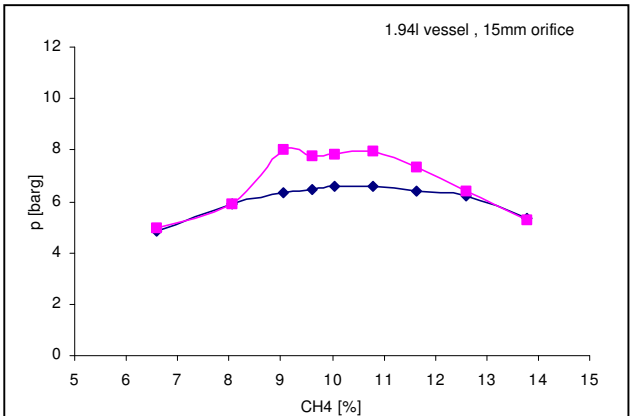

CH4	6,60	8,05	9,05	9,60	10,05	10,80	11,65	12,60
p1	4,88	5,93	6,33	6,48	6,58	6,59	6,42	6,20
p2	4,96	5,92	8,03	7,76	7,82	7,97	7,32	6,40

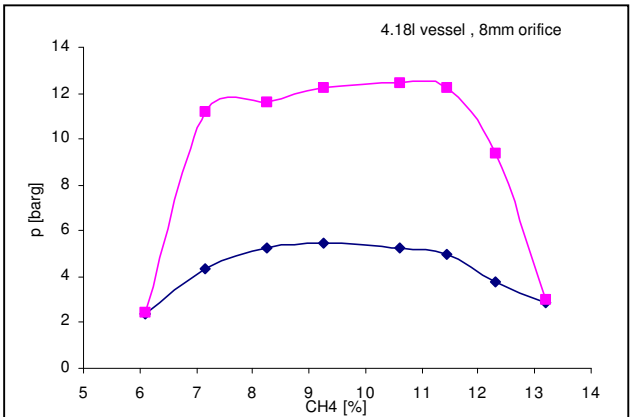

CH4	6,10	7,15	8,25	9,25	10,60	11,45	12,30	13,20
p1	2,40	4,32	5,28	5,44	5,28	4,96	3,76	2,88
p2	2,48	11,20	11,64	12,24	12,44	12,28	9,36	3,02

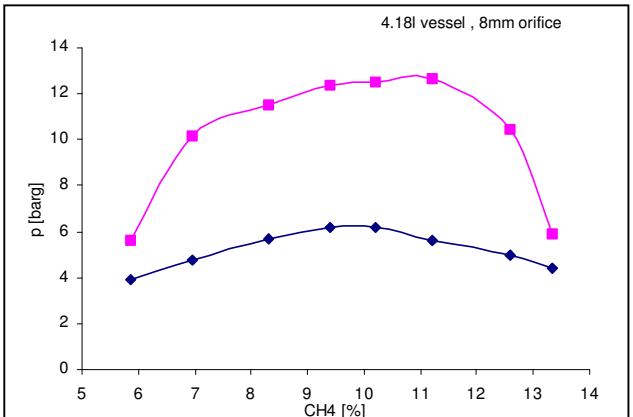

CH4	13,35	12,60	11,20	10,20	9,40	8,30	6,95	5,85
p1	4,40	4,96	5,60	5,90	5,88	5,66	4,76	3,92
p2	5,88	10,44	12,68	12,50	12,40	11,54	10,16	5,60

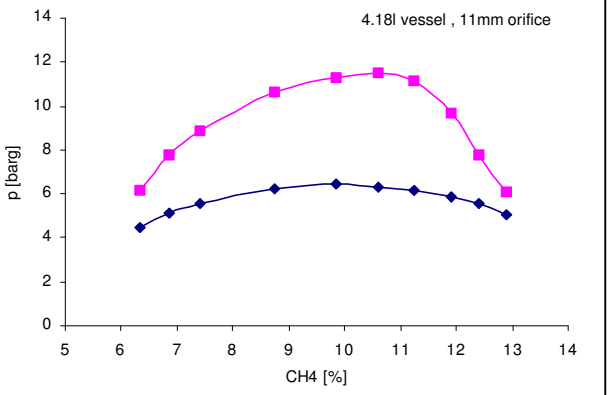

CH4	6,35	6,85	7,40	8,75	9,85	10,60	11,25	11,90
p1	4,48	5,15	5,60	6,24	6,43	6,32	6,16	5,84
p2	6,19	7,76	8,90	10,64	11,28	11,53	11,16	9,65

CH4	12,40	12,90						
p1	5,60	5,04						
p2	7,76	6,05						

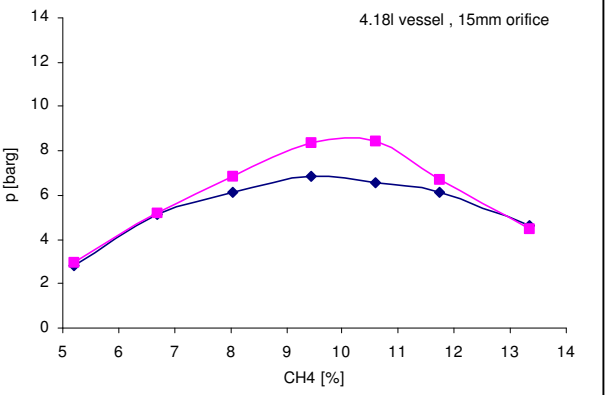

CH4	5,20	6,70	8,05	9,45	10,60	11,75	13,35	
p1	2,81	5,10	6,13	6,88	6,60	6,16	4,64	
p2	2,95	5,16	6,87	8,40	8,43	6,69	4,51	

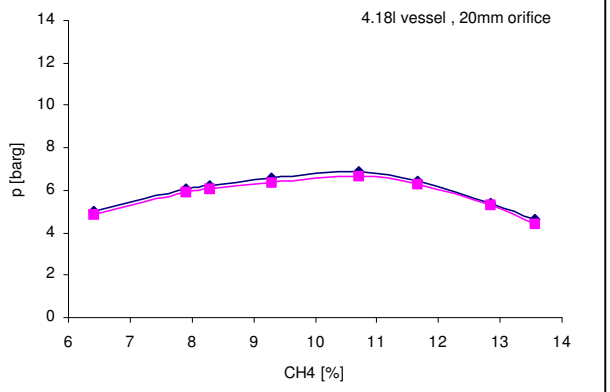

CH4	6,4	7,9	8,3	9,3	10,7	11,65	12,85	13,55
p1	4,98	6,08	6,21	6,56	6,86	6,42	5,36	4,64
p2	4,88	5,92	6,08	6,4	6,64	6,28	5,3	4,44

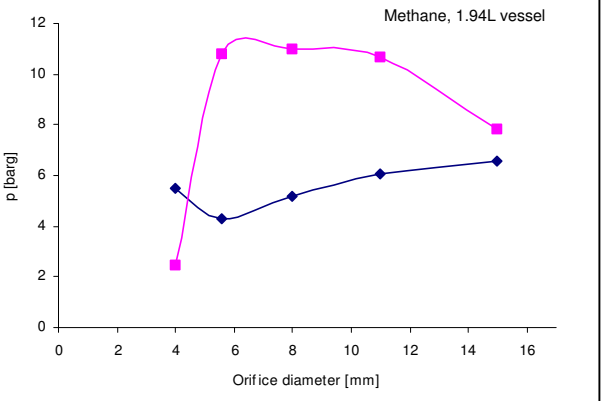

Orifice	4	5,6	8	11	15			
p1	5,50	4,32	5,21	6,09	6,58			
p2	2,48	10,77	11,02	10,7	7,82			

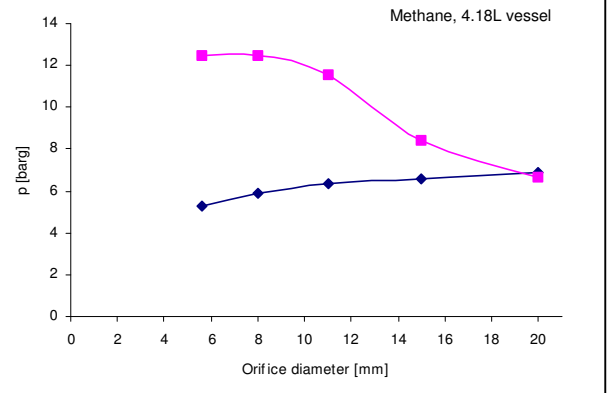

Orifice	5,6	8	11	15	20			
p1	5,28	5,9	6,32	6,6	6,86			
p2	12,44	12,5	11,53	8,43	6,64			

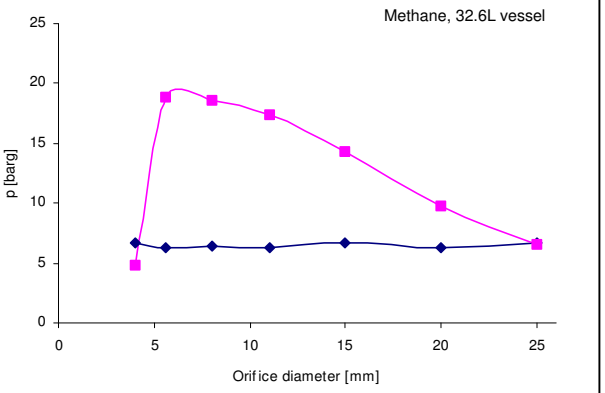

Orifice	4	5,6	8	11	15	20	25	
p1	6,63	6,24	6,40	6,24	6,72	6,24	6,72	
p2	4,80	18,88	18,61	17,39	14,29	9,71	6,56	

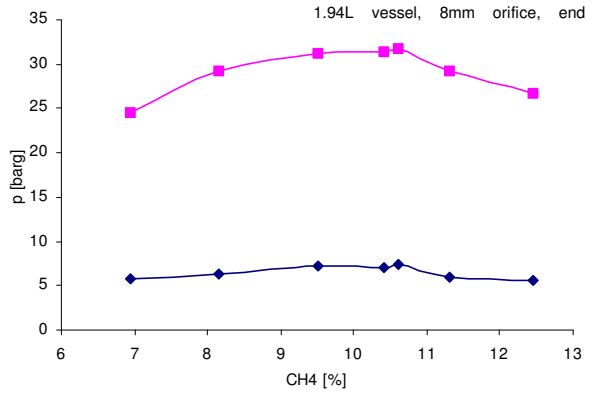

CH4	6,95	8,15	9,5	10,4	10,6	11,3	12,45
p1	5,76	6,24	7,20	6,96	7,44	6,00	5,52
p2	24,48	29,28	31,20	31,44	31,68	29,28	26,64

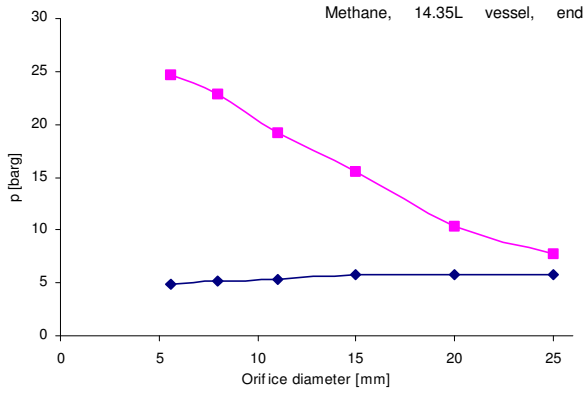

Orifice	5,6	8	11	15	20	25	
p1	4,8	5,12	5,28	5,76	5,76	2,83	
p2	24,72	22,8	19,2	15,6	10,32	7,81	

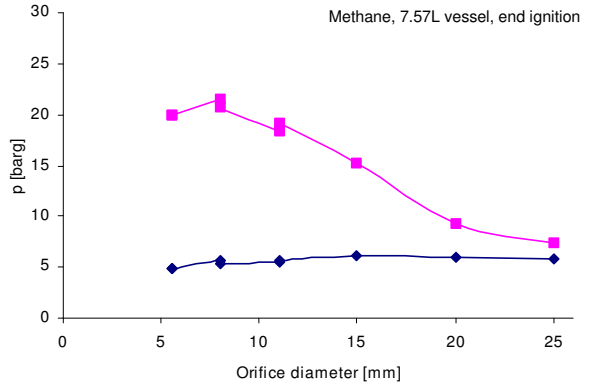

Orifice	5,6	5,6	8	8	11	11	15
p1	4,94	4,86	5,6	5,28	5,44	5,6	6,08
p2	19,89	19,93	21,44	20,8	18,4	19,2	15,2

Orifice	25						
p1	5,76						
p2	7,36						

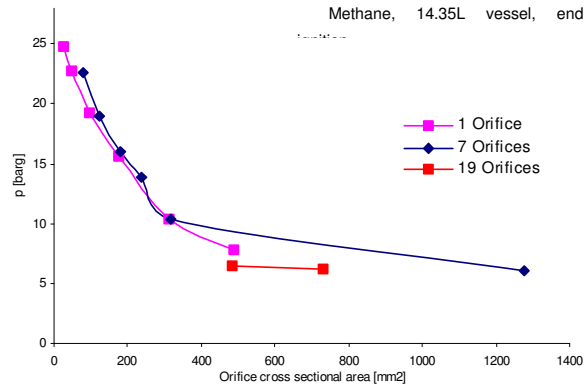

Orifice (1)	5,6	8,0	11,0	15,0	20,0	25,0	30,0	40,0
P1	6,63	6,66	6,20	6,15	6,61	6,54	6,70	7,12
P2	8,97	10,88	13,23	16,57	20,51	21,63	20,56	19,90
Area	24,60	50,3	95,0	176,7	314,2	490,9	706,9	1256

Orifice (7)	3,8	4,7	5,7	15,0	20,0	25,0	30,0	40,0
p1	6,66	6,38	6,48	6,15	6,61	6,54	6,70	7,12
p2	11,87	12,63	16,33	16,57	20,51	21,63	20,56	19,90
Areal	79,3	121,4	178,5	176,7	314,2	490,9	706,9	1256

Orifice(19)	5,7	7,0						
p1	6,52	6,72						
p2	18,75	17,43						
Areal	484,8	730,8						